ISA Activity Report

No. 2.

November 1998

Updated September 1999

Table of Contents

Introduction

Two years have passed since ISA was defined as a National Laboratory through a contract signed by the University of Aarhus and the Danish Natural Science Research Council. The aim of the contract was to ensure the running of ISA as an international competitive centre for basic and applied research, the education of young researchers and to constitute a link between the University of Aarhus and industry. A budget guarantees the operational expenditure, new developments and staff costs. The laboratory is operated under the University of Aarhus with a Board, a Scientific Advisory Committee and beam committees.

The new budget has created a highly dynamic period for ISA. New staff members have been employed, not just on the technical side, but also researchers in order to strengthen especially the use of synchrotron radiation (SR) in physics, chemistry, biology and astronomy.

New SR-beamlines have been installed or are under construction as shown in the laboratory layout on the inside front cover. These include in particular the recently commissioned SGM-2 monochromator (page 24), the SGM-3 monochromator presently under construction and the planned UV-1 monochromator for photobiology, so in coming SR periods, ISA can allocate beamtime on 7 SR-beamlines. The Miyake monochromator with its associated ion beamline also deserves mention, producing its first results at the time of writing this report.

In the laboratory layout is also shown the new developments on the injection side, specifically the electron injector (Microtron) is now used full time for producing pulsed thermalised positrons outside ASTRID I injection periods. Such a positron source is unique worldwide and a large research program is on the way (see pages 19-20).

The ion injector is now followed by an EBIS-ion source so that highly charged ions can be injected into ASTRID I. This injector can also be used for separate research programs.

A completely new Windows NT based control system for all ISA accelerators has been developed and installed to replace the old system which was based on Norsk Data minicomputers.

The new electrostatic storage ring (ELISA) is commissioned and different molecules and clusters (eg. C_{60}) have been stored. In 1998 the designer of ELISA, S. P. Møller, ISA, won the European Accelerator Prize for having made a *recent, significant, original contribution to the field.* In 1996 another Aarhus physicist, J. Hangst, won the prize, which is awarded biennially.

During the past year, ISA has signed collaboration agreements/contracts with DANFYSIK, Jyllinge, Denmark, Daresbury Synchrotron Radiations Laboratories (CLRC), Warrington, UK, Institute for Nuclear Research of the Russian Academy of Sciences, Moscow, Russia and Danisco Ingredients, Brabrand, Denmark.

These new developments have broadened research programs considerably and brought in many new users from specific disciplines that have not been represented before. More than 100 Users utilise the ISA-facility and many PhD/M projects have been carried out. ISA activities in general were reviewed in late 1997 and to quote:

> "*The present research activities at ISA and ASTRID I are of a very high standard... and bear on important problems in a wide range of areas that extend from basic atomic physics, through molecular and solid state physics, biology and medicine as well as accelerator and storage ring physics.*"

The many activities of today have led to the proposal of a new dedicated synchrotron radiation source ASTRID II, which in the ultraviolet and soft X-ray region has a performance equal to or

better than the best sources in Europe, USA and Japan. A layout of ASTRID II is found on the inside front cover. ASTRID II will operate at two energies i.e. 600 MeV for UV/VUV and 1.4 GeV for producing X-rays to biotechnology, medical and materials sciences. Tracking calculations for ASTRID II have shown, that the general concern about unacceptable reductions in dynamic aperture for such machines does not apply to our special lattice. The beam lifetime can be increased (>10h) by increasing bunch length using RF phase modulation and Landau cavities. With ASTRID II the old ring – ASTRID I - will be dedicated to ion storage.

The main arguments for the ASTRID II project can be summarised as follows:

ASTRID II : 600 MeV operation - A State-of the-Art VUV/SXR source
Fulfils a distinct and increasing need for such sources.

ASTRID II : 1.4 GeV operation gives hard X-rays for Biology and Materials
- And back-up for large international facilities

A unique centre for basic and cross-disciplinary research
- A rich research milieu is already established in Aarhus

A centre for accelerator technology
- High technology spin-off and training for Danish Industry

A University link to Industry
- Faster exchange of results between basic and applied research

At the time of writing, the funding of the ASTRID II project is not finalised.

The many contributions from ISA activities found below show that the laboratory today is the scene of a wide range of research, using SR from infrared to X-rays and positive/negative ions, molecules and clusters.

Aarhus in October 1998

Erik Uggerhøj
Director of ISA

Update September 1, 1999:
On the ISA board meeting of June 22, 1999, we were asked to write an activity report covering the period from 1996, when the contract was signed, until today. For this overview we have updated the most recent ISA Activity Report from November 1998. Significant activities since November 1998 are appended to the various contributions.

Notable developments are new SR-beamlines for electron scattering experiments and low energy surface science - both coupled to the undulator. Also a beamline for UV experiments (1.5 - 15 eV) has been installed. New activities have started on the slow positron facility. ELISA is now part of the ion storage program.

Unfortunately, ASTRID II has not yet been funded - a new and cheaper, dedicated UV facility, ASTRID 2000, has been designed. This 3rd generation facility will cover some of the European lack of UV facilities.

1/9 1999 Erik Uggerhøj

Accelerator Physics
and
Machine development

The Storage Ring / Synchrotron ASTRID

S.P. Møller
Institute for Storage Ring Facilities, University of Aarhus

I. The Facility

ASTRID is the first facility which combines a storage ring for ions with a synchrotron-radiation source. The motivation for this was to make a relative expensive piece of equipment available to a wider user community. The layout of the storage ring and injectors is shown in fig. 1.
The electron injector is placed in a separate well-shielded cave. There is no radiation shielding

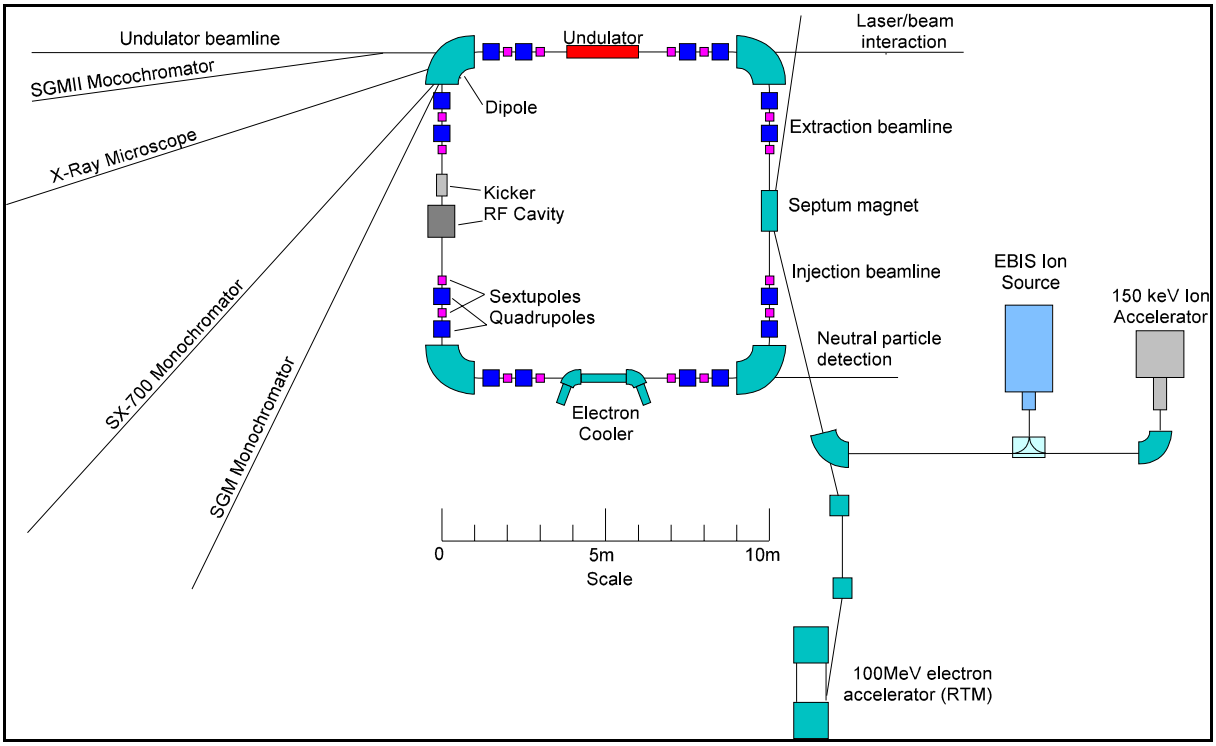

Figure 1: Overview of the ASTRID storage ring, injectors and beamlines.

around the storage ring; hence the ring hall is evacuated during filling of the ring. Scrapers in the ring are left close to the electron beam to give a well-defined beam dump.

A. The injectors

Ions are preaccelerated in an isotope separator using a very stable (RMS<1 V) 200 kV high-voltage supply. A variety of ion sources for both positive and negative ions can be used with the separator to produce singly-charged ions and molecules of almost any type. A charge exchange cell has been installed after the separator magnet to produce negative ions by electron capture in a Na, K or Cs vapour. Differential pumping in the injection beamline separates the high-pressure ion source (10^{-2} torr) from the ring vacuum (10^{-11} torr).

A pulsed (10 Hz) race-track microtron has been built to produce the 100 MeV electrons for the storage ring.

B. The storage ring

The "ring" is a square as formed by two 45° bending magnets in each corner, excited by a common coil. The lattice functions for ASTRID are shown in fig. 2. The quadrupoles are grouped in four families, so that the dispersion in two opposite straight sections can be varied continuously from 0 to 6 m without changing the tunes. Figure 2 shows the lattice functions in ASTRID with four superperiods, and with two superperiods giving two dispersion-free straight sections.

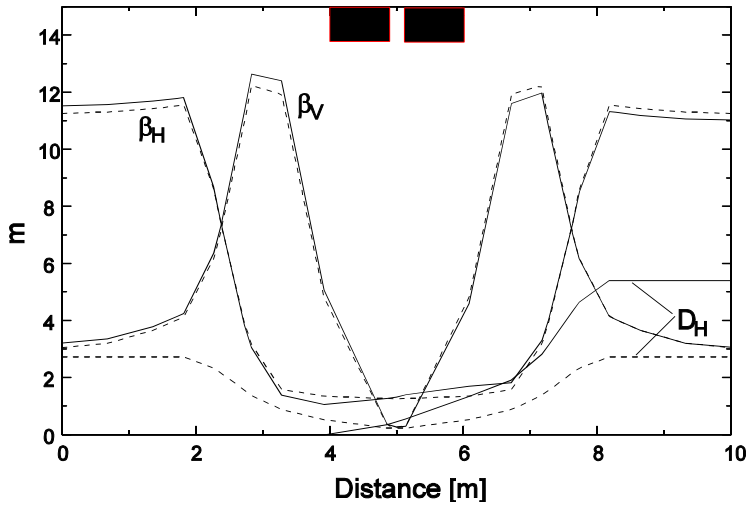

***Figure 3**: Lattice functions of ASTRID in one superperiod for Q_H=2.29 and Q_V=2.73. The black rectangles indicate the position of the bending magnet.*

Two families of 8 sextupoles are available for chromaticity corrections. Superimposed on the air-cored sextupoles are 8 horizontal and 8 vertical correction dipoles. Furthermore 4 horizontal correctors are available as back-leg windings on the main dipoles.

The vacuum system is designed for the 10^{-11} torr region, as required for long storage times of the ions. Hence the system has been vacuum fired and a 150° C in-situ bake-out is performed after each venting of the ring. There is installed a total of 20 ion pumps and 24 sublimation pumps in the ring. Presently an average pressure around $2 \cdot 10^{-11}$ torr is accomplished, with the usual dominance of hydrogen in the residual gas.

Two different RF systems are used:

For ion beam acceleration the old ferrite-loaded cavity has now been changed to a drift tube acceleration setup. All the old low-level electronics has been retained, and only the final-stage amplifier has been changed. The amplifier presently used is a standard 10 W broadband amplifier, which limits the maximum energy gain to ~70 V per turn. A new, matched amplifier extending the maximum energy gain to ~200 V per turn is being designed. This amplifier will also have a better amplitude characteristic (especially at lower frequencies). At present the available frequency range is 0.5 – 5 MHz limited by the low-level electronics. It is being considered to change the low-level electronics with a new direct digital synthesiser (DDS) extending the frequency range. This may also include a stage with an arbitrary waveform generator, so other curve forms than sinusoidal can be exploited. The limited frequency range means that for an injection energy of 150 keV, the maximum energy achievable in a single step is 6.5 MeV. Higher energies has been obtained by a two-step acceleration, where the beam is debunched and rebunched at a lower harmonic at an intermediate flat-top.

For the electrons, a capacitively loaded coaxial TEM cavity operating at 104.9 MHz is used. This cavity was fabricated in steel, which was then copper plated. The obtained Q is around 9000.

Ions and electrons are injected with a magnetic septum (dc) and a kicker placed diametrically opposite. For the ions, the electrostatic kicker excited by a square pulse injects one turn. For the electrons, a magnetic kicker excited by a half-sine pulse is used to accumulate electrons. The dc septum has a maximum bending power of 1.3 Tm and an effective thickness of 11 mm. This rigidity allows injection of heavy ions and also extraction of a low-intensity 580-MeV electron beam.

The kicker/RF-system and the undulator/laser-cooling vacuum chamber are the only

components being exchanged when swapping between electron and ion operation.

Clearing electrodes covering around half the circumference are installed in the ring to reduce ion-trapping effects during electron storage..

A variety of diagnostics instruments are installed in ASTRID. At strategic locations four scintillator screens (Al_2O_3, Cr-doped) are inserted into beam path under 45^0, viewed by TV

Operational Parameters of ASTRID

General:				
Magnetic rigidity	1.87 Tm			
Circumference	40 m			
	Electrons:		**Ions**:	
Injection energy	100 MeV		5-150 keV	
Hor., vert. tune	2.208	2.640	2.29	2.63
Hor., vert. chrom.	-4.3	-7.1	-3.4	-7.5
Corrected chrom.	+1	+1		
Momentum compaction	0.068		0.053	
Injected current	< 265 mA		1 pA - 10 μA	
Accelerated current	< 235 mA		0.1 - 3 μA	
Max. energy	580 MeV		85 MeV (H_2^+)	
Horizontal emittance	0.14 mm mrad			
Critical energy	0.36 keV			
Critical wavelength	35Å			
Energy loss/turn	8.3 keV			
Beam lifetime (Touschek)	20-30 hours (at 150 mA)			
Number of bunches	14		1-28	
RF frequency	104.9 MHz		0.5-5.0 MHz	
RF voltage	125 kV		70 V	

cameras. They are used for beam guidance at injection giving position and approximate size.

The beam position monitor system in ASTRID must accurately measure the position of beams over a wide range of intensity. Split-electrode electrostatic Pickups are used to monitor the position of the beam because of their good low frequency response and high linearity. Depending of beam intensity, the 8 horizontal and 8 vertical positions can be measured with a resolution down to a fraction of a mm. For ions a front-end-processor with low noise wide-band pre-amplifiers provides the difference (intensity dependent position signals) and sum signals (intensity signals) in the 1 kHz to 50 MHz range, followed by a signal processing system with a narrow frequency band selection in the frequency domain (Network Analyser) and a wide-band system (digital oscilloscope) both high precision position measurements and analog observations in the time domain are possible. Time domain observations are important for single turn observations and as a diagnostic tool during, e.g., beam injection. With electrons in the ring another front-end-processor providing the difference and sum signal down converted from ≈105 MHz to 10.7 MHz excludes the observation in the time domain. Both front-end processor outputs are sent as differential signals in double screened coax cables via the reception amplifiers and the multiplexers to the network analysers (HP 4195, HP8753D) and the digital oscilloscopes (LeCroy 9400, LeCroy 9361).

Synchrotron light beam size is measured by a CCD camera and a frame grabber.

The intensity of the circulating beam is measured with two beam current transformers placed near a ceramic gap in one of the straight sections. A DC-transformer (PCT from Bergoz) with a DC to 100 kHz frequency range having a resolution ≤ 5 μA RMS in two current ranges

of 10 mA and 250 mA is mainly used for electrons. For Ions where the intensities are in the 0.1 - 10 µA range a Beam Current Monitor (ICT and a Bunch Charge Monitor from Bergoz) with a resolution ≈ 10 nA RMS is used.

A Shottky pick-up monitor with a low noise, high Q resonant amplifier is used to measure the energy spread of the low velocity ion beams. The monitor provides a selection of frequency ranges with an electronically Q-value control to match different ion velocities.

The control system is based on a a network of PC's running Windows NT. Autonomous function generators are used for all dynamical parameters for acceleration and similar operations. See also separate contribution to this report

II. RUNNING ASTRID WITH IONS

Since the start up of the facility many different ions have been stored in the ring; a list is given in table 2.

The ion

: Mg netic tg ardeyri ltnac.t. Mld tnct: 87 Tn C

ua.nMf dti Mg netnac.4
^{2}C^{+} tttt^{4}0 d^{+} tttt^{6}I n^{+} tttt^{7}I n^{+} tttt^{16}j $^{+}$ tttt^{19}o^{+} tttt^{20}Vd^{+} tttt^{24}5 - $^{+}$ tttt^{40}: 1^{++} tttt^{151}k y^{+} tttt^{166}k l^{+} tttt0 $_{2}^{+}$ tttt

ua.nMf dtg ardeyri ltnac.4
0 C^{+} tttt0 $_{3}$j $^{+}$ ttttH0 $_{3}^{+}$ tttt^{13}Hj $^{+}$ tttt^{14}V^{15}V^{+} tttt^{12}Hj $^{++}$ tttt^{13}Hj $^{++}$ ttttj $_{2}^{+}$ ttttH8 $_{2}^{++}$ ttttH$_{48\text{-}60}^{+}$ ttttH$_{60}^{++}$ ttt H$_{70}^{+}$

Vd-i Mf dti Mg netnac.4
0 $^{-}$ ttttC $^{-}$ tttt^{3}0 d^{-} tttt^{4}0 d^{-} tttt^{9}, d^{-} tttt^{11}, $^{-}$ tttt^{12}H^{-} tttt^{16}j $^{-}$ tttt^{19}o^{-} tttt^{28}8 n^{-} tttt^{32}8 $^{-}$ tttt^{35}Hr^{-} tttt^{40}Hi $^{-}$ tttt^{56}od $^{-}$ ^{88}8 l^{-} ^{138}t, i $^{-}$ ^{174}v 2^{-}

Vd-i Mf dtg ardeyri ltnac.4
^{4}0 d$_{2}^{-}$ ^{12}H$_{2\text{-}8}^{-}$ j 0^{-} : r$_{1\text{-}12}^{-}$ H$_{48\text{-}60}^{-}$ H$_{70}^{-}$

The stored ion beams had rigidities between 7 MeV/c for 6 keV $^{4}He^{-}$ and 300 MeV/c for 85 MeV H_2^+. Many of the ions were accelerated to around 6 MeV. The most complicated operation procedure of ASTRID has been acceleration of H_2^+ from 0.15 to 4 MeV with harmonic 6, debunching and rebunching at harmonic 1, followed by acceleration from 4 to 85 MeV, stored for laser interaction, and then deceleration from 85 MeV to 4 MeV for recombination with the electron beam.

The lifetime at injection energy of stored beams of positive ions was limited by the vacuum, typically a few 10^{-11} torr, giving lifetimes around ten seconds. Injected currents for the positive ion beams were in the 1-10 µA range.

The lifetime of a negative ion beam is determined by rest gas stripping, intrabeam stripping and field stripping (in the bending magnets). A new stripping mechanism has been identified for loosely bound ions. Black-body radiation can ionize ions with small electron affinities like Ba^-, Ca^- and He^-. Furthermore some ions are metastable and autoionise on time scales around a msec.

Most negative ions can only be produced in small quantities, leading to currents in the pA-nA range. Hence they can only be observed with 'neutral' detectors monitoring the decay of the stored beam by counting neutralized ions at the end of the straight sections. An electron multiplier, a semiconductor and a microchannel-plate detector have been used in ASTRID for this purpose.

III. RUNNING ASTRID WITH ELECTRONS

The 100-MeV race-track microtron routinely delivers 10-15 mA pulses of 1 µsec width. This 3 GHz beam is injected into the ring and captured by the 105 MHz RF system. The current captured per injection is around 2-5 mA, and the optimal injection frequency is around 0.2 Hz, to be compared to transverse damping times of 4 secs. This rather low injection frequency is caused by the rather thick septum used. During the early commissioning it was realized, that beam loading in the rf-system limited the maximum accumulated current to 1-2 mA per bunch for rf-voltages around 8 kV. In our case this limitation can not be cured by running with a higher rf power, since a good accumulation efficiency is needed owing to the low injection frequency. A rf power of less than 10 kV is needed to keep the bucket height smaller than the ring acceptance (1%). Hence an amplifier feedback system was built, which reduce the effective cavity impedance as seen by the beam. This feedback system has raised the beam-loading threshold to 20 mA per bunch. The largest current accumulated to date is 265 mA. Up to 235 mA has been accelerated to 580 MeV in less than min. without significant losses. Coupled bunch oscillations are observed at high energy with large circulating currents. The circulating current during a production run is shown in figure 3.

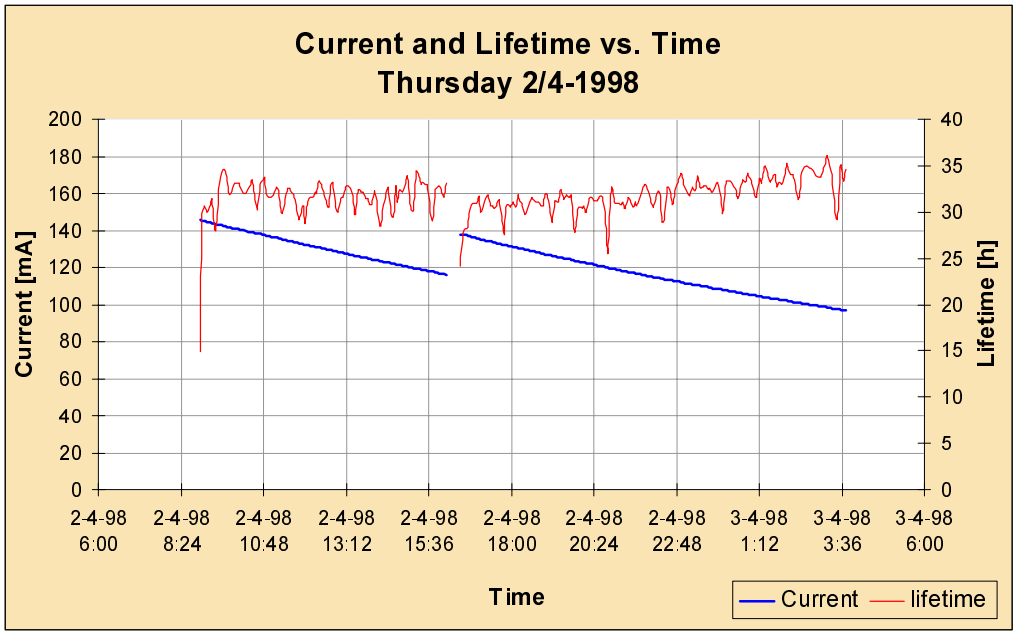

Figure 3

After installation of the narrow-gap undulator vacuum chamber, accumulated currents are usually around 150 mA. At present the lifetime is larger than 30 hours. See separate contribution to this report.

The beam size has been measured using the optical part of the synchrotron radiation at 580 MeV. The horizontal and vertical beam size at the entrance to the dipole have been measured to 0.73×0.10 mm^2 (RMS). From this we deduce a coupling of less than one %, and an increase in the horizontal beam size of around 60 % owing to the bunch oscillations.

The electrostatic storage ring, ELISA

Søren Pape Møller and Ulrik Vindelev Pedersen
Institute for Storage Ring Facilities, University of Aarhus

The electrostatic storage ring, ELISA, whose design was mentioned in the last ISA activity report, has been constructed and is now in operation. The experiments envisaged at ELISA are continuations of some of the experiments performed at ASTRID, such as lifetime experiments of metastable ions and experiments with fullerenes and clusters. Also some new experiments are foreseen, in particular experiments exploiting the advantages of ELISA, in particular the possibility to store very heavy molecules. Here we will describe the design briefly, and give a few highlights from the initial commissioning; for details, we refer to refs. 1 and 2. The layout of ELISA is shown in the figure below.

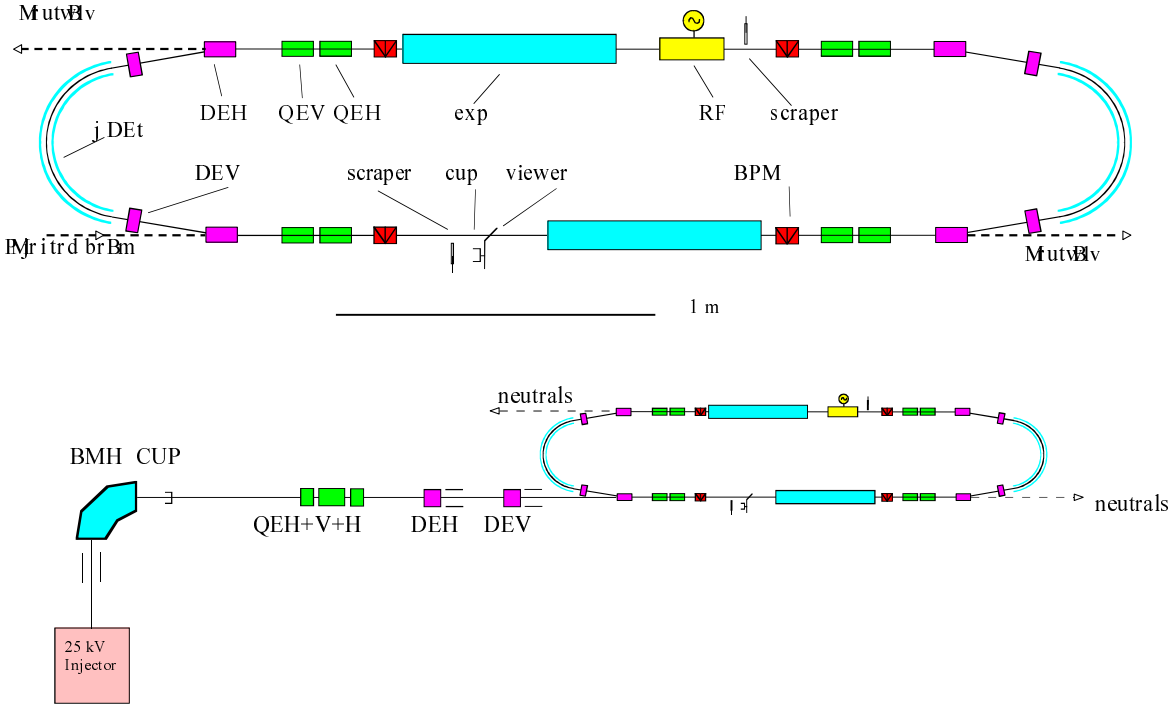

Figure 1: Top: A detailed view of ELISA. Bottom: ELISA with injector and injection beamline.

The lattice is defined by the two 160≈ spherical electrostatic deflectors (SDEH), each having on each side a 10≈ parallel-plate electrostatic deflector (DEH) and an electrostatic quadrupole doublet (QEH, QEV). The resulting lattice functions are shown in the figure below, calculated by standard lattice programs.

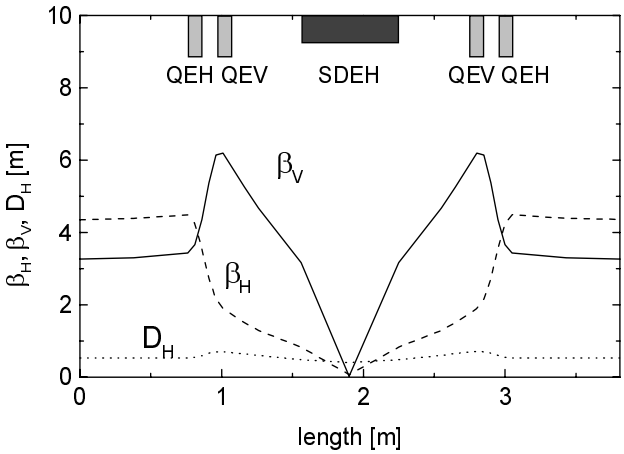

The strong focussing from the 160≈ bends results in a very strong waist in the middle of the bend with a betatron amplitude of only 0.05 m. The two 10≈ bends allow observation of neutral atoms created in the straight sections, and they can also be used as spectrometers in connection with detectors for charge- and mass-changing reactions in the straight sections. One of the 10≈ bends is also used for injection.

The tunes corresponding to the lattice shown above are 1.25 and 1.42 for the horizontal and vertical planes, respectively, but tunes in the range between 1 and 2 are readily possible. Closed-orbit correction can be performed with the four vertical correctors (DEV) and the four horizontal 10≈ bends.

The ELISA lattice has also been simulated by a tracking program taking the actual electric fields, including fringe fields, into account. Ions have been tracked, "flown", through the system for hundreds of turns showing the required stability.

ELISA parameters

General parameters		*10 ° deflectors*	
Maximum energy	25 keV	Plate distance	50 mm
Circumference	7.62 m	Plate length	100 mm
Revolution time	3.5 μs (p) 93 μs (C_{60})	Nominal voltages	± 2.2 kV
Betatron tunes Q_H, Q_V	1.25, 1.42	*Electrostatic Quadrupoles*	
Chromaticities α_H, α_V	-1.9, -1.4	Inscribed radius	26.2 mm
Momentum compaction α_p	0.41	Electrode length	50 mm
160 ° spherical deflectors		Nominal voltages	± 0.47 kV
Electrode radii	235 & 265 mm	*RF*	
Nominal voltages	±3.0 kV	Frequency	10-500 kHz
		Voltage	< 50 V

A single turn injection is performed by means of a chopper in the injection beamline and one of the 10≈ deflectors used as a pulsed inflector. The injector is a standard isotope separator with the possibility of easy exchange of ion sources for production of the various ions. A beamline is used for steering and matching the beam to the ELISA lattice, and for differential pumping. No acceleration is envisaged in ELISA, but a RF system is necessary for bunched-beam observations. Hence, a non-resonant driven drift-tube is used for bunching. The required frequency range is 10-500 kHz.

In order to ensure a smooth commissioning and daily operation of ELISA several diagnostics devices are mounted in ELISA. The positioning of these is shown in figure 1. For steering and focussing into ELISA, a viewer (fluorescent plate and camera) and a Faraday cup is used. Four sets of horizontal and vertical beam-position monitors will be used for bunched-beam observations, either with a chopped beam or with a bunched beam. The pick-ups will provide an intensity proportional sum signal (Σ) and a position-proportional difference signal (Δ/Σ). The noise on the amplifier system corresponds to around 10^7 ions stored in ELISA. Hence, signal averaging is useful to obtain good signal-to-noise ratios. Furthermore, new amplifiers with a noise figure reduced by a factor of 10 are being prepared. Analysis of Schottky-noise and bunched-beam current-transformer measurements is also planned. Finally, observations of neutral atoms at the end of the straight sections are very useful.

Here, we also point out that an electrostatic storage ring is mass independent, and hence can be set up with an intense beam before turning to the, possibly weak, interesting beam.

The vacuum system has been built from stainless steel, according to usual UHV principles. The vacuum system is equipped with four 300 l/s ion pumps and six 1000 l/s sublimation pumps. The system is baked by means of an easily mountable insulation box and one heating element placed centrally. Two Bayard-Alpert ionisation gauges with modulator and a restgas analyser measure the pressure.

At low energy, the stored currents are usually limited by the space-charge tune-shift. Hence we should be able to store currents similar to that in ASTRID, i.e. several µA. Electron-capture or –loss from restgas collisions determines the lifetimes of singly charged ions at low energies. Cross-sections for these processes are slowly varying at low energies, and hence longer lifetimes than in ASTRID are expected in ELISA, since the traversed target thickness becomes smaller for decreasing velocity. Hence, lifetimes in the 1-1000 seconds range are expected. Intra-beam scattering times are around 1000 seconds for typical beams of around 1 µA.

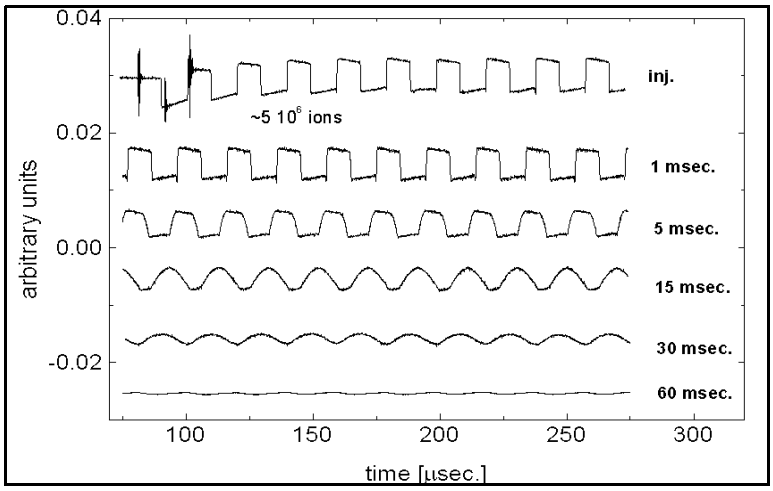

At present the pressure in ELISA is around $2*10^{-11}$ mBar, and beams of many different negative and positive ions have been stored during the one year since the commissioning started. In this figure, we show the sum signals from a pickup for a 22 keV N_2^+ beam chopped to half a ring circumference. The debunching of the beam is clearly seen.

Another example of a beam stored in ELISA is shown in this figure, where the rate of neutral fullerenes from a 22 keV C_{60}^- beam is shown as function of time. The fast initial decay is from a type of thermo-ionic emission process[3], whereas the long-lived component is from interactions with the residual gas. At the same time, the mass independence of the settings of the lattice elements has been verified since fullerene beams of C_{36}^- to C_{96}^- were stored with the same ELISA parameters

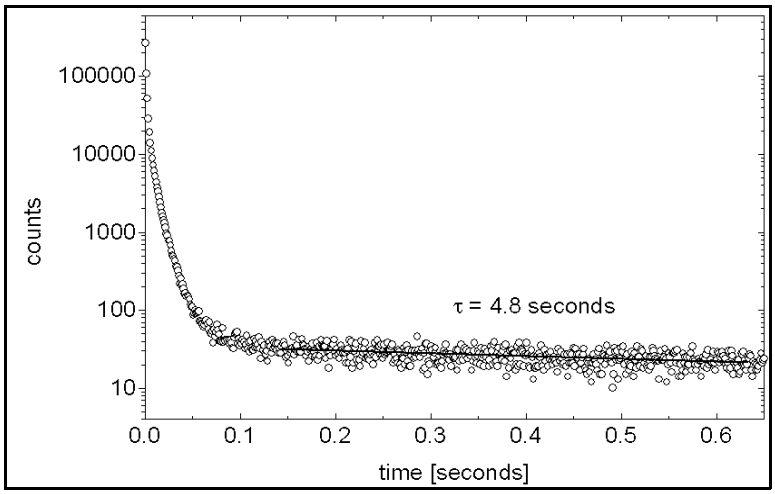

Added September 1999:

Since the cross sections for residual-gas interactions (capture and loss) are almost constant in the low-energy range, the storage times will scale inversely proportional to the velocity. We have measured the lifetime of a O^- beam at 22 and 11 keV to be 26 and 33 sec., respectively, in accordance with this scaling. The longest lifetime observed at room temperature is 36 sec. for a circulating Xe^+ beam at 22 keV. Longer lifetimes for the low intensity beams can be obtained by reducing the residual-gas pressure in ELISA. One possibility to obtain this is to cool the whole ring with liquid nitrogen, and a temperature of −40°C has been reached several times reducing the pressure to a few times 10^{-12} mBar. The cold environment has another very important feature, namely a reduction in the flux of thermal photons stemming from the blackbody radiation from the vacuum chamber walls. This allows new and more reliable measurements of lifetimes of

weakly bound negative ions, and ongoing studies are performed on the He^- and Ba^- ions.

A programme studying the thermionic emission from cluster anions, specifically fullerenes, Ag, Al and Cu clusters has been performed. Also laser excitation has been studied.

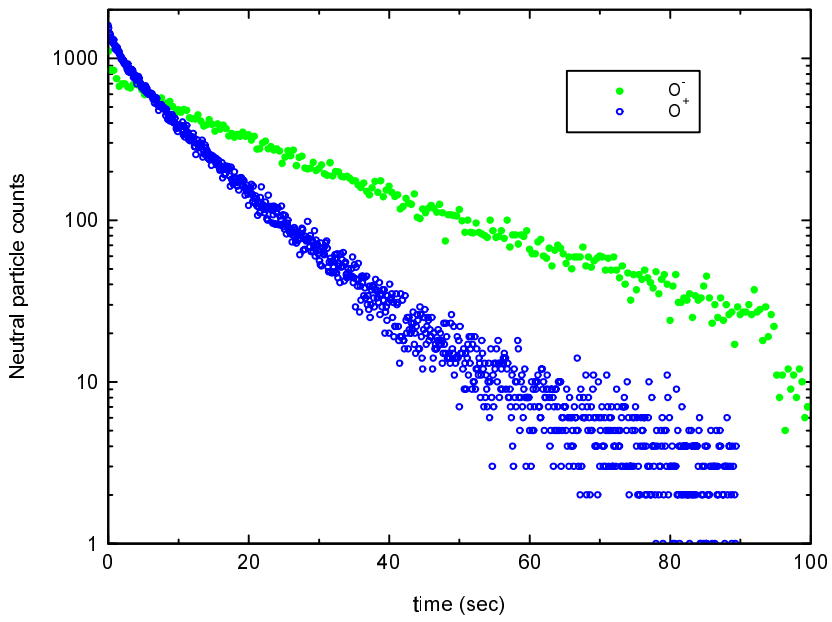

A comparison of residual-gas dominated lifetimes of a positive and negative oxygen beam at 22 keV is shown next. The different exponential decay time for the two species, 11 sec. and 26 sec. for O^+ and O^- respectively, can be explained by the fact that the electron capture cross section of O^+ is approximately three times larger than the electron detachment cross section of O^- at low energies.

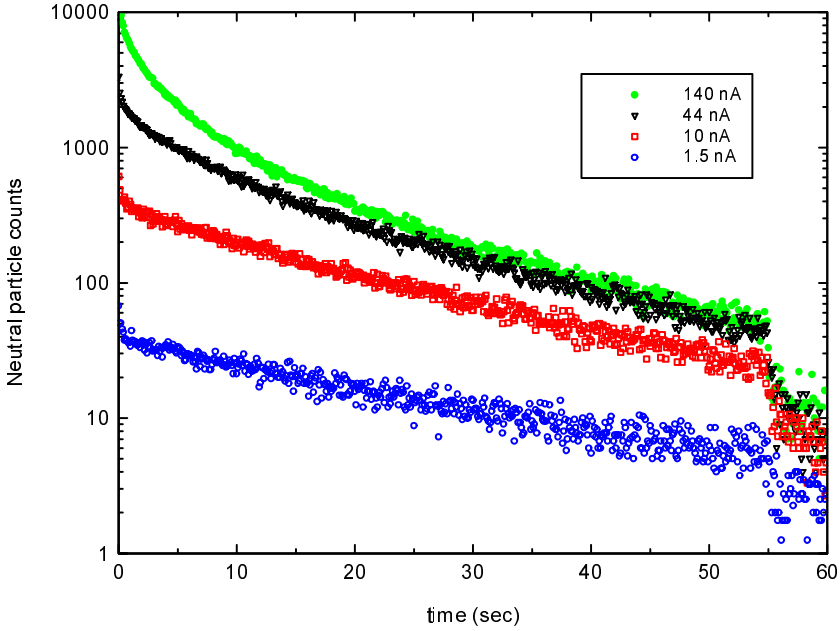

The next figure shows the neutral particle yield for four different injected currents of O^- at 22 keV, where the remaining beam is kicked out after 55 seconds to obtain the background level. For large currents, a reduction in the lifetime is seen at early times, i.e. an intensity dependent lifetime. The origin of this effect is not yet understood[4].

References:

1 S.P. Møller, Nucl. Instrum. Methods in Physics Research A **394** (1997).

2 S.P. Møller, Proceedings of the Sixth European Accelerator Conference, Stockholm, 22 to 26 June 1998, IOP Publishing.

3 J.U. Andersen, C. Brink, P. Hvelplund, M.O. Larsson, B. Bech Nielsen, and S. Shen, Phys. Rev. Lett. **77** (1996) 3991.

4. S.P. Møller and U.V. Pedersen, Proceedings of the 1999 Particle Accelerator Conference, New York, 1999, p. 2295.

The EBIS ion source

U.V. Pedersen[1], N. Hertel[1], P. Hvelplund[2], and L. Liljeby[3]
[1]*Institute for Storage Ring Facilities, University of Aarhus*
[2]*Institute of Physics and Astronomy, University of Aarhus*
[3]*Manne Siegbahn Institute, Stockholm University, Stockholm, Sweden*

The EBIS (**E**lectron **B**eam **I**on **S**ource) is intended to be a source of moderately charged ions for injection in ASTRID. For elements lighter than oxygen, ions of all charge states can be produced with sufficient intensity for injection. For heavier ions, the limit is for charge states up to ~10.

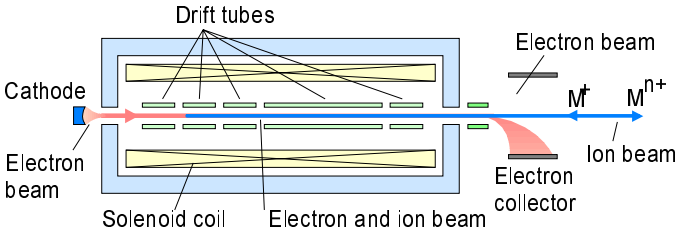

An EBIS consists of an electron gun producing an electron beam which is compressed and confined in the axial magnet field of a solenoid. At the exit of the solenoid the beam is expanded and collected on an electron collector. Since only intermediate charge states are needed, this version is a 'warm' source, i.e. the required current density can be produced in a room-temperature solenoid. To trap ions a potential-well is created, which is formed radially by the space charge of the electron beam and axially by a system of cylindrical electrodes surrounding the beam. Due to successive ionizing collisions with the energetic electrons, the charge state of the trapped ions increases gradually as a function of the confinement time. When the desired charge state is reached, the ions are extracted axially through the electron collector by lowering the potential on the end electrode.

The EBIS source will be loaded through the electron collector with singly charged ions produced by the ASTRID heavy ion injector. The advantages of external ion injection are decreased gas load, increased range of ions, and isotopically clean beams. The ions are retarded from an energy of 100 keV to less than 1 keV prior to being trapped in the EBIS. After 'cooking' for 1 ms to 1 s, they are extracted and accelerated for injection into ASTRID. Since the time of the last activity report, the EBIS has been moved to the new ISA laboratories. Improvements have been made concerning the properties of the electron beam which now fulfil the design values (see below). In a preliminary beamline equipped with a low energy separator, an electrostatic deflection switch needed to direct ions in and out of the EBIS has been tested successfully. A 17 keV N^+ beam was injected all the way through the EBIS and detected at the electron gun end. It was, however, not possible to decelerate and trap the N^+ ions in the EBIS due to the lack of focussing optics in the preliminary beamline. Residual gas particles present in the EBIS have been trapped, ionized, and extracted. After the acceleration stage and deflection in the electrostatic switch, the different charge states in the extracted pulse have been separated by time of flight. The figure below shows a time of flight spectrum from the residual gas after 200 ms confinement in the EBIS.

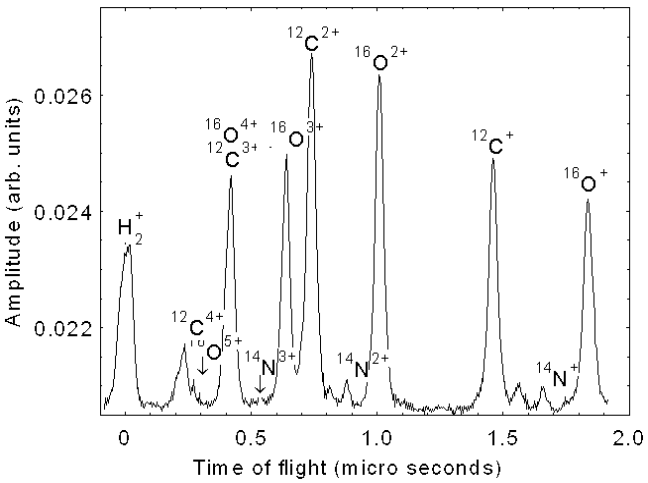

The EBIS is presently being installed in the new beamline for the ASTRID ion injector (see separate report). This beamline will provide the beam optics needed to focus the injected ions in the EBIS.

The main EBIS parameters are given below:

Maximum axial magnetic field	0.1 Tesla
Length of solenoid	0.6 m
Electron current	0.05-0.25 A
Electron beam energy	2-7 keV
Confinement time	< 1 s
Number of ions (charges/pulse)	$<10^{10}$

The ISA Slow Positron Facility

Jonathan Merrison[1], Niels Hertel[1], Helge Knudsen[2], Stefan Stahl[3]
[1]*Institute for Storage Ring Facilities, University of Aarhus, Denmark*
[2]*Institute of Physics and Astronomy, University of Aarhus, Denmark*
[3]*University of Mainz, Mainz, Germany*

An intense pulsed slow positron beamline has been constructed based on ISA´s 100MeV Microtron electron accelerator. Since February 1998 this facility has routinely produced microsecond long pulses containing over 20,000 positrons with a repetition rate of up to 15Hz. Using a specially designed fast switching buncher these pulses have been compressed to around 10ns in length. An extensive physics program utilising this unique European facility has already begun. As part of a European collaboration for highly charged ion cooling a cryogenic Penning trap from the University of Mainz is currently being installed. This will allow accumulation and cooling of the positrons to produce a dense single particle plasma. Positrons can then be extracted to form an ultra-low energy, ultra-high resolution beam. This would be the first facility of its kind and allow matter/antimatter interactions to be studied in a new regime.

The operation of the positron facility relies on pair production from high-energy α-rays. These α-rays are emitted when 100MeV electrons strike a dense (platinum) target. Using two acceleration and moderation stages the relativistic positron flux is converted into a well-resolved slow beam. The electron accelerator is pulsed with microsecond long pulses, therefore the positrons arrive in the laboratory also in pulses which contain over 20,000 particles. Temporal compression of these pulses can be performed with the use of a specially designed ´buncher´, which simply accelerates those positrons at the rear of the pulse in order to catch up with those at the front. Pulse lengths of around 10ns have been obtained.

Such a pulsed positron source is ideal for studying the lightest and arguably most simple of all atoms (or anti atoms), namely positronium which is the bound system of

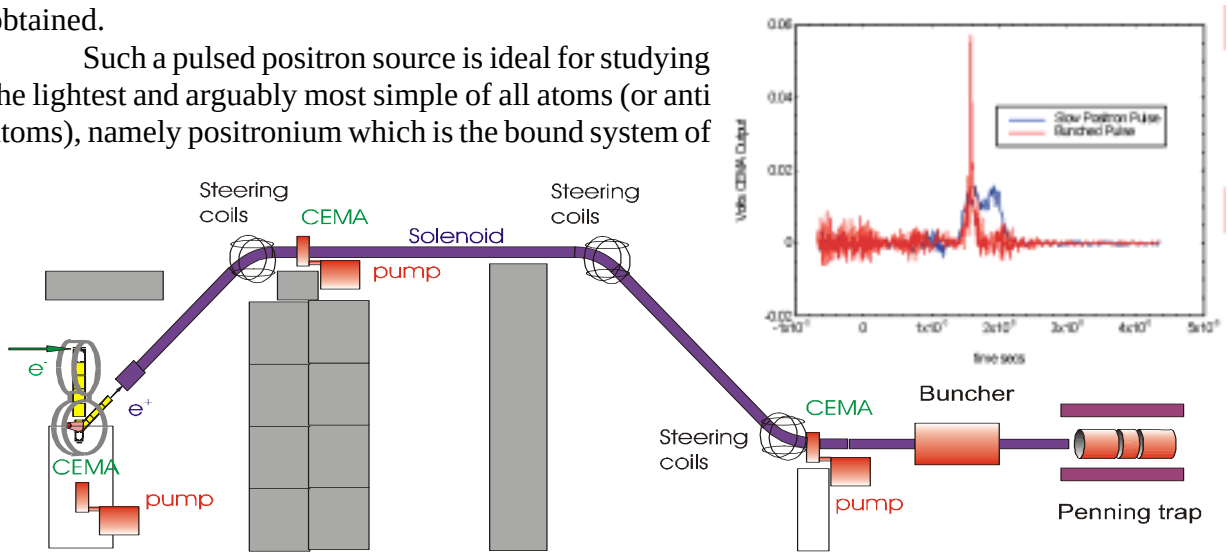

an electron and positron. An extensive program of research involving positronium atoms has already begun with an attempt to observe multiphoton ionisation of positronium and more specifically above threshold ionisation. Here an intense (pulsed) infrared laser is used to irradiate the positronium and by absorbing many (7 or more) photons ionisation can occur. These studies are intended to continue next year. A list of such collaborative projects is presented on the next page including the name(s) of additional collaborators.

The special time structure of the bunched positron beam makes it well suited for injection into a cryogenic Penning trap. Here positrons can be accumulated and cooled to a temperature of a few Kelvin at densities close to the space charge limit (around 1million particles per cubic mm). These positrons may be used for cooling highly charged ions in order to allow higher precision mass spectroscopy measurements. We are presently in a large European collaboration for this

purpose which is funded under the EUROTRAP EU network. Here the unprecedented resolution and beam intensities anticipated can be used for precision studies of matter/antimatter interaction. A program of positron atomic physics at ultra low energies (meV) is planned. Also with the use of a tuned circuit the number of trapped positrons can non-destructively be measured, something which cannot be done with conventional slow positron beams.

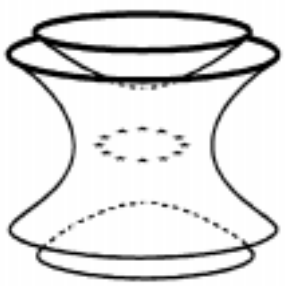

An exciting technique, which has been applied to trapped ions, may now be applied to positrons. This involves exciting the so called ´magnetron´ motion, this is the oscillatory motion of the particles about the trap axis. The effect is that the particles are centered on the axis of the trap. With this technique the radius of the trapped positrons could be reduced to less than 1μm. A positron beam with an energy resolution of 1meV and a size of 1μm would constitute the first of a new class of beam or ´microbeam´.

Internationally the largest use of positrons is for characterising defect and impurity concentrations, specifically for the semiconductor industry. Positrons are unique tools in this regard since by analysing the gamma radiation emitted when a positron annihilates with an electron in the material details of that electrons properties, such as its momentum, can be obtained. This is a sensitive probe of the electrons environment and thus of the structure of the material. With the recent acquisition of a scanning electron microscope, 3D defect and impurity mapping may be performed in the ISA slow positron laboratory. This can be done by injecting (instead of electrons) a well-resolved positron beam and studying the annihilation radiation. This is one use of a positron microbeam.

Added September 1999:

The ISA Positron Microscope

Positrons are widely used for solid state and surface physics, in fact solid state investigators are the most prolific users of positrons. Several large dedicated positron facilities (accelerator/reactor based) exist, for example at Lawrence Livermore National Laboratory (USA), KEK (Japan), Delft University (Holland) and The Munich Research Reactor (Garching, Germany). Many more groups (in at least 10 different countries) apply a large variety of positron techniques to solids and surfaces. In most cases the motivation is the study of electron structure by observing the gamma rays emitted after positron annihilation. This is a sensitive and non-destructive probe of the sample structure and defect/impurity concentration. The use of a so-called positron microprobe - such as the one currently under construction at Aarhus - one can map such features in 3D. Lack of exchange allow positron studies to be cleaner than similar electron studies and significantly more surface sensitive, hence their increasing application in surface science.

With current technology in order to produce a positron micro-beam (with a diameter of around 1 μm) one must employ several stages of acceleration, focussing and moderation, also with the use of thin film metal moderators. Aarhus is one of the only institutes, which manufactures thin single crystal metal films of sufficiently good quality and in fact supplies several other positron groups world-wide. Since the optics in a standard electron microscope utilises (almost solely) magnetic lenses it functions equally well for positrons or electrons, as the sign of the charge is irrelevant. Hence one can simultaneously observe a sample with electrons and perform positron annihilation analysis. This requires only minor modification to an electron microscope such that a well-resolved positron beam can also be focussed into the lens system. An operational electron microscope at ISA is presently in the process of being modified such that it is compatible with positron injection. The primary positron beamline and electrostatic transport is under construction. The final stages of the positron optics are in the design stage. Final construction and preliminary trials should begin in early 2000.

The developments of positron trap technology may lead the way for the long-term future of positron microscopy. With the huge improvements in intensity and beam quality one could

envisage real time positron imaging. Also if positrons are to be applied in an industrial environment it is clear that an inexpensive, rugged and compact system must be developed which has large instantaneous intensity and high resolution. The application of positron trapping is making this possible.

New mass spectrometric techniques for the characterisation of biomolecules: Positron capture dissociation of proteins.

Mass spectrometry (MS) is one of the most important physical methods in analytical biotechnology. A particular advantage of MS compared to other molecular spectroscopies is its high sensitivity so that it provides one of the few methods that is entirely suitable for the identification or quantitative measurement of trace amounts of chemicals.

Today many MS instruments consist of two mass analysers arranged in a tandem called "Tandem mass spectrometry or MS/MS".

Here the first analyzer selects a specified m/z value and then this is directed into a collision cell to collide with gas molecules, ions or recently electrons - hereby fragmentation is induced. The second mass analyzer separates these fragments for detection. Tandem MS has become a powerful method for obtaining detailed structural information of peptides. In particular, the use of collisionally activated dissociation (CAD) of peptides to yield characteristic fragment ions for determining their primary structure is well established.

The dissociation of peptides by CAD is an ergodic process. This means that the internal energy acquired by the ion upon collisional activation is redistributed among all internal degrees of freedom before bond cleavage takes place (i.e., the rate of internal energy randomisation is much faster than the rate of fragmentation). The energy randomization leads to a scrambling of the amide hydrogens, which makes CAD unsuitable for investigating hydrogen/deuterium exchange sites of peptides and proteins (vide infra). A new fragmentation method, which generates sequence specific fragment ions without inducing H/D scrambling, will be extremely useful for the analysis of the dynamics of protein molecules.

Fragmentation by positron/electron capture

In the mid-nineties it has been demonstrated that capture of positrons by small organic molecules yields a number of fragment ions which are specific for the given molecule. The positron-electron annihilation process (in closed shell ions, such as deprotonated/protonated peptides) results in the formation of excited radical ions, which are similar in nature to the radical ions formed by electron capture. Recent results strongly suggest that the dissociation of such ions is also a nonergodic process and has been demonstrated to occur without H/D scrambling. Very recently, it has been shown that the capture of low energy electrons by protein cautions causes specific cleavage of the peptide backbone in contrast leave product ions formed by CAD2. In comparison with CAD electron capture cleaves many more sites (of the backbone of the protein) thereby yielding a greater number of sequence specific fragment ions, so fragmentation of macromolecules using low energy electrons/positrons is a very promising new technique.

In the present project large molecules (proteins) are trapped first and then bombarded with intense (10^6) low energy positron beams. A completely new and unique research facility in the analysis of proteins and other biomaterials.

Positron Trapping – Cooling and Accumulation

The application of Penning traps is revolutionising slow positron beam technology. As a device for in-beam cooling and accumulation they can provide many orders of magnitude enhancement in resolution and instantaneous intensity [1]. This is proving to be vital for the most ambitious and exciting experiments using positrons [2,3,4]. This is the motivation for the positron trapping program at the ISA positron facility. We presently trap around 1000 positrons per pulse (10000 per second) in a 6 Tesla cooled Penning trap. An exciting and potentially important observation has been made. Due to the high radial compression of the beam on entering the strong

magnetic field, in-beam coulomb scattering becomes a rapid and efficient process for mixing axial and radial energy components. Also observed was rapid cooling (around 100μs) of the positron cloud by evaporation of the hottest positrons. This may be used as an efficient source based trapping scheme for positron accumulation and cryogenic cooling to compete with present trapping schemes which are either inefficient or use a dense buffer gas and are therefore inconvenient [this is being prepared for publication].

Proposed Projects for the ISA Pulsed Positron Facility

Positronium in Strong Laser Fields	[P.Balling, M.Raarup]
Positron and Positronium Compounds (eg Lie^+)	[T.Andersen]
COLTRIMS using Positrons	[V.Mergel]
Positronium Spectroscopy	[R.Ley, G.Werth]
Laser Cooling of Positronium (Photon Recoil)	[M.Drewsen]

Positron Trapping and Cooling

EUROTRAPS: Heavy Ion Cooling	[S.Stahl, R.Ley, G.Werth, M. Charlton, L.Jørgensen]
Cluster Ionisation and Cooling	[L. Schweikhard]
Positron Microprobe (Solids and Surfaces)	[L.Jørgensen]
Antihydrogen (Physics/Technology)	[M.Charlton]

An Ultra High Resolution (meV) Slow Positron Beam

Positron Scattering at Low Energy	[D.Field, S.Lunt]
Near Threshold Ionisation	[N.Laricchia]
Atomic Excitation (eg. He)	

The new ion injection beamline

Søren Pape Møller, Kåre Iversen, and Lars Therkelsen
Institute for Storage Ring Facilities, University of Aarhus

A new ion injection beamline for ASTRID has been designed and built and is presently being installed in the ring hall and the new injector room. This new beamline is a consequence of moving the 150-keV isotope separator into the new injector room, where also the EBIS is installed. The beamline is shown in figure 2 on the next page. It is designed to transport ions from the injector into the EBIS source, and subsequently transport the EBIS ions into ASTRID. Furthermore, ions can be transported directly from the separator to ASTRID. This new beamline will in addition allow tests and developments of new ions from the separator during electron runs; an option previously not available. Furthermore, the beamline will improve the differential pumping between the ion source and the ring, a key issue when using noble gasses in the ion source.

The isotope separator including separator magnet and the first Faraday cup is unchanged. The first electrostatic quadrupole triplet creates a beam waist inside the EBIS source, or it transports the beam to the second quadrupole. This second quadrupole produces a beam waist immediately in front of the wall, where a charge exchange cell will be placed. The beam then passes through the third quadrupole, a new 90≈ analysing magnet, a fourth quadrupole and finally the beam is matched to the ASTRID lattice by the fifth quadrupole. Apart from the first Faraday cup immediately following the separator magnet, there are four additional Faraday cups along the beamline, and one beam viewer. The beam is steered by 4 new electrostatic steerers, and the old steering magnets in the injection beamline. A vertical beam chopper is used to chop the beam to a pulse corresponding to the circumference of ASTRID. In addition, there is a chopper immediately after the EBIS switchyard and a channeltron to analyse the charge state of the EBIS ions. An electrostatic deflector with two Faraday cups after the charge-exchange cell will be used to monitor the charge-exchange process. The optics of the beamline is shown in figure 1.

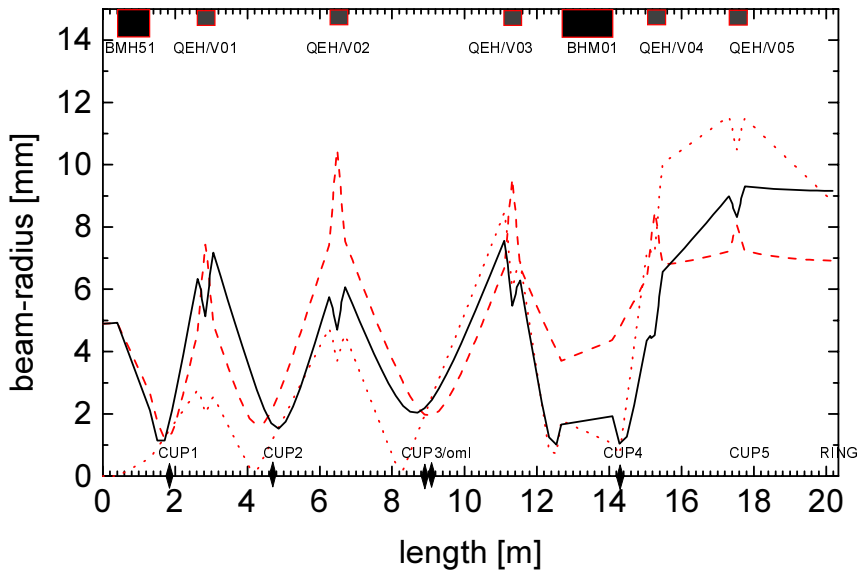

Figure 1: Beam optics in the new ASTRID injection beamline.

Added September 1999:

The new ion injection beamline was brought into operation in the last ion run of 1998 and it has been used since with a good performance. The transmission efficiency is close to 100 %, and there are a sufficient number of steering elements. Also a reasonable matching to the ring lattice can be made; this has in particular been demonstrated during the Mg^+ -laser cooling runs, where the diagnostics based on flourescence light has been used to characterise the beam. Also the vacuum characteristics are acceptable; in particular, a reduced inlet of noble gases into the ring has been observed, when operating an ion source with a high pressure of a noble gas.

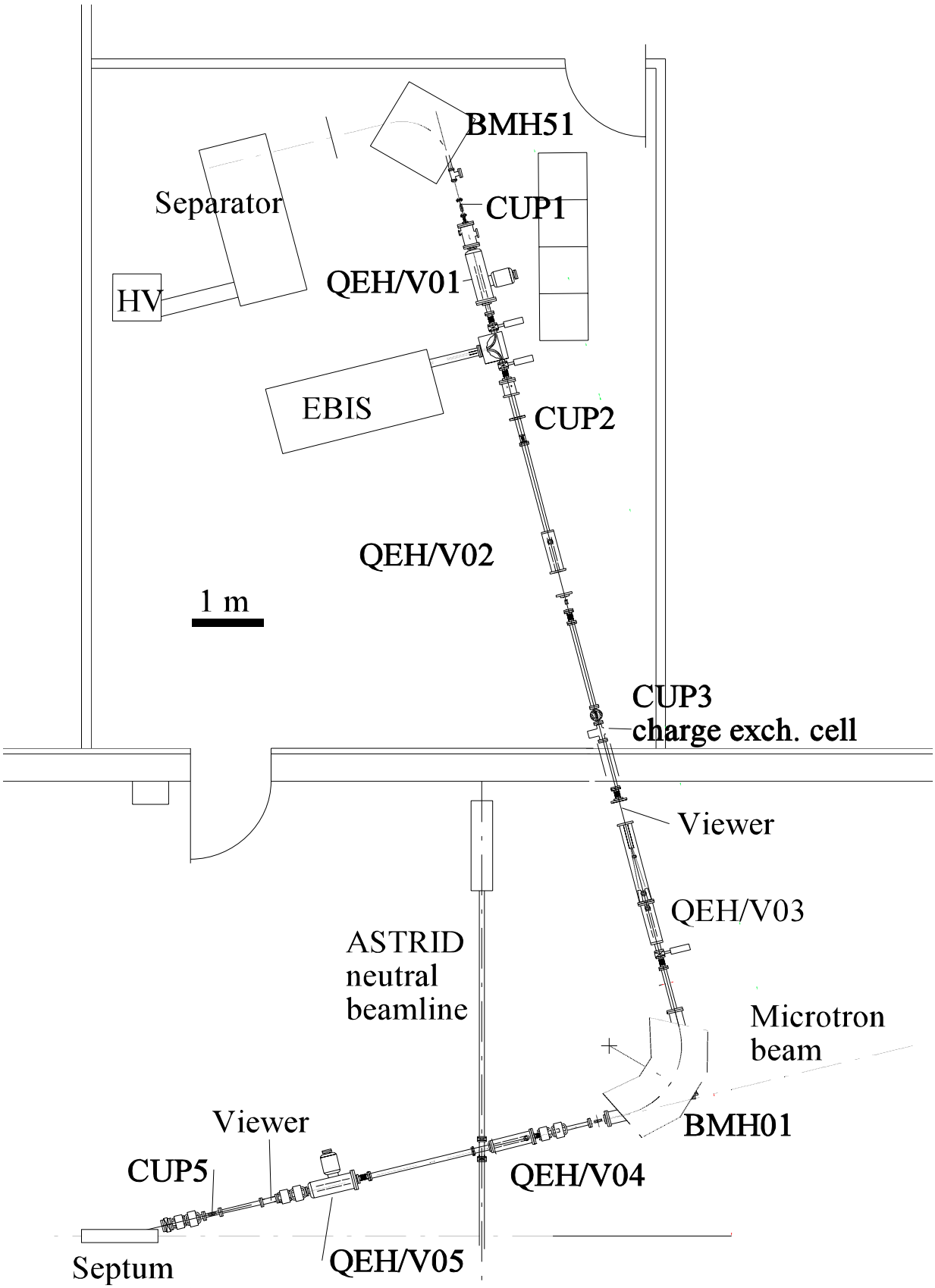

. ayout of the new ASTRID ion injection beamline

Synchrotron Radiation Beamlines (Revised Sept. 1999)

S. L. Lunt
ISA, University of Aarhus.

The period following the publication of the previous activity report has been one of consolidation and expansion for the synchrotron radiation (SR) beamline program. Five beamlines operate routinely, a sixth is nearing completion and a seventh under construction. The characteristics of these seven SR beamlines are summarised in the table below. Research areas noted in the final column span the fields of Physics, Chemistry, Biology, Surface and Materials Science affirming the multi-disciplinary nature of the ISA SR program.

The SX700 beamline, which is also the oldest, comprises a Ziess plane grating monochromator (PGM) of the Petersen design [1] and a dedicated surface science endstation, equipped with the usual surface science tools. References to published research using this line will be found later in the report.

SGM I is another surface science station consisting of a plane folding mirror spherical grating monochromator [2] and a UHV surface preparation and analysis facility. The primary analytical tool is a Scienta electron energy analyser for photoemission studies. This beamline is fully operational and references to work carried out can be found later in the report.

The X-ray Microscope (XRM) [3] is another station in full production, capturing images of human sperm at different stages of maturation, images of iron-precipitating bacteria (which have been considered as 'biological filters' in the preparation of drinking water supplies) and of blue-green algae to name but a small sample of the current projects. As before, further references to the work on the XRM will be found later in this report.

The next station is the MIYAKE beamline, which couples an order-sorting plane grating monochromator of the Miyake design [4] with the ASTRID undulator. Differing from conventional bending magnet sources of SR, undulators provide flux enhancement through constructive interference as the electron beam 'undulates' in a permanent magnet array. This leads to a series of peaks in the output spectrum as opposed to the smooth distribution from a dipole magnet. By varying the undulator gap, and sometimes the energy of the electron beam in the ring, it is possible to scan continuously over a wide range of photon energies. Typical flux outputs are enhanced by some two or three orders of magnitude as compared to bending magnet sources. The output from the MIYAKE monochromator is currently merged with singly charged ions of $\approx$100 keV from an ion beamline in order to measure absolute photoionisation cross-sections of atomic ions.The first results from this apparatus were taken during the latter half of 1998 resulting in new data on C^+, K^+, Mg^+ and Al^+ ions, to name but a few.

ISA's newest operational beamline, SGM II, was completed in the first half of 1999. This beamline operates in a time-sharing mode with the MIYAKE beamline, using the same undulator source of radiation but now coupled to a spherical grating monochromator of the Chen design [5]. The performance of the monochromator has proved to be outstanding. With slit settings of 10 microns, a resolution of 0.75 meV FWHM has been measured in the sharp autoionising Ar** $3p^5(^2P_{1/2})$ 11s resonance, superposed on the broad 9d' resonance, in the photoionisation of argon at 786.5Å. This is to be compared to the figure of 0.73 meV, calculated from optical ray tracing. This beamline supports a low energy electron-molecule scattering experiment using a beam of photoelectrons generated by the argon photoionisation scheme noted above to measure absolute scattering cross-sections in various gaseous molecular targets. The high photon flux of the undulator source coupled with the high resolution of the monochromator has enabled electron beams with an energy resolution of $\lesssim$1 meV to be produced down to kinetic energies of 5 meV yielding new data on many molecular species.

Using virtually identical components to SGM II, a third monochromator (SGM III) is nearing completion. This monochromator will also share the output from the undulator but will span a larger wavelength range than SGM II and terminate in a surface science work station concentrating mainly on photoemission studies. We are presently only awaiting delivery of the gratings before

embarking on the commissioning of the beamline. The mechanical assembly is complete and the end station is undergoing characterisation..

The final beamline is UV1. It is currently under construction and uses a very simple normal incidence monochromator with a toroidal pre-mirror and grating to provide a high flux of linearly polarised ultra-violet (UV) and vacuum ultra-violet (VUV) photons at moderate resolution. Intended applications for this beamline include; circular dichroism spectroscopy (CDS) of biological materials, particularly in the important protein absorption region around 200 nm, absorption spectroscopy of chemical and biological samples, photoconductivity measurements of thin films and semiconductor wafers and photon-induced oxidation of iron bearing minerals.

Station	Source	Performance	Applications
SGM1 (operational)	Dipole 2 downstream tangent	30 to 700 eV (3 gratings) R= 5,000 to 14,000	Surface Science
SX700 (operational)	Dipole 2 downstream tangent	6 to 2,000 eV (2 gratings) R = 200 to 2,500	Surface Science
XRM (operational)	Dipole 2 centre tangent	α = 1.5 to 3 nm	X-Ray Microscopy, Imaging
MIYAKE[(1)] (operational)	Undulator	15 to 180 eV R ≈ 2,000	Atomic/Molecular Physics
SGM2[(1)] (operational)	Undulator	12 to 40 eV R = 20,000 [(2)]	Atomic/Molecular Physics
SGM3[(1)] (under construction)	Undulator	8 to 150 eV [(3)] 3 gratings R ≈ 15,000	Surface Science
UV1 (under construction)	Dipole 1 centre tangent	1.5 to 15 eV 2 gratings R ≈ 5,000	CD spectroscopy, Photobiology, VUV Spectroscopy

[(1)] shared operation - switchable via premirror.
[(2)] measured at 786.5Å
[(3)] lower limit of 8 eV possible by reducing ASTRID beam energy, normal limit 14 eV.

[1] H. Petersen. *Optics Communications* **40**, 402, (1982).
[2] J. van Elp, C. Thiel, F. Folkmann, A. Baurichter, C.S. Mythen and B.N. Jensen. *NIM*, **A381**, 548, (1996).
[3] R. Medenwaldt and E Uggerhøj. *Rev.Sci.Inst*, **69**, 2974 (1998).
[4] K.P. Miyake, R. Kato and M. Yamashita. *Sci.Light*, **18**, 39, (1969).
[5] C.T. Chen. *NIM*, **A 256**, 595, (1987).

Commissioning of the SGM2 undulator beamline

S. V. Hoffmann, Z. Li and S. L. Lunt.
Institute for Storage Ring Facilities, University of Aarhus

A new Spherical Grating Monochromator (SGM) has been built and commissioned on the ASTRID undulator beamline. The SGM is of the dragon type with a fixed entrance slit, and a moveable exit slit. The first optical element is a horizontally deflecting and focussing spherical mirror (HFM). This HFM can be retracted vertically from the beam in order to let it pass into the Miyake monochromator, or it can be rotated by about 180° to deflect the undulator beam into a third branch (SGM3), currently under construction. After sideways deflection into the SGM2 branch, the beam is deflected vertically upward, and focussed onto an entrance slit. This entrance slit acts as a source for a spherical grating, which focusses the beam onto the exit slit, with the final beam direction in the horizontal plane.

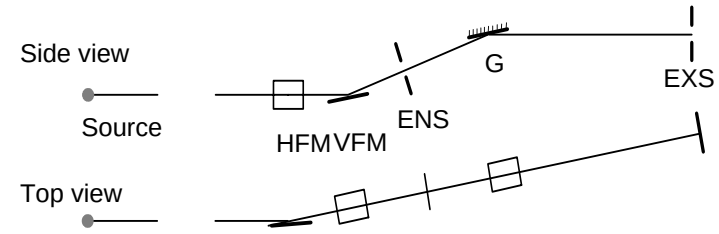

Figure 1: Optical layout of SGM2. The abbreviations used are HFM: Horizontal focussing mirror, VFM: Vertically focussing mirror, ENS: Entrance slit, G: Grating and EXS: Exit slit.

The SGM2 beamline is constructed to scan a wavelength range of 400Å to 1000Å (12eV to 30eV), and the resolution of the instrument has been optimised at a wavelength of 785Å by minimising the major optical aberrations at this wavelength. To cover the entire wavelength range with high resolution, the exit slit must be able to travel over a distance of 400mm, but initially the travel distance has been limited to 100mm, in order to accommodate an Electron Molecule Scattering (EMS) experiment.

The resolution of the SGM has been checked by recording the photoionisation spectrum of Argon. An elliptical mirror was used to refocus the photon beam into a PhotoIonisation (PI) cell filled with Argon at a pressure of 0.15mtorr. The photoemitted electrons were extracted by a small potential difference across the PI-cell, accelerated and focussed with a 4-element lens system, and finally detected by a channeltron. This setup is part of the EMS experiment, which has a high transmission for electrons formed close to zero energy.

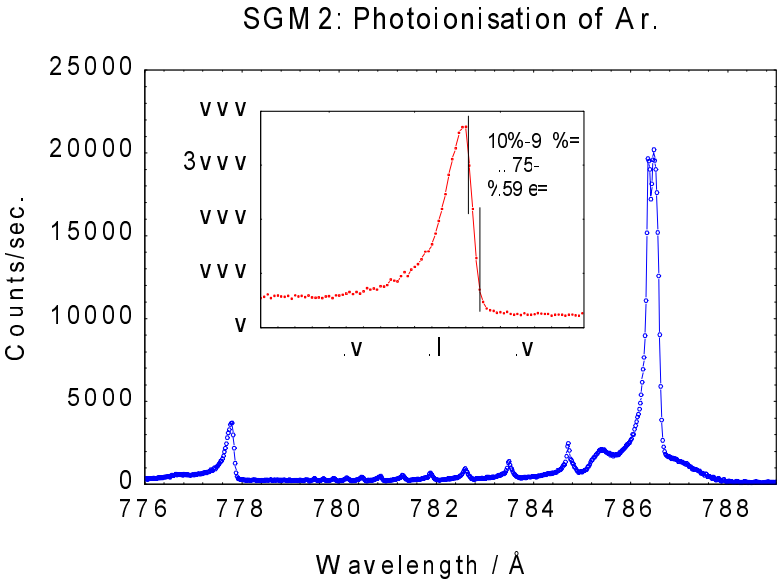

Figure 2: Photoionisation spectrum of Argon, recorded with the Electron Molecule Scattering experimental setup. The FWHM resolution of the SGM can be determined from the width of the 10% to 90% peak height interval of the Ar-$^2P_{1/2}$ onset, and is found to be 1.5meV.

Figure 2 shows a photoionisation spectrum recorded with the EMS setup over the wavelength range 789 to 776 Å. Clearly seen in the figure are the two Ar-$^2P_{3/2}$ and Ar-$^2P_{1/2}$ ionisation thresholds at 786.7Å and 777.9Å respectively. The natural onset of the Ar-$^2P_{1/2}$ threshold is very sharp (<0.1 meV). Thus, the main component to the observed rise in the onset comes from the instrumental resolution. From figure 2, the FWHM resolution can be determined by measuring the interval between 10% and 90% of the peak height, which is better than 1.5meV, very close to the design value of 1.3meV.

New orbit measurement in ASTRID: Quadrupole shunts

Jørgen S. Nielsen
Institute for Storage Ring Facilities, University of Aarhus

ASTRID has from the start been equipped with 16 pickups (8 in each dimension), that mechanically were aligned together with the rest of ring. Vertically it has always been quite easy to achieve good positions (overlap with lasers, etc.), but horizontally, good positions were always difficult to achieve. The mechanical position of one pickup was then remeasured, and found to be displaced 2.5 mm inwards. For long it was then believed that this was true for all of the pickups. Good horizontal orbit control was however still difficult to achieve. It was therefore decided to install a quadrupole shunt on each quadrupole, which would enable measurements of the beam positions in the quadrupoles. By aligning the beam to the centres of the quadrupoles it has now been possible to calibrate the offsets in the pickups, which for unknown reasons have been found to vary quite a lot (from -2.0 mm to +2.5 mm). These large and varying offsets explain the difficulty previously encountered in beam positioning.

Principle of measurement

The 16 pickups located close to the dipole magnets allow measurement of beam position to within ~½ mm. Using a least-square closed-orbit correction method this allows the beam to be positioned within a few mm in all of the machine if the pickup offsets are known. Previously these were unknown, resulting in position uncertainties of more than 10 mm. See table 1 for some of the parameters of the pickups.

For more accurate beam positioning, and calibration of offsets in the pickups, the beam positions can be measured in the quadrupoles by shunting their current. If the beam is not in the centre of a quadrupole, changing the strength of the quadrupole will cause a change in the deflection of the beam. This will in turn cause a change of positions around the machine, which can be measured by the pickups. The quadrupole shunt based beam-position measurements allows the beam to be positioned to within one mm in the entire machine.

As part of the new control system, a new positioning program is being made. This will ease positioning and hopefully lead to an improved machine performance.

Pickups:	
Electrostatic type (diagonal cut "shoe-box") with Σ- and Δ-signals	
Nr of pickups (horz, vert):	8, 8
Short term precision:	~30 μm
Long term accuracy:	~0.5 mm
Quadrupole shunts:	
Installed autumn 1996	
Shunts one Q-pole at the time	
Shunt current:	0 – 30 A
Precision (of resulting beam position measurement):	0.2 – 0.5 mm

Table 1: Some parameters of the ASTRID beam positioning system

Development in electron beam lifetime at ASTRID

Jørgen S. Nielsen
Institute for Storage Ring Facilities, University of Aarhus

Vertical excitation (t = 10-15 h) (before Autumn 1997): Being a small ring the "natural" (Touschek limited) lifetime is quite low (only 1-2 hours at 100-200 mA). As the users mostly have been interested in flux, and not so much brilliance, the vertical emittance has been increased by a factor of ~10, with corresponding lifetime increase, by excitation at the first vertical betatron sideband.

Phase modulation (t = 15-20 h) (Autumn 1997): At the 5th ESLS in Lund 1997 it was reported by Peter Kuske, Bessy that phase modulation of the acceleration RF field at approximately three times the synchrotron frequency had lead to an increase in lifetime at Bessy I.
Phase modulation was subsequently tried at ASTRID, where it was found that the lifetime of the "natural" beam increases by a factor of 2-3 by applying a (small) phase modulation at any harmonic (up to the fourth) of the synchrotron frequency. The gain in lifetime increases as current is increased. The gain is however reduced to approx. 50% when the vertical excitation is applied. Phase modulation together with the vertical excitation, however still led to a lifetime of 15-20 h, which was a significant increase, and phase modulation was then applied routinely, with a frequency of 57 kHz (third harmonic).
To our knowledge there is no theory which completely explains what happens to the bunches when phase modulation is applied, but a model which describes some of the features has been suggested (in the spring of 1997) by Yu. Senichev. The key point in this theory is that particles with small synchrotron amplitude are made to oscillate in longitudinal phase space, whereas the motions of large amplitude particles are not affected. The overall effect is that the particle density is reduced in the bunch centre, which reduces the Touschek scattering, but as the large amplitude particles are not affected the overall bunch length is not increased very much.

Better orbit (t = 30-35 h) (spring 1998): Following an orbit change associated with commissioning of the undulator, the lifetime jumped to 30-35 h (vertically excited and with phase modulation on). Without phase modulation the lifetime is now normally 15-20 h, but sometimes we get the long lifetime even without phase modulation. The reason for this is not fully understood, but it has been correlated with an uneven fill of the machine (different bunches have different currents), and it may therefore be a microwave instability, which causes bunch lengthening. This is also consistent with the fact, that the bunch lengths have been seen to increase in the first minutes after acceleration.

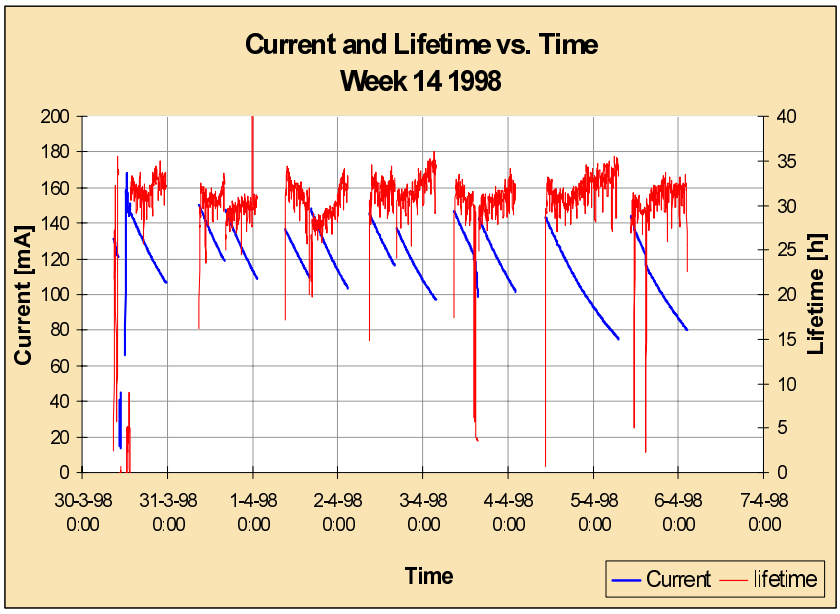

Phase modulation is still routinely applied, as we newer have seen any disadvantages from it. (We do not presently have users, which perform time-resolved experiments.)

Mechanism of rf phase modulation to increase the lifetime of beams in synchrotron radiation sources

Yu. Senichev
Institute for Storage Ring Facilities, University of Aarhus

The proposed lattice for a third generation synchrotron light source, ASTRID II, is designed to provide a low electron emittance of 5 nm at 1.4 GeV and 1 nm at 0.6 GeV. In such low emittance SR sources a key concern is the decrease in lifetime due to enhanced scattering, the Touschek effect. In principle an improvement in the beam lifetime can be obtained by increasing the emittance coupling or by increasing the longitudinal bunch dimension, however, both methods affect the whole bunch and have an adverse effect on the light quality.

To address these problems we have developed a method of RF field phase modulation, where the energy gain of the electron is modulated with an amplitude ψ_m and frequency ω_m:

$$\frac{dW}{dt} = eU\sin\left[\varphi + \psi_m \cos(\omega_m t + \theta)\right] - \widetilde{W}_r$$

where U is the peak RF voltage, φ is the particle phase angle relative to the RF field zero with fixed phase, θ is the initial phase of the phase modulation.

The nature of this method is based on the parametrization of the radiation damping decrement in the longitudinal plane due to the modulation of the energy deviation relative to the bunch centre:

$$W - W_o \propto \left[1 + \chi \cdot e^{i\left[(\omega_m - \Omega_s)t + \theta - \varphi_i\right]}\right]$$

where α_s is the synchrotron frequency for the small amplitude oscillation and

$$\chi = \frac{\Omega_s^2}{\omega_s^2 - \Omega_s^2}\frac{\omega_m}{\Omega_s}\frac{\psi_m}{\psi_i}$$

is the factor of the parametrization. From this expression we can see that under fixed $\delta\omega = \alpha_s - \omega_m$ the magnitude of the energy modulation is determined by the ratio between the coherent RF phase modulation amplitude ψ_m and the incoherent oscillation amplitude ψ_i of the particle . Figure 1 shows the phase trajectories of a particle with the different oscillation amplitudes at the same phase modulation. With a change of the amplitude ψ_i the shape of the curves varies as well.

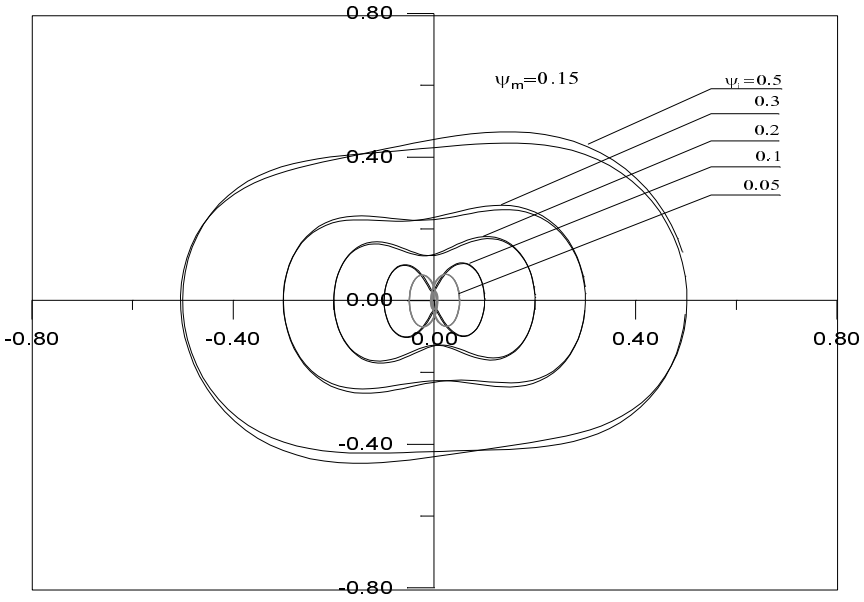

Figure 1. *The phase trajectories of a particle with different amplitude of oscillation under the same RF phase modulation amplitude.*

Taking into account the spontaneous character of radiation emission, the stationary distribution is determined by the balance of the quantum excitation and the radiation damping processes:

$$\sigma_E^2 = \frac{\dot{N}_{tot}\left\langle \varepsilon_{ph}^2 \right\rangle}{4\xi_o\left(1 - \frac{\chi}{2}\cos 2\Theta\right)}$$

where $\dot{N}$ is the total rate of the quantum emission, $\left\langle \psi_{ph}^2 \right\rangle$ is the mean square quantum energy and α is the total phase of the particle. The decrement modifies the distribution in two directions, extending in one direction and compressing in another perpendicular to the first (see figure 1). Making the correct adjustment of the phase of the phase modulation we can determine the extension in the length of the bunch and the compression in the momentum spread. The degree of this redistribution depends on how far the particle is from centre of the bunch. It is leading to a lower density in the bunch core and consequently a lower probability of the intrabeam scattering. The balance of the quantum excitation and the radiation damping processes determines the equilibrium longitudinal emittance. We modify this balance for the growth of the phase area, occupied by the particles in the central part of the longitudinal plane. We show that phase modulation with a frequency three times that of the synchrotron oscillation excites the core growth with an increment greater than the decrement of the radiation damping process. Varying the RF phase modulation strength, we can change the phase area, where the distribution is modified. The parametrization effect can be reached by RF amplitude modulation as well and the nature is similar.

For results with the phase-modulation technique in ASTRID, see the previous contribution.

The proposed third generation synchrotron light source *ASTRID II*

Y. Senichev, S.P. Møller
Institute for Storage Ring Facilities, University of Aarhus

The main features of third generation light sources are the small electron emittance, typically less than 10 nm and many long straight sections for wiggler and undulator insertions. Obviously in order to reach such a small emittance, the dispersion function in the lattice has to be minimised. Unfortunately, with the necessary value of the dispersion, the sextupole efficiency required to correct the chromaticity becomes extremely low and the dynamic aperture of the ring takes an unacceptably small value. Besides, each long straight section gives an additional growth of the natural chromaticity. To satisfy these two contradictory conditions we have developed a racetrack lattice with two second-order achromatic arcs and many long dispersion-free straight sections[1]. The layout of the new ASTRID II storage ring is given in fig. 1. Electrons will be injected from a 500-MeV booster synchrotron, identical to the booster for the ANKA storage

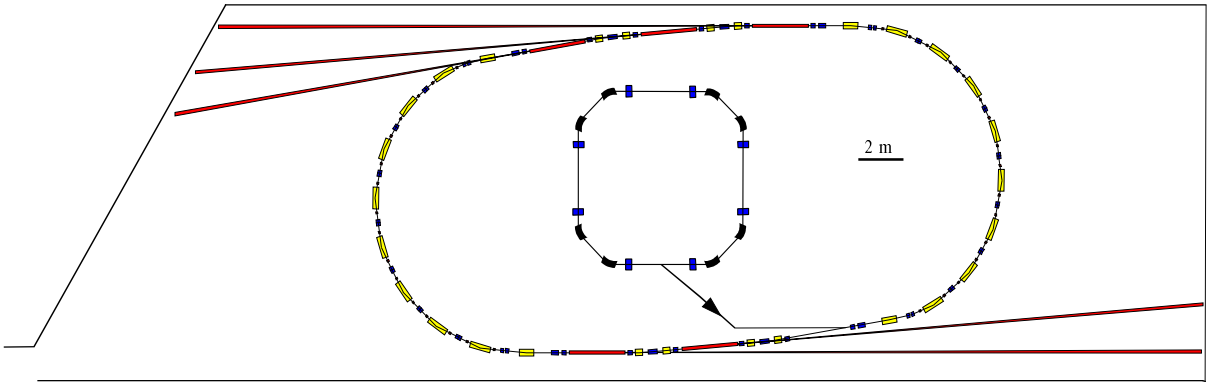

Figure 1 *Layout of ASTRID II with insertion device beamlines and synchrotron injector.*

ring[2]. ASTRID II is planned to operate at two energies, one around 600 MeV and another at 1.4 GeV. At the lower of these energies, ASTRID II would be optimised for the production of vacuum ultra-violet (VUV) and soft X-ray (SXR) radiation, providing high brilliance through the use of insertion devices and by optimisation of the machine parameters to minimise the natural electron beam emittance. Operation at the higher energy of 1.4 GeV will provide sufficient flux of harder X-rays (~10 keV). The brilliance of the photon beams from bending magnets, wigglers and undulators at ASTRID II are compared to the brilliance from ASTRID I and DORIS in fig. 2.

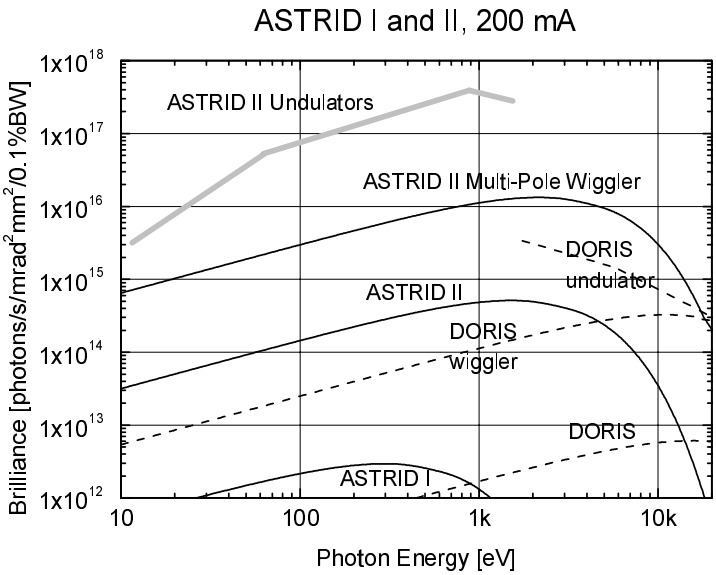

Figure 2 *Brilliance curves for ASTRID I and II for bending magnets, wiggler and undulators. Corresponding curves for the DORIS ring at DESY are also shown*

When considering various lattice layouts, it is desirable to provide sufficient flexibility in the optics, if possible, to take advantage of any future advances in insertion device technology, perhaps by a renewal of the straight sections without a significant disturbance. The type of facility envisaged would include either two, or four, or six straight sections, with each having a length of up to 10 m, 5 m and 3 m, respectively.

The proposed lattice has the following parameters:

- horizontal emittance of the electron beam less than 1 nm at 600 MeV, or 5 nm at 1.4 GeV;
- dispersionless straight sections between 3 m and 10 m in length;
- flexible straight sections decoupled from the bending sections;
- convenient method to correct the chromaticity by the sextupoles;
- large dynamic aperture, about 100 mm mrad;
- small number of families of the magnetic elements.

With these parameters, the source is far from diffraction-limited in the X ray regime and the brightness is governed by the electron beam emittance. Conversely in the VUV regime the source is completely diffraction-limited, and the brightness is dominated by diffraction. Thus, in order to produce tuneable radiation from 5 eV to 100 eV and from 1 keV to 10 keV the lattice has to be optimised for two extreme regimes at 600 MeV and 1.4 GeV. The classic ring structure of a number of identical achromat cells arranged in a highly symmetric circular form has been used in the vast majority of synchrotron sources until now. In particular, a modified Chassman-Green layout was proposed in an earlier design study by V. Lebedev for ASTRID II[3]. Due to the requirements mentioned above, it soon became apparent that a large circular lattice capable of achieving the desired performance should be discounted in favour of a more compact racetrack layout.

The lattice

The proposed racetrack lattice geometry consists of two identical arcs separated by two similar optical channels consisting of one, two or more straight sections. Between the arc and the straight sections a matching section is required to control the parameters for the beam in the insertion devices. A significant advantage of such a design is the ability to separate the functions of the arcs and the straight sections, with the former largely determining the final equilibrium emittance and the latter, with the inclusion of small additional elements, able to tune the Σ functions as required.

In the proposed racetrack lattice each arc includes eight periodical cells, containing combined function bend magnets and focussing quadrupoles. Figure 3 shows a lattice of arc and straight section. A reduction in symmetry can lead to a reduction in the dynamic aperture. However, if we could tune the arcs in the horizontal and vertical planes to a value of $n_{x,y} \times 2\psi$, we form a second-order pseudo-achromat and it would be possible to maintain an acceptable dynamic aperture. The most appropriate values of tune for our arc are the integer numbers n_x=3 and n_y=2, corresponding to a phase advance per cell equal to 135° and 90°. To a first approximation in this condition, the non-linear action of each n^{th} sextupole is compensated by $(n+4)^{th}$ in the horizontal

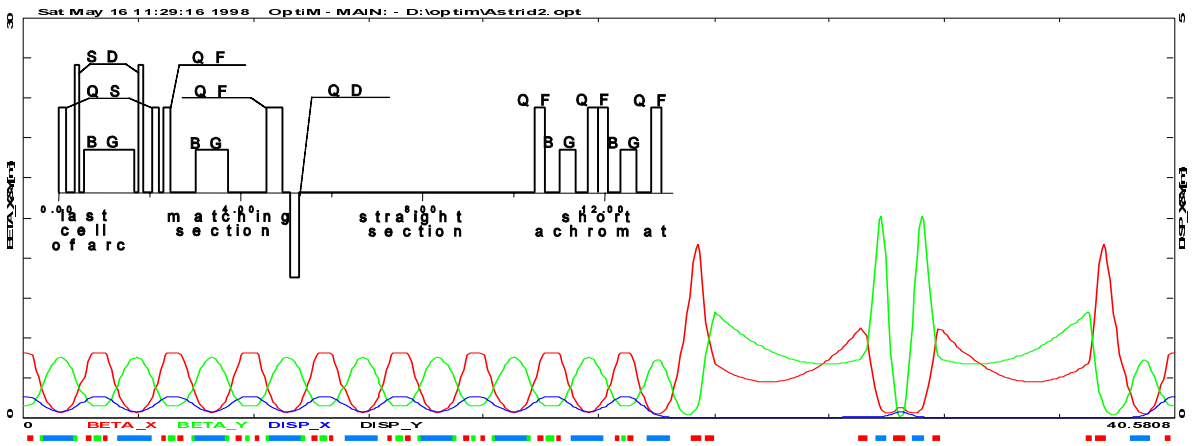

Figure 3 *The lattice of arc, matching section and straight section (QF, QD –focusing and defocusing quadrupole, QS-focusing quadrupole incorporated with sextupole, SD-defocusing sextupole, BG-combined function bend magnet with negative gradient).*

and $(n+2)^{th}$ in the vertical planes correspondingly. Figure 3 shows the scheme for two families of sextupoles in which one is incorporated in the focussing quadrupole. Tracking calculations indicate very good values of the dynamic aperture, about 100 mm mrad. In another variant with independent sextupoles and quadrupoles the dynamic aperture has approximately the same value. As a comparison, the dynamic aperture of a modified circular Chasman-Green lattice with the same number of sextupole families is smaller by a factor of three.

With such a scheme, we are able to use the simplest cell periodicity in constructing the arcs, removing the small inter-cell straight sections with a consequent reduction in overall length. This is a very simple and compact lattice with one family of focussing quadrupoles and one combined function bending magnet. The maximum in the dispersion function is concomitantly reduced, resulting in an equilibrium emittance of 4 nm.rad at 1.4 GeV.

Since we would like straight sections much longer than the cell of arc, we have to increase the beta function just at the entrance to the straight sections. This solution is achieved through a weaker focussing quadrupole and a longer combined function bend magnet in comparison with the "half-angle" option. In figure 3, upper part, we show an arc cell, the matching section and a straight section. The matching section consists of two focussing, one defocusing and one combined function bending magnet.

It is possible to install several insertion devices in the "straights" joining the arcs by dividing them into smaller sections separated by short bend achromats, of perhaps 2×5°, reducing the bending angle of the arcs by the appropriate amount. The number of sections could easily be increased either to three or reduced to one in order to increase the length available for insertion devices. Such a super-long straight section could be used for a free electron laser (FEL) or a very long undulator, perhaps with helical geometry or rotated field sections.

References

1Yu. Senichev, Proceedings of the 6th European Particle Accelerator Conference, EPAC'98, Stockholm, 22 to 26 June 1998

2 N. Hertel et al., this activity report, page 36

3 ISA Activity Report 1996.

CONSYS– A New Control System for ASTRID and ELISA

J.S. Nielsen, K.T. Nielsen[§], and T. Worm
Institute for Storage Ring Facilities, University of Aarhus, Denmark

In the mid nineties it was realised that the old control system for the ASTRID storage ring would soon become obsolete, and it did not have room for further upgrades. Therefore, a new control system had to be designed. The development of the new control system, ConSys [1], was started at ISA in the beginning of 95. The aim of the project was to develop a general site and machine independent control system. Taken into consideration was also the possibility of new facilities in Århus.

As operating system, Windows NT was chosen, as it fulfils the requirements for an operating system for a control system. It is a multi user environment with good reliability, good network support (TCP/IP), good network security, and it runs concurrent processes with different priorities. Furthermore, it has a powerful graphic interface, which is well known to most users, and good development tools. From the start it was the intention to use commercial software wherever possible.

The system is based on the standard model for modern control systems - an Ethernet based system with distributed front-ends and console/client computers. There is a central server for domain management, file server and configuration database. The control system is connected to the in-house network, so parameters can, with the right software, be accessed from everywhere. Since front-ends, as well as console computers, are PC's running Windows NT, it has been possible to use the same control-system core-software on all computers.

The overall model follows the so-called publisher/subscriber model. When a client application wants data from or control access to a parameter on a device, it first has to subscribe to the parameter. When the value of the parameter is changed, the new value is automatically transmitted to the client.

The system consists of three parts: The kernel, devices, and client programs. The kernel, common for all computers, handles all communication between devices and client programs, be it locally on the same computer or across the network. The devices store the values of the parameters on the system, and handle all the input/output communication to the hardware under control through device drivers etc. For interaction with the operators, a number of client programs have been developed, of which the major one is the Console. The tri-partition of the system allows very easy addition of new devices and client programs, as new types of hardware needs control, and as new needs for utility programs arise. The computer-code is highly object-oriented reducing code size and development time. The system is fully software configurable with all addresses, conversions, and display properties stored in an ODBC compliant database.

The major client application are:

- **Console:** The main program to display and adjust parameters. It is completely machine independent – all console pages are fully defined in the database. It has three views: A list view, which lists the parameters sequentially, a graphics view with parameter values on top of a bitmap, and two control bars with "analog" display of two parameters. The set values in the control bar can be adjusted by two digital potentiometers, so an

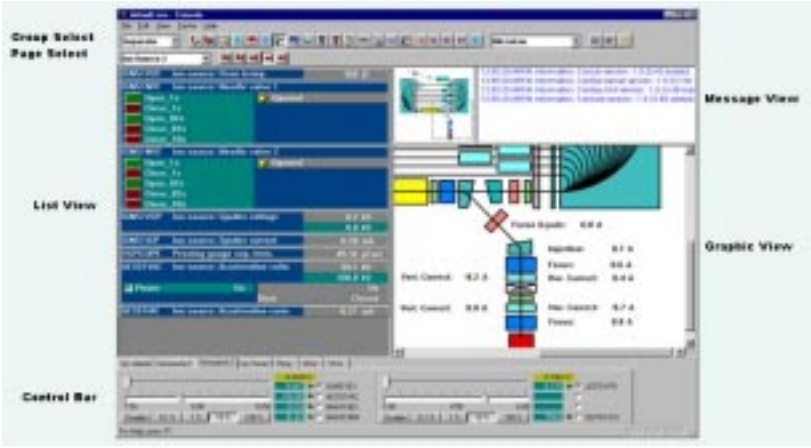

The ConSys Console.

"analog" feel is obtained.

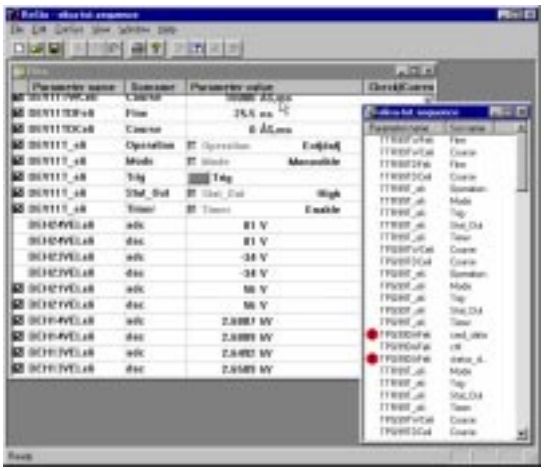
ReSto.

- **ReSto:** A general-purpose program to store and restore parameters on the system. Uploads parameters from one or more machines (or machine parts). Which parameters to download are specified in a so-called sequence file, which has to be applied to the setup file before download.
- **DAFLoader:** A program to load DAFs (Dfi Autonomous Function generator). Reads an ASCII file generated by Excel (or any other suitable program) with the vector description of the function-generator ramps and load the vector tables into hardware. It has options for pre-processing the vector data, as for instance parabolisation of bends or small energy changes. The DAFLoader also has options for automatic fileread and load when the Excel file is changed. The use of Excel gives very good possibilities for automatic calculation of magnet settings based on simple inputs (beam energy).


The DAFLoader.

- **RampControl:** A general-purpose program to perform slow (≈1 Hz) ramping of parameters. It can ramp floating point values in either specified time or at specified rates. It also has options to set binary values, as well as possibilities for synchronisation of different ramps, including waiting for a specified time or for a given parameter value to be reached. One use is an injection sequencer, which performs the necessary changes between the different parts of an electron fill (Alignment, Accumulation, Acceleration, Storage, Dump). Another use is for bakeout of the vacuum chambers.
- **RangeControl:** A small general feedback program. Used to increase/decrease a parameter based on the value of another parameter. One example is automatic increase of RF power as the accumulated electron current grows.
- **SimpleWebWriter:** Writes parameter values to a file based on a template file at regular intervals. Used to make HTML files for status display on the WWW.
- **Datalogger:** A general-purpose program to log run-time data values to the database. It is possible to set up different logging conditions, so logs are only performed if specific criteria are fulfilled. Standard logs are electron current, electron lifetime, radiation level, and vacuum pressures.
- **ConSysManager:** The system set-up program. With this program a system set-up file can be made, which specify the system database, and other system parameters. Likewise it is also here, it is specified which computers participate on which systems, as well as specification of which devices to load on individual computers, and the set-up of the devices.

AstridElOp.

- **DatabaseEditor:** A system program to ease set-up and maintenance of the system database. It gives an object oriented editing of the ConSys tables, based on description tables.
- **AstridElOp:** A small special dialogue application to ease fill control. From this program there is an easy access to the most used status parameters. Note that it is not in this program the settings are changed when stepping from Align to Accumulate. This is done by a RampControl sequence.

Besides these general applications there are a number of more specific (and usually smaller) applications: AstridTune (A program to assist in change of tune), BeamCurrentDisp (A small dialogue application to display electron current and lifetime), MassScan (A program to perform mass scan of the separator output).

There is also a number of "intelligent" devices which perform different helpful tasks. Examples of these are:

- **TableConversion:** Takes the value of one parameter and based on a table it writes a new value to another parameter. The values in the table are linearly interpolated. The table is loaded at runtime and can be changed at any time. This is presently used to convert the undulator gap to an energy setting, and to set the frequency for the vertical excitation, which depends on the undulator gap.
- **Digitizer Control:** This is a special device, which takes care of selecting the correct digitizer/multiplexer when cups and viewers are taken in or out of the beam.
- **Lifetime Calculation:** The electron lifetime is calculated in a device, which means that it is available system-wide and that computer power is only spent once for lifetime calculation.

The system is presently controlling ELISA [2] and ASTRID [3]. The last parts of the old control system for ASTRID were transferred to the new system in August 98. At present there are 2758 parameters defined in our database divided into 782 groups. (One group is typically one supply.) There are six dedicated front-ends, one combined front-end/client computer, seven dedicated client computers, and a number of user data-taking computers and office computers participating in the ISA ConSys control system.

The system core (transport layer, data structures, database interface) is fully implemented, as well as the core client applications (Console, Store/Restore, Soft Ramps, DAFLoader, Datalogger). A few important auxiliary applications (General plot program, Orbit correction, and an Alarm and Surveillance program) are still missing.

The overall experiences with the system development have been very good, and generally there has been a high satisfaction with the chosen tools. The stability of the Windows NT operating system (both server and workstation editions) has been very good. The stability of the ConSys system as a whole has been reasonable. For the dedicated front-ends, which do not have client applications, the stability has been quite good, but client applications may fail in some cases. The performance of the system is very good. The data rates are most often limited by display capabilities on console computers. Typical update rates are several Hertz.

More information on the system can be found on http://isals.dfi.aau.dk, where all system documentation, including user manuals, is available.

References

[1] See for instance J.S. Nielsen, K.T. Nielsen, and T. Worm: "Consys - A New control system for ASTRID and ELISA", TUP46G, Proceedings of EPAC 98, Sixth European Particle Accelerator Conference, Stockholm, 22-26 June 1998, p 1679. Available at http://www.cern.ch/accelconf/ or see documentation at http://isals.dfi.aau.dk

[2] S. P. Møller, This activity report, page 14.

[3] S. P. Møller, This activity report, page 9

[§]Now at CERN, PS Division, 1211 Geneva 23, Switzerland

The Antiproton Decelerator at CERN

H. Bluhme[1], J.F. Hangst[1], H. Knudsen[1], N. Madsen[1, 2], J. Merrison[1],
U. Mikkelsen[2, 3], S.P. Møller[3] , K.T. Nielsen[2, 3] and E. Uggerhøj[3]
[1]*Institute of Physics and Astronomy, University of Aarhus*
[2]*CERN, Geneva, Switzerland*
[3]*Institute for Storage Ring Facilities, University of Aarhus*

Foreseeing the closure of the Low Energy Antiproton Ring, LEAR, at CERN at the end of 1995, it was soon realized that a wide range of nuclear, atomic and particle physics experiments would be out of reach without a new antiproton facility. For this purpose, a feasibility study[1] was made to investigate the possibility of restructuring the Antiproton Collector (AC), which was initially built to increase the intensity of antiprotons to the Antiproton Accumulator (AA) for the p-pbar operation of the SPS. This machine, the Antiproton Decelerator (AD), is presently being commissioned at CERN. As opposed to the previously used sequence of accelerators, AC, AA, PS and LEAR, the AD will alone collect, decelerate, cool and eject the antiprotons at 100 MeV/c with an intensity of 10^7 per 200-300 ns burst, once a minute.

So far, three experiments have been approved for the AD: ATHENA, ATRAP and ASACUSA and all experiments will take place within the circumference of the AD. The commissioning of the AD is expected to be completed mid-1999.

The primary goal of the two collaborations ATHENA and ATRAP is initially the production and detection of antihydrogen which was first found at LEAR in 1995. Subsequently a capture and storage of a few thousand of these is aimed for. With antihydrogen atoms nearly at rest the possibility of a detailed comparison to spectroscopic measurements in normal hydrogen is opened for. According to the fundamental CPT theorem, these radiative transitions should be the same in matter and anti-matter, thus the aim is to test CPT-invariance to an accuracy of better than 10^{-15}. Moreover, it has been proposed to do experiments to test the influence of gravity on these fundamental entities of the anti-matter world that according to the Weak Equivalence Principle should be affected by gravity as normal matter.

The third experiment, ASACUSA, aims to continue the investigations of the antiprotonic helium `atomcule' initiated at LEAR. In this exotic state, one electron of the He has been replaced by an antiproton and subtle effects of QED influence its transition energies, such that one can measure eg. the fine-structure constant to extremely high precision[2]. Furthermore, this collaboration includes members of the former PS194 group at LEAR, who will pursue the studies of ionization by antiproton impact at very low energy[3], the study of antiproton stopping - in particular the Barkas effect – and the development of antiproton channelling at low energy[4]. To be able to decrease the energy even further than the 5.3 MeV available from the AD, ASACUSA will employ a novel scheme where a Radio Frequency Quadrupole will be used for deceleration[5] to obtain kinetic energies down to 10 keV. A Penning trap situated in a 6 Tesla superconducting magnet will be able to catch and cool these antiprotons, and they can then be extracted as a beam of energies down to a few tens of eV.

IFA and ISA have contributed to the development and construction of the AD in terms of both manpower and money. In particular, we have been involved in control system software development, new low-intensity pick-up amplifiers, beamline design and vacuum performance. The ATHENA and ASACUSA collaborations both have participation from researchers in Aarhus.

Added September 1999:
The commisioning of the AD has been succesful so far in 1999: First the lattice was verified (tune, chromaticity etc.) for antiprotons and then stochastic cooling was applied at 2.0 GeV/c and electron cooling at 300 MeV/c and 100 MeV/c for protons in the 'reversed' machine. The overall deceleration efficiency is around 30% with a cycle length of 140 s, about a factor of 2 too long and a relatively low efficiency compared to the design goal. However, during the final stages of

the commisioning, these insufficiencies should be repaired and it is expected that antiprotons fulfilling the design values can be delivered in november ’99.

For the ASACUSA collaboration, the Radio Frequency Quadrupole Decelerator (RFQD) is nearly ready and will be tested with the 5.3 MeV proton beam available at the Aarhus Tandem in the fall of ’99. This will constitute a major milestone towards achieving antiprotons of very low energy (0-120 keV) with a large deceleration effciency compared to deceleration in foils. Furthermore, the test in Aarhus will show if – as expected – the RFQD principle works and with what tolerances, transmissions etc.

Lastly, the Aarhus group have finished the design of the apparatus to be used for energy loss measurements and it is now being built. Initial testing is foreseen to take place in the early spring of 2000, before transport to the AD at CERN.

References:

1 S. Baird *et al.*, CERN/PS 96-43 (AR), 1996

2 J. Eades and F.J. Hartmann, acc. for publ., Rev. Mod. Phys., 1998

3 H. Knudsen *et al.*, Phys. Rev. Lett. **74**, 4627 (1995)

4 S.P. Møller *et al.*, Phys. Rev. A **56**, 2930 (1997)

5 J. Bosser *et al.*, CERN PS/HP Note 97-36, 1998

The ANKA injector

N. Hertel[1], S. P. Møller[1], L. Præstegaard[1,2], and staff at Danfysik
[1]*Institute for Storage Ring facilities, University of Aarhus, DK-8000 Aarhus C, Denmark*
[2] *Danfysik A/S, DK-4040 Jyllinge, Denmark*

INTRODUCTION:

The ANKA injector is a 500 MeV electron injector for the 2.5 GeV ANKA synchrotron which presently is being built at Forschungszentrum Karlsruhe, Germany[1] The injector complex shown in Fig. 1 consists of a 53 MeV racetrack microtron pre-injector, a 500 MeV booster synchrotron, a transfer line between the microtron and the booster synchrotron, and a transfer line from the booster synchrotron to the ANKA synchrotron[2]. The construction of the injector is accomplished by the company Danfysik, Denmark with assistance from ISA, providing expertise on accelerator physics issues related to the design, construction and commissioning of the injector. The entire ANKA injector will be commissioned in the autumn of 1999.

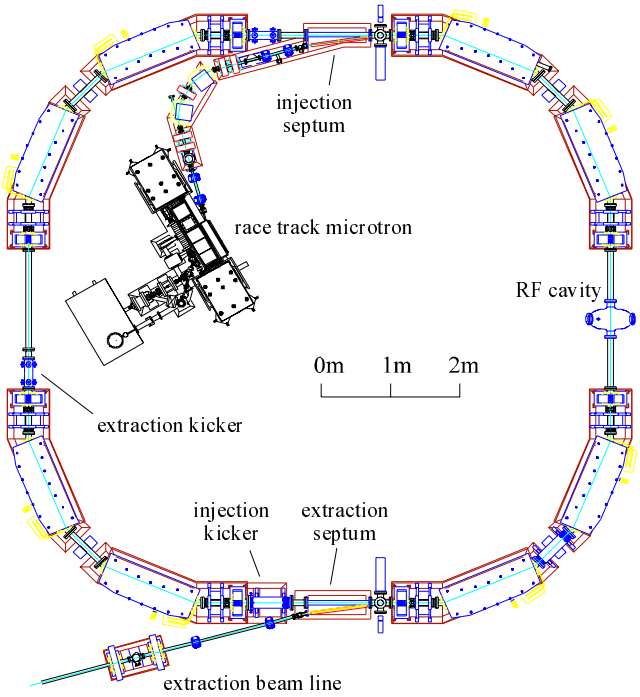

THE RACETRACK MICROTRON:

A racetrack microtron has been chosen as pre-injector due to its small energy spread, compactness, ease of operation and low price; all characteristics which are superior to those of a linear accelerator.

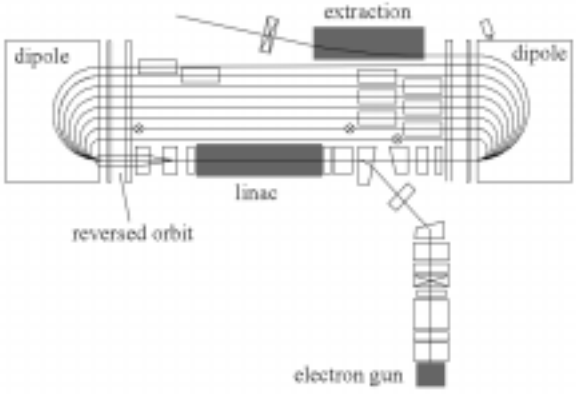

Figure 2: Schematic layout of the racetrack microtron

RF Frequency (Ghz)	2.9986
Resonant Energy Gain	5.3 MeV
Final Energy	53 MeV
Pulse Current	>10 mA
Pulse Length	0.5-1 µs
Repetition rate	1-10 Hz
Energy Spread	<0.3%
Emittance (h/v)	~0.2 mm mrad

The schematic layout of the microtron is shown in Fig. 2, while its main parameters are listed in the table above. The electron gun is a standard spherical Pierce type with a BaO cathode which provides ~500 mA of electrons in a 0.5-1µs long pulse. After the electron gun, the electron beam is deflected onto the axis of the linac which is of the Los Alamos side coupled standing wave type, allowing acceleration in both directions. The resonant energy gain of the linac is 5.3 MeV, implying that the speed of the electrons after the first passage of the linac differs from the speed of light by 0.5%. Hence, in order to avoid a phase lag in the first orbit, the beam is reversed in the left dipole and sent back on the axis of the linac with the aid of two small dipole magnets (see Fig. 2). After two passages of the linac, the velocity of the electrons is sufficiently close to the

speed of light that the synchronous condition is fulfilled without any significant phase lag. In addition, the reversed orbit has the advantage that the first real orbit is sufficiently far away from the common axis to clear the linac. After ten passages of the linac, the electron beam is extracted with a 15≈ bending magnet.

THE BOOSTER SYNCHROTRON:

The four-fold symmetric lattice of the Booster synchrotron is shown in Fig. 1, and its main parameters are listed in table 2. The lattice has eight 45≈ rectangular dipole magnets, defining in total four short and four long straight sections. A family of horizontally focusing quadrupoles are located symmetrically in the long straight sections, while vertical focusing is provided by the edge focusing at the end-faces of the dipole magnets; a scheme only feasible for dipole magnets, having a rather small bending radius. The length of the long straight sections have been selected with the aim of confining the horizontal and vertical betatron tunes Q_x and Q_y between the systematic resonances $3Q_x+2Q_y=8$ and $Q_x+2Q_y=4$. In addition, this choice ensures clearance between the transfer lines and the nearby quadrupoles. No sextupole magnets have been included in the lattice because the hail-tail instability is of little significance for circulating currents below 40 mA, roughly a factor of three higher than the specified value. Finally, the acceleration is performed by a 500 MHz RF cavity inserted in the center of one of the long straight sections. Having separate power supplies for dipole and quadrupole families, the horizontal and vertical tunes can vary in the ranges 1.5-1.95 and 1.33-1.15, respectively. The smallest emittance of 0.15 mm mrad is obtained for the design parameters.

Final energy	500 MeV
Circumference	26.4 m
Dipole field	1.00 T
RF frequency	500 MHz
Pressure	$<10^{-7}$ mbar
Horizontal tune (design value)	1.50-1.95 (1.776)
Vertical tune (design value)	1.33-1.15 (1.173)
Horizontal chromaticity	-0.29
Vertical chromaticity	-2.69
Momentum compaction factor	0.27
Horizontal emittance	0.15 mm mrad
Repetition frequency	1 Hz
Circulating current	>15 mA
Extracted current	>7.5 mA

References:

1 H. O. Moser *et al.*, ANKA, A Synchrotron Light Source for Microstructure Fabrication and Analysis, PAC 95, May 1-5, Dallas, Texas, USA (1995)

2 H. Bach, D. Einfeld, N. Hertel, S. P. Møller, B. R. Nielsen, F. Perez, L. Præstegaard, U. Ristau, and R. Rossmanith, The ANKA injector, EPAC 98, June 22-26, Stockholm, Sweden

Added September 1999:

The 50-MeV racetrack microtron was first commissioned in Denmark before shipment to Karlsruhe. Pulse currents in excess of 10 mA in a pulse of more than 1 Σsec were routinely demonstrated. The microtron and the booster components were transported to Karlsruhe in the spring, and the initial commissioning was done in June. Currents of more than 15 mA were injected into the booster, and more than ½ mA was accelerated to the full energy: 500 MeV. A re-alignment was subsequently performed, and the extraction system was installed. The final commissioning will take place in the fall of this year.

Added September 1999:

ASTRID 2000

Søren Pape Møller & Yurij Senichev
Institute for Storage Ring Facilities, University of Aarhus

The storage ring, hereafter called ASTRID 2000, is designed to provide VUV and soft x-ray synchrotron radiation with the highest possible brightness. Dipole radiation will be available up to 1-2 keV and undulator radiation from around 10 eV to around 500 eV. It will be a internationally competitive source, where hardly any alternatives exist world-wide.

Injection will be made at 100 MeV from the existing racetrack microtron, which will allow accumulation of currents of 200 mA during 5 minutes. Two storage energies are envisaged, a low energy around 500 MeV for low-energy undulator radiation (down to 10 eV) and a high energy around 800 MeV for high-energy undulator and dipole radiation. The machine is designed with 6-fold symmetry, which will leave space for 4 undulators; the two other straight sections will be used for the injection system and for the RF system. The length of the straight sections is 2.8 m between the quadrupoles, as compared to 2.2m for ASTRID. The straight sections can be longer (up to 4 m) without deteoriation of the lattice performance. A dynamical aperture of more than 100 mm mrad can easily be obtained with this symmetric lattice.

It is planned to follow recent experience, where an in-situ bake-out system is omitted. This leads to a significant saving, but requires baking of the vacuum system prior to assembly in the ring. Furthermore, this assembly has to be made under clean dry-atmosphere conditions. In this way, the only sacrifice is a somewhat longer conditioning time of the system.

The RF system for ASTRID 2000 will initially be taken over from ASTRID, since it is directly able to deliver the required power. At a later stage, a new cavity would be needed in order to exploit fully the small emittance of the ASTRID 2000 ring. A significantly better cavity in terms of higher order modes than the present ASTRID cavity can be built at a minor hardware cost.

The lifetime is Touschek-effect dominated, and is hence inversely proportional to the current and to the product of the bunch-length and the vertical and horizontal emittances. The lifetimes are estimated using bunch lengthening by a factor of 2 as compared to the natural bunch length. Two possibilities exist for this bunch lengthening, namely by use of a Landau cavity or by phase modulation. A further increase in lifetime can be obtained by an emittance increase.

The parameters of the ring are given in the table below together with those of ASTRID, and the size of the ring in the laboratory can be seen from the figure on the next page.

Table 1

	ASTRID at 580 MeV	**ASTRID 2000 at 100 MeV**	**ASTRID 2000 at 500 MeV**	**ASTRID 2000 at 800 MeV**
Dipole field	1.6 T	0.15	0.75 T	1.2 T
Char. Energy Σ_c	358 eV	1 eV	125 eV	510 eV
Char. Wavelength Δ_c	35 Å	12400 Å	99 Å	24 Å
Current	150 mA	200 mA	200 mA	200 mA
1'st harmonic of ASTRID undulator	210-1090 Å 11-59 eV		290-1270 Å 10-43 eV	110-580 Å 21-113 eV
Energy loss per turn U_0	8.3 keV	4 eV	2.5 keV	16.3 keV
Total power P	1.2 kW	-	0.5 kW	3.3 kW
Horizontal emittance	140 nm	-	2-5 nm	6-12 nm
Vertical emittance	14 nm	-	1 nm	1 nm
Lifetime	30 hours	-	10 hours	10 hours
Circumference	40 m	45.7 m	45.7 m	45.7 m
RF harmonic number	14	16	16	16
Straight section length	2.2 m	2.8 m	2.8 m	2.8 m
Diffraction limit at 10 eV			10 nm	
Diffraction limit at 100 eV				1 nm

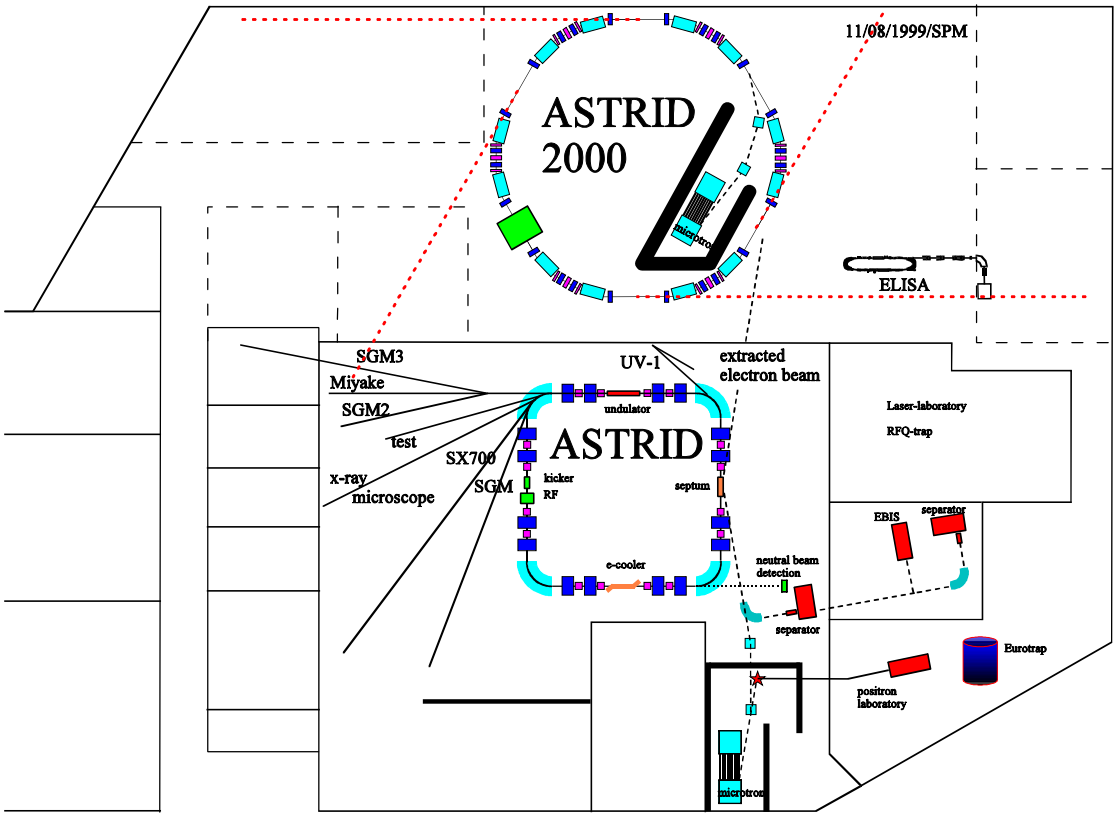

Synchrotron Radiation Activities

Electron scattering experiments using ASTRID

Stuart Lunt[1] , Robert Gulley[2,3], David Field[1,3], Tom Field[4],
Jean-Louis Lemaire[5], Jean-Pierre Ziesel[6] and Søren Hoffmann[1]
[1]*Institute for Storage Ring Facilities, University of Aarhus*
[2]*Australian National University, Australia*
[3]*University of Bristol, UK*
[4]*University of Nottingham, UK*
[5]*Observatoire de Meudon and Université Cergy-Pontoise, France*
[6]*Université Paul Sabatier, Toulouse ,France*

When electrons collide with atoms, molecules or ions, the target species may enter an excited state or may undergo chemical change. Electron collisions occur in gas plasma which in varying composition, density and temperature are found in planetary atmospheres, for example in the ionosphere, and which make up the greater proportion of the material of stellar and interstellar gas. Closer to home, the lights by which you may be reading this article contain plasma and operate through collisions of electrons with gas atoms, causing target species to become electronically excited and emit light. Electron collisions may also cause molecules to become rotationally and vibrationally excited. Cross-sections for rotational excitation can be very large indeed for molecules with large dipole moments. For example, recent data on chlorobenzene (see below) show rotationally inelastic scattering cross-sections in excess of 1500 $Å^2$ below 20 meV electron impact energy. Because of these high cross-sections, rotationally inelastic scattering dictates how low energy electrons diffuse through polar gases.

Electrons may also attach to molecules. For example SF_6 is very efficient at quenching fires because it has a strong propensity to form negative ions, soaking up the electrons which are therefore no longer available for maintaining a flame. Electron attachment may be followed by dissociation of the molecule into fragments, one of which is a negative ion and the other a neutral. The overall process is then called "dissociative attachment" (DA). The probability that excitation or attachment (or DA) may occur depends upon the kinetic energy, E, of the electron colliding with the target molecule. Electron attachment occurs with increasing probability (or cross-section) as the collision energy falls. As in the case of rotational excitation, molecules may present cross-sections of hundreds of $Å^2$ or more at electron energies equivalent to a few tens of degrees Kelvin, that is a few milli-electronvolts (meV) energy. For example the cross-section for attachment to SF_6 to form SF_6^- for electrons of energy equivalent to 100K is ~500 $Å^2$. It is therefore no surprise that in low energy laboratory plasmas and in astrophysical plasmas, electron attachment may play a dominant role in determining the electron concentration, the electron energy distribution and the plasma chemistry. This has important practical implications since electronegative plasmas containing SF_6, CF_3 Br etc. are constituents of gases widely used in plasma and reactive ion etching in microcircuit device fabrication. In astrophysical chemistry some of the most eagerly sought data are the cross-sections for low energy electron scattering, attachment and dissociative attachment for polycyclic aromatic hydrocarbons – "PAHs". These species are strong candidates for the missing link between carbon atoms, small carbon chain species (such as C_6H) and larger particulate matter, called "dust" or "grains" by astronomers. The formation and evolution of particulate matter is fundamental to an understanding of stellar evolution and planet formation.

The final step in any chain of chemical reactions for the formation of astrophysical molecules (of which there exist about one hundred inorganic and organic species), involves an electron combining with a protonated positive ion to give neutral products. The concentration of electrons in molecular clouds in space is therefore very important in determining the concentration of molecular species. The efficiency of larger molecules such as PAHs in removing electrons from astrophysical plasma may therefore be a key factor in astrophysical chemistry. The study of PAHs also has a distinguished place in the history of molecular orbital theory. Hückel,

discussing reactions involving alkalis, invoked the picture of an electron entering the lowest unoccupied molecular orbital of a PAH, that is the lowest anti-bonding Σ* orbital of the unsaturated PAH, just as in electron attachment.

Despite the considerable interest in electron scattering and attachment to PAHs and related species, there are no high resolution electron beam data at low energy, that is, in the energy range of a few meV to 100 meV. The reason for this lack of data reflects the experimental difficulties associated with forming and controlling low energy electron beams. Experiments on synchrotron sources both at LURE (Université Paris-Sud) and at Daresbury Laboratory have however shown that low energy high resolution beams may successfully be generated through a photoionisation technique[1,2,3]. Using monochromatised synchrotron radiation, electrons are formed by photoionisation of Ar at the intense autoionising resonance Ar** $3p^5$ ($^2P_{1/2}$)11s at 786.5 Å, close to the $^2P_{3/2}$ threshold. The energy resolution in the photoelectrons is equal to the energy resolution of the ionizing photons. Typically this resolution lies between 3 and 4 meV but was degraded to 10 meV (see below) in the work performed here. The photoelectrons, formed in a small volume, are expelled from the region of ionization in a very weak electric field of <0.1V per cm. In order that transverse components of the motion should not cause the electron beam to disperse at the very lowest energies, the electrons may be confined in an axial magnetic field of 20 Gauss (2 x 10^{-3} Tesla). The low energy electron beam, guided with the aid of an electrostatic lens, enters a chamber containing the target gas. A proportion of the incident electrons are scattered and the cross-section for scattering may be evaluated from the simple "Beer-Lambert" relationship through which cross-section is given by log (incident/transmitted current) divided by the product of the number density of the target gas and the interaction cell length. In the absence of a magnetic field, the total scattering cross-section for scattering into 4Σ steradians is measured. In the presence of the magnetic field, the cross-section for scattering into the backward hemisphere is recorded. Using the Miyake monochromator on ASTRID working at a best resolution of 9 to 10 meV, experiments have been performed using PAH and PAH-related target species such as anthracene, naphthalene, azulene, perylene etc. Backward scattering data obtained for naphthalene are shown in the figure to the left. A set of values, some of them preliminary, for scattering cross-sections for a variety of species at 25 meV electron impact energy are shown in the table below. For all these species, spectra between ~10 meV electron impact energy and a few hundred meV have been recorded. Data for benzene, and deuterated derivatives have recently appeared in J.Phys.B At.Mol.Opt.Phys. **31** (1998) 2735-1751, Gulley, Lunt, Ziesel and Field.

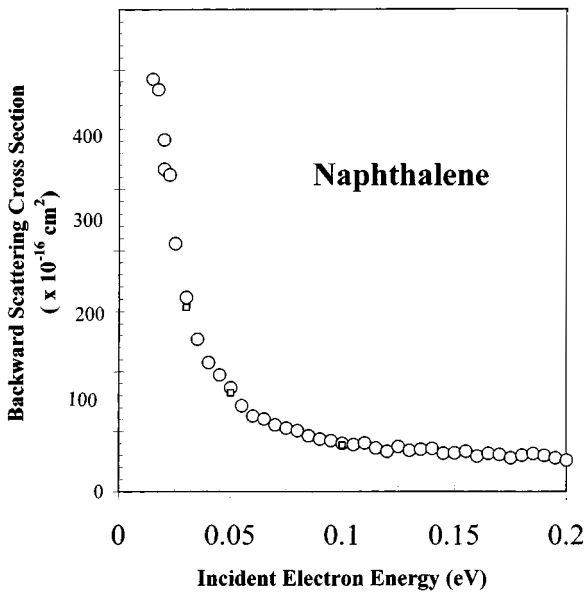

Figure 1:Backward scattering data for Naphthalene

The data shown are in fact very remarkable and provide strong evidence for low energy electron attachment to PAHs. It is quite unexpected that molecules with zero dipole moment should show large scattering cross-sections at low electron impact energy, as do benzene, naphthalene and perylene, the latter a regular structure composed of five benzene rings. The behaviour is also quite erratic: biphenyl composed of two benzene rings joined by a single bond shows only weak scattering whereas a single benzene moiety shows a cross-section several times larger. Again, anthracene, with three benzene rings, shows a much smaller cross-section than naphthalene with two benzene rings. Some of this work is presently being prepared for publication and further experiments are planned in the very near future using the new undulator-SGM2 beamline presently under test.

Material	*Cross-section for back ward scattering at 25 meV*	*Molecular dipole moment*
Benzene	78 Å^2	zero
Toluene	80 Å^2	0.36D
Chlorobenzene	1370 Å^2	1.69D
Biphenyl	15 Å^2	zero
Naphthalene	270 Å^2	zero
1-methyl naphthalene	180 Å^2	?
Anthracene	30 Å^2	zero
Azulene	50 Å^2	0.8D
Perylene	720 Å^2	zero

References:

1 Field D, Knight DW, Mrotzek G, Randell J, Lunt SL, Ozenne JB, Ziesel JP 1991, Meas.Sci.Technol. 2 (J.Phys.E) 757
2: Randell J, Field D, Lunt SL, Mrotzek G, Ziesel JP, 1992, J.Phys. B 25, 2899
3: Randell J, Lunt SL, Mrotzek G, Ziesel JP, Field D, 1994, J.Phys. B 27, 2369

Added September 1999:

As mentioned above, an aim of our work has been to study electron scattering in molecules of atmospheric importance. The group at University College London, headed by N J Mason, has brought to Aarhus two sizeable preparative rigs to make ozone (O_3) and chlorine dioxide (ClO_2), both of which are highly reactive and poisonous and must be made in situ. The importance of ozone in the atmosphere is very well known. We have measured the first scattering cross-sections for ozone in the low energy region of relevance to the earth's atmosphere, that is from 9 meV and above (to 10 eV) in electron collisional energy (Gulley et al. 1998b). Rotationally inelastic scattering is observed, but with cross-sections which are lower than those predicted by the first order Born point dipole model below 50 meV impact energy. This latter point is important. One of the general aims of our work is to study rotationally inelastic scattering at very low energies, a phenomenon that no other apparatus is able to address. The predictive capabilities of the Born approximation are valuable to ascertain, since such calculations are the only means to obtain essential data for reactive plasma modeling. Rotationally inelastic scattering in dilute plasmas involving polar gases is the major determinant of the electron temperature, which in turn influences the plasma potential and the nature of plasma and reactive ion etching (see for example YP Song, D Field and DF Klemperer J.Phys.D 1990, **23**, 673). A number of the most fascinating aspects of low energy electron scattering are displayed in the behaviour of chlorine dioxide (ClO_2) (Gulley et al. 1998b, Field et al. 1999a). Our recent data for both total integral and backward scattering are shown in Fig.2 and the ratio of backward to integral scattering cross-sections in Fig. 3. The latter data illustrate the need for high resolution in the energy of the incident electron beam - the peak in the ratio in Fig. 3 is of a width of only 4 meV FWHM. The rise in the scattering cross-section in Fig. 2 down to ~100 meV fits closely with predictions of Born theory (upper

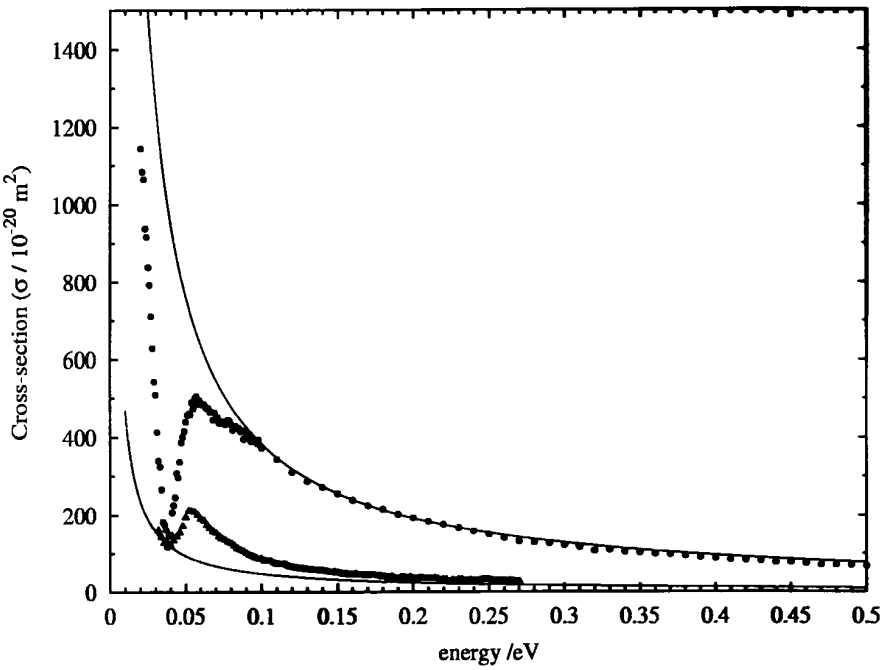

Figure 2: the variation of the total integral and backward scattering cross-section for electrons by ClO_2 as a function of electron kinetic energy

solid line). Below 60 meV impact energy, the cross-section falls sharply. The high value of the apparent ratio of the backward to the integral scattering cross-sections (reaching unity at 38 meV - Fig.3) is indicative of electron attachment, as described in detail for example in Gulley et al. 1998a. It is unclear why electron attachment to ClO_2 suppresses rotational excitation in

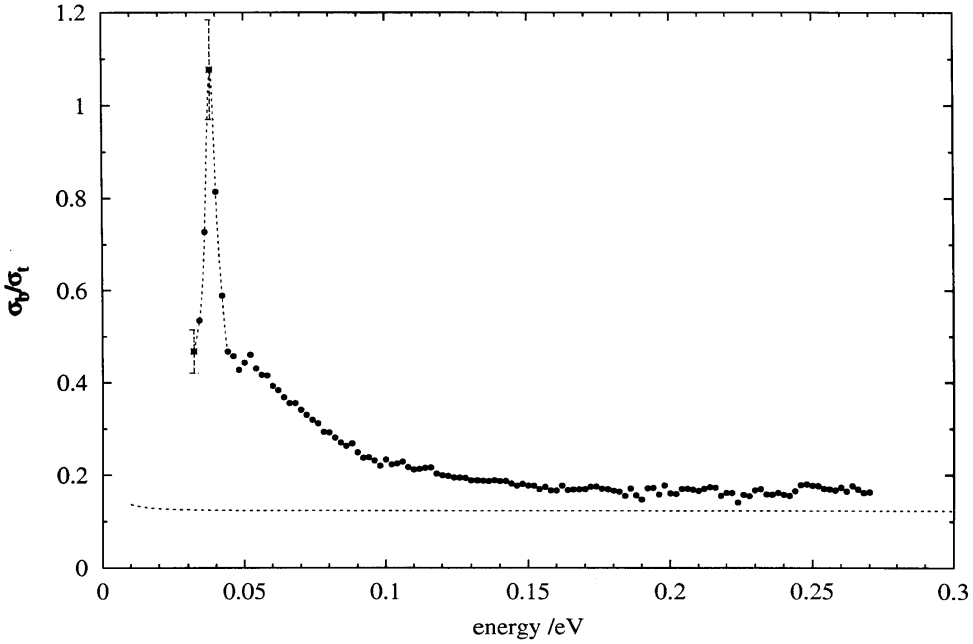

Figure 3: the variation of the ratio of backward to integral scattering cross-sections for ClO_2 as a function of electron kinetic energy

the 30 to 100 meV region. A possible explanation is that the incipient ClO_2^- formation causes the target species to become increasingly linear, thus reducing the dipole moment. Walsh diagrams for the excited states of ClO_2^- - accessible through the large electron affinity of ClO_2 - support this hypothesis, as does an SCF calculation on the ground state of ClO_2^-. ClO_2 has a group of electrons in various orbitals which are rather close in energy to that of the HOMO (highest occupied molecular orbital); the HOMO itself is known to be of b_1 symmetry. The impacting electron mixes the target states, at the same time inducing nuclear motion. At all

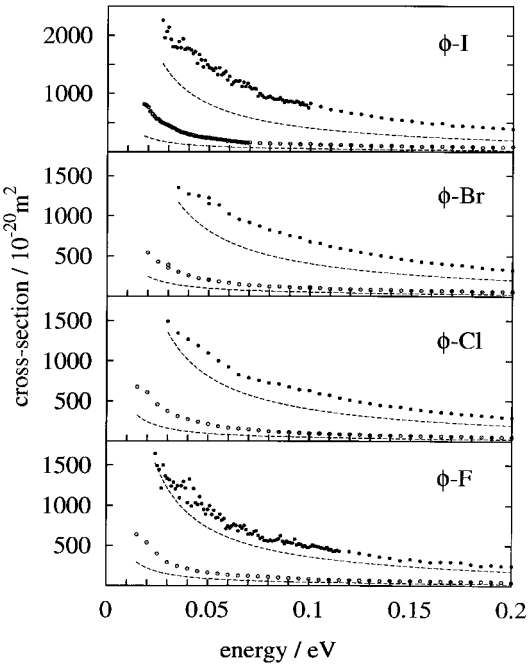

Figure 4: The variation of the total integral and backward scattering cross-sections for electrons by halobenzenes as a function of electron kinetic energy. Upper sets of data: integral, lower sets of data backward scattering cross-sections. Dashed lines: first order Born point dipole approximation calculations. ($\phi \equiv C_6H_5$)

events, the electron attachment is clearly p-wave in character, rising with increasing energy (Fig. 3), as dictated by the orbital symmetry of ClO_2. The data of Fig.2 and 3 represent a very nice illustration of p-wave electron attachment, one of the very few, or perhaps the only demonstration of this phenomenon - certainly the only one at such low energy and with such high energy resolution (~1.0 meV FHWM in the electron beam in this case). Data for Cl_2 (Gulley et al. 1998c) show similarly complex behaviour to that of ClO_2, again requiring the involvement of electronically excited states of Cl_2^- to yield an interpretation of the data.

Turning to pure rotational excitation, the work on the halobenzenes illustrates this very well. A compilation of data is shown in Fig. 4, taken from Lunt et al. 1999a. Very large scattering cross-sections are found at low energies, and the agreement with the Born model is middling. Significantly, the ratio of the backward to integral cross-sections is considerably greater than the Born prediction, the observed values lying between 0.15 and 0.25, and the calculated values around 0.1, for these species with dipole moments of ~1.7 Debyes. This indicates a breakdown of the Born approximation at low energies. There is considerably more forward scattering than predicted, suggesting that only a few partial waves are important in the scattering rather than the large number inherent in the Born model. Similar data for nitromethane are shown in Fig. 5 (Lunt et al. 1999b). In this case the backward scattering cross-section remains a very small fraction of the integral scattering cross-section, with ratios lying between 0.05 and 0.025. In this case (and in other nitro- derivatives) the Born model may turn out to be more accurate because of the very high dipole moment of the target (3.46 Debyes). Other species which we have studied during this period, e.g. ethanol and methanol (Field et al. 1999c), give further insight into the subject of rotational excitation through electron collisions. Further work is necessary with more species with a variety of dipole moments, and this will be carried out in future runs on ASTRID.

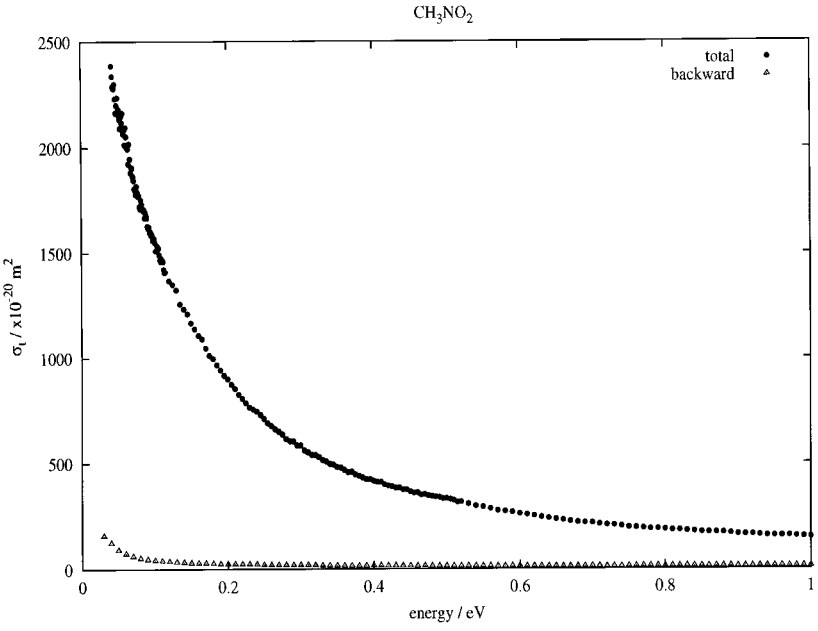

Figure 5: The variation of the total integral (upper data set) and backward scattering cross-sections (lower data set) for electrons by nitromethane (CH_3NO_2) as a function of electron kinetic energy

Photoionization of positive ions using the ASTRID undulator

Henrik Kjeldsen[1], Martin S. Rasmussen[1], Finn Folkmann[1], Helge Knudsen[1], Torkild Andersen[1], Jan van Elp[2] and John West[3]

[1] *Institute of Physics and Astronomy, University of Aarhus*

[2] *Institute for Storage Ring Facilities, University of Aarhus*

[3] *Daresbury Laboratory, CLRC, Warrington, United Kingdom*

A chamber is set up where synchrotron radiation over a distance of 60 cm interacts with ions, both with a diameter of a few mm. After that, a magnet separates higher charge states. The aim of the planned experiments is to continue previous measurements[1] of absolute photoionization cross sections to other ions of special interest, e.g. for stellar atmospheres, such as C^+ and Mg^+, for which the cross sections are expected to be smaller.

A Miyake monochromator[2,3,4] with a plane grating and a cylindrical mirror of radius 2.4 m selects an energy in the range 15-170 eV from the horizontal undulator[5] in ASTRID. It has first been tested at an adjacent bending magnet beamline. Later it was put after the undulator, so we could directly observe the increase of intensity at selected energies, determined by the gap of the undulator. The increase was a factor of 175 for the 3rd harmonic at 42 eV and 80 for the 5th, 7th and 9th harmonics at 70, 98 and 126 eV. To focus the synchrotron radiation to a diameter of 2 mm in the interaction region we have placed a horizontal focussing mirror in front of the monochromator deflecting 5^0 and behind the mono a vertical focussing mirror and a plane mirror to get the beam out in the horizontal plane. The intensity we measure from the monochromator and the undulator is shown in fig. 1. We used an Al diode at the very end of the beamline and an exit slit of 50 μm inside the monochromator and normalized to a fractional resolution of αE/E=0.001 (bandwidth =0.1%) and an electron current of 100 mA.

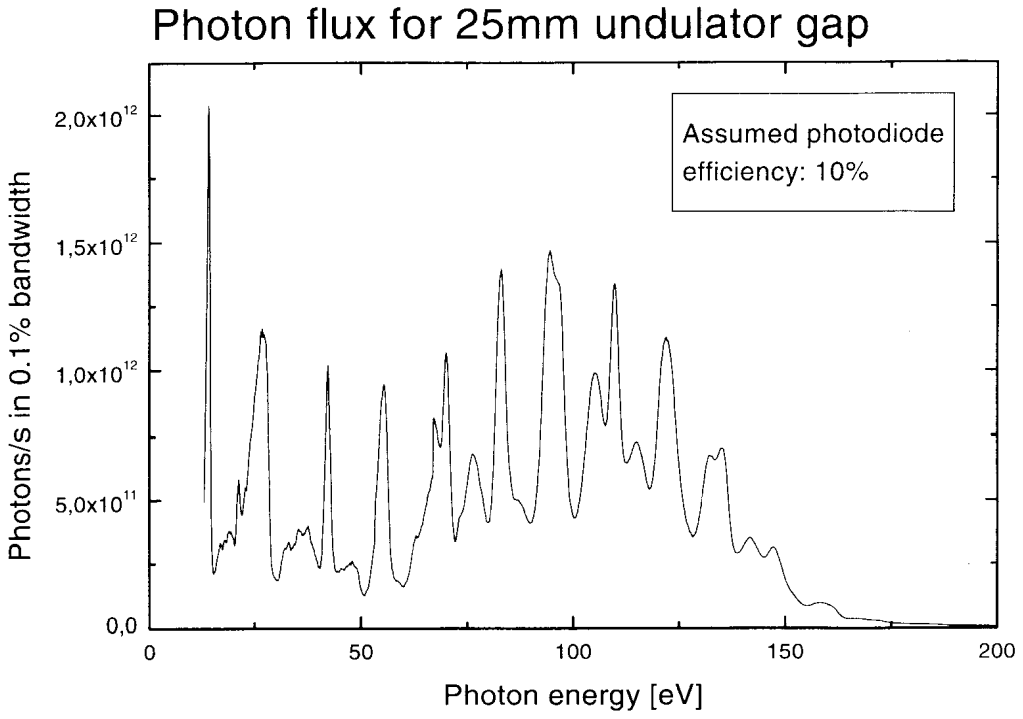

Figure 1. Photon yield from ASTRID undulator and Miyake monochromator.

Ion sources of various types are run at voltages 2000 to 5000 volt and currents of typically 100 nA are analysed by a magnet and merged by an electrostatic deflector with the synchrotron radiation as shown in fig. 2. After the interaction region the synchrotron radiation continues

straight into a photodiode PD and the positive ions are deflected in a magnet and analysed according to their charge.

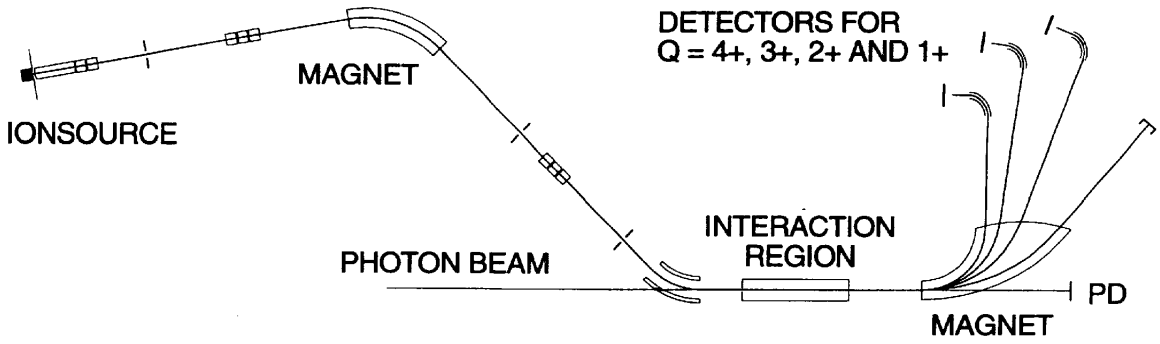

Figure 2. Plan for the ion source optics merging the photons.

The interaction region has 5 profilers with 0.2 mm wide slits in both the horizontal and the vertical plane. In fig. 3 is shown the central photon profiles in both the horizontal an the vertical plane. The horizontal profile depends on the order of the harmonic from the undulator and has one peak for the fundamental, two peaks for the 2nd harmonic and e.g. three peaks for the 3rd harmonic: a strong central one with smaller wing peaks at each side which we will mask to get a well defined overlap with the ion beam. The ion beam is a little broader and we will try to extract absolute cross sections from our measurements.

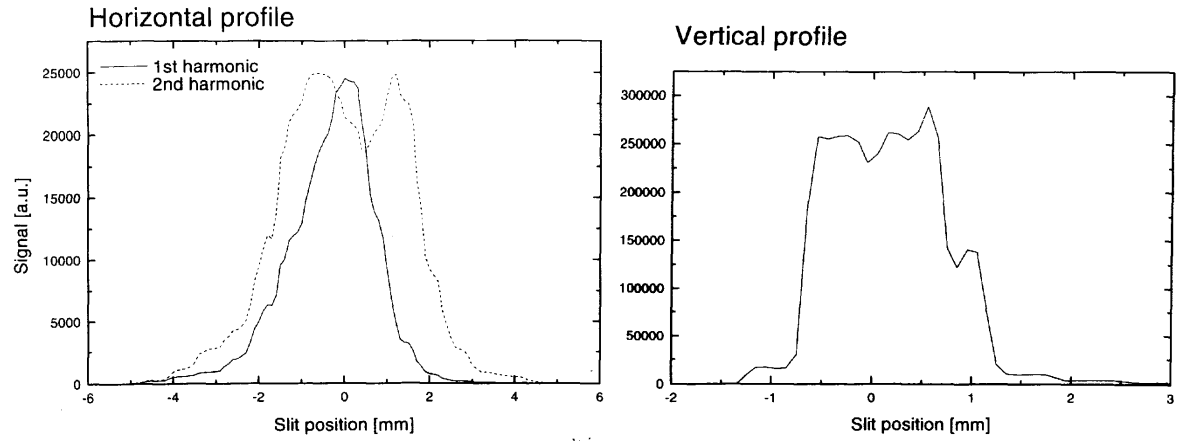

Figure 3. Horizontal and vertical profile of the photon beam.

Added September 1999:

Photoionisation of positive ions in the photon energy range from 20 to 200 eV

The aims of this project are mainly laboratorie astrophysics. It is crucial for the development of quantitative theoretical models of astrophysical objects such as stellar atmospheres to have reliable data for the interaction of light with atoms and ions, which can lead to removal of electrons (photo ionisation)

So far the inputs to the various models have been properties predicted theoretically by means of computational methods, but the accuracy of the predicted values for photo ionisation has never been tested, since it is very difficult to obtain accurate absolute data for neutral atoms due to lack of techniques to determine the atom density and for ions due to the low density available in beams. Thus very intense photon sources are needed to measure absolute cross sections in the range 0.1-10 Mb. With the access to an undular beamline at ASTRID the present photon-ion project was launched in 1998.

Research Goals:
Measurements of absolute photoionisation cross sections for ions of astrophysical importtance such as C+, C++, N+, O+, Mg+, Si+, Fe+ and later on also for selected ionic systems of interest for atomic and molecular physics.

Results.
A unique merged photon-ion apparatus has been constructed and the first results obtained during the spring 1999. The equipment available can be used for a large number of systems, atomic and molecular, positively or negatively charged. The results obtained for C^+ have tested the calculations for the most important ion for astrophysical modelling, showing deviations from the theoretically predicted absolute cross sections up to 35 % and the presence of significant resonances in the cross section, which until now had been neglected in the calculations. The Mg+ results have led to a reassignment of the absorption spectra for the Mg^+ ion, whereas the K^+ data have demonstrated the potentially of the new setup allowing measurements of absolute cross sections down to 0.1 Mb or less, a factor of 100 improvement above the only previous study of absolute photoionisation cross section for ions. Similar setups are under construction in Paris and at Berkeley.

References:

1. I.C. Lyon, B. Peart, J.B. West and K. Dolder, J. Phys B **19**, 4137-4147 (1986)
2. J.B. West, K. Codling and G.V. Marr, J. Phys. E **7**, 137-144 (1974)
3. M.R. Howells, D. Norman, G.P. Williams and J.B. West, J. Phys. E **11**, 199-202 (1978)
4. J. van Elp and F. Folkmann, ISA Activity Report **1**, 81-82 (1996)
5. S.P. Møller, ISA Activity Report **1**, 46-47 (1996)

The SGM/SCIENTA beamline

J H Petersen[1], C Søndergaard[1], S V Hoffmann[2] and D L Adams[1]
[1]*Institute of Physics and Astronomy,University of Aarhus*
[2]*Institute for Storage Ring Facilities, University of Aarhus*

The SGM/SCIENTA beamline consists of an experimental system for photoemission studies of the electronic and geometrical properties of surfaces at the end of a spherical grating monochromator (SGM).

The SGM has three sets of gratings and folding mirrors to be used within the following photon energy ranges, 30-80eV, 80-250eV and 250-600eV. The energy resolution is determined by the width of the entrance- and exit slits. The ultimate resolving power $E/\alpha E$ is 5000-14000.

The vacuum system consists of two spherical mu-metal chambers (Vacuum Generators) mounted vertically and connected by an all-metal gate valve. The upper chamber is used for sample preparation and contains facilities for sputtering, gas-dosing, metal deposition, residual-gas analysis, and LEED. The lower chamber, which is connected to the SGM monochromator, is used for surface analysis, primarily via electron spectroscopy. In addition the lower chamber has an X-ray photon source for use particularly in the periods when ASTRID is not operating as a synchrotron. The two chambers can be pumped and baked separately. The sample is transferred between the two chambers by a VG Omniax manipulator with 60cm vertical travel, and with facilities for polar and azimuthal rotation and for sample cooling using liquid nitrogen (and liquid helium if a suitable transfer line is constructed).

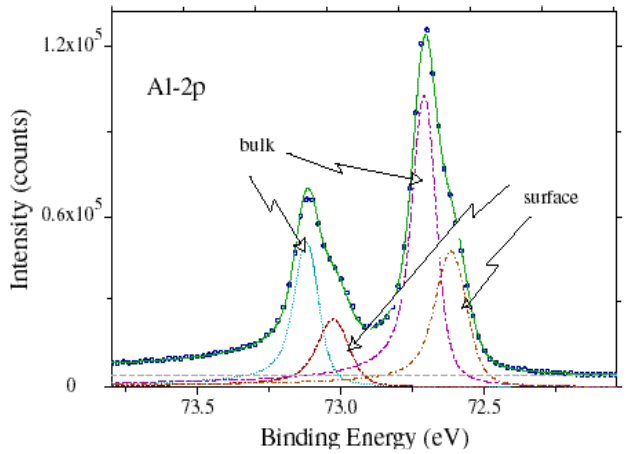

Al-2p spectrum of a clean Al(100) surface illustrating the high count rate and resolution of the system. The spectrum was measured in 2 min at 132.5 eV photon energy. The instrumental resolution ≈ 55meV is high enough to resolve the surface core-level shift of Al(100).

The main analytical component of the system is a high transmission / high resolution electron spectrometer from Scienta, which is attached to the lower vacuum chamber at an angle of 40≈ to the beam line direction. The Scienta spectrometer contains a five-element electron lens, which focuses photoelectrons emitted from the sample on to the entrance of a 20 cm radius hemispherical electron energy analyser. The electrons passed by the analyser are registered by a detector consisting of a 4cm diameter microchannel plate, fluorescent screen, and externally-mounted video camera. The detection is energy-dispersive, allowing simultaneous measurement of a spectral range of about 10% of the pass energy of the analyser. The pass energy is selectable in nine steps from 2eV to 1000eV. The ultimate resolution of the spectrometer is less than 5.0meV.

The beamline has by now (Sep. 98) been operating on an experimental basis for a year. Several interesting results have been obtained, as described elsewhere in this report. The figure shows an Al-2p spectrum taken with an instrumental resolution (SCIENTA + SGM) of 55 meV. The spectrum and the derived surface shift in binding energy are in excellent agreement with a previous result from MAXLAB

References:

[1] J. Van Elp, C Theil and F Folkmann, ISA activity report 1996, p. 34
[2] R Nyholm, J N Andersen, J F Van Acker and M Qvarford., Phys. Rev. B **44**, 10 987 (1991)

A high-resolution core-level spectroscopy and low energy electron diffraction study of the Li on Al(100) surface alloy.

J H Petersen[1], C Søndergaard[1], S V Hoffmann[2], A Mikkelsen[1], and D L Adams[1]
[1]*Institute of Physics and Astronomy,University of Aarhus*
[2]*Institute for Storage Ring Facilities, University of Aarhus*

The adsorption of Li on Al(100) has been studied by high-resolution core-level spectroscopy and low energy electron diffraction (LEED) at different Li coverages and temperatures at the SX-700- and the SGM/SCIENTA surface physics beamlines.

Adsorption at room temperature leads to the formation of a c(2x2) phase, first observed at a coverage of 0.15 monolayer (ML) and fully developed at 0.5ML. Li-1s and Al-2p core-level spectra show that the 0.5ML structure contains a single type of Li and three types of Al. This is consistent with the results of a recent LEED analysis, which shows that the c(2x2) phase is a surface binary alloy in which every second Al atom in the first layer is substituted by Li. Al-2p core-level spectra taken after adsorption at 120K followed by annealing indicate that reconstruction of the Al substrate begins to occur at temperatures as low as 140K.

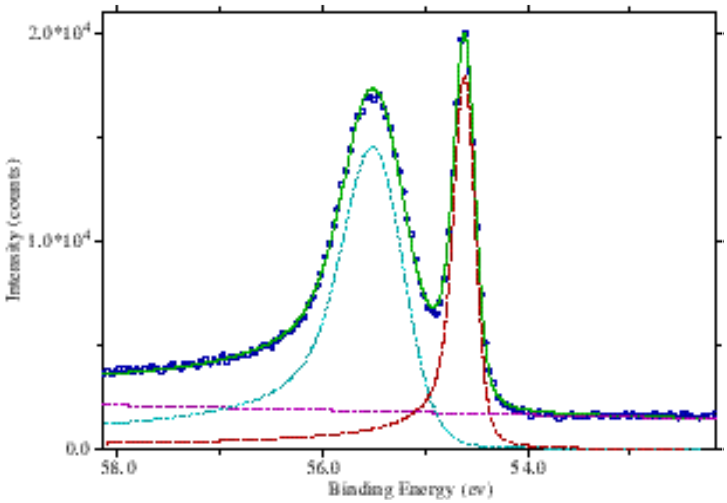

:*Li-1s spectrum measured at 132.5eV photon energy after adsorption of 1 ML of Li at RT.*:

At coverages above 0.5 ML the Li-1s spectrum contains a second peak shifted by 1eV towards lower binding energies as shown in the figure, clearly indicating the presence of a second layer of adsorbed Li. Due to enhanced surface vibrations the peak corresponding to the outermost Li-layer is much broader than the other. The observation that only minor changes occur in the Al-2p spectra and the LEED pattern on going from 0.5 ML to 1 ML suggests that the second Li layer is a chemisorbed layer on a mixed Al-Li c(2x2)-layer.

References

[1] Submitted for publication.

Lithium promoted oxidation of Al(100) studied by XPS

C S Søndergaard[2], J H Petersen[2], S V Hoffmann[1] and D L Adams[2]
[1]*Institute for Storage Ring Facilities, University of Aarhus*
[2]*Institute of Physics and Astronomy, University of Aarhus*

Oxidation of the clean Al(100) surface and oxidation of the Al(100) surface with pre-adsorbed Li has been studied by XPS using the SGM/SCIENTA beam line at ASTRID.

The oxidation of clean aluminum low-index surfaces has previously been experimentally studied with a wide range of surface specific techniques including XPS. A motivation for these studies has been the fact that clean aluminum at room temperature oxidizes and a stable surface layer of aluminum oxide (Al_2O_3) is formed that protects the bulk against further oxidation. Due to the improved resolution of the SGM/SCIENTA system we observe an additional

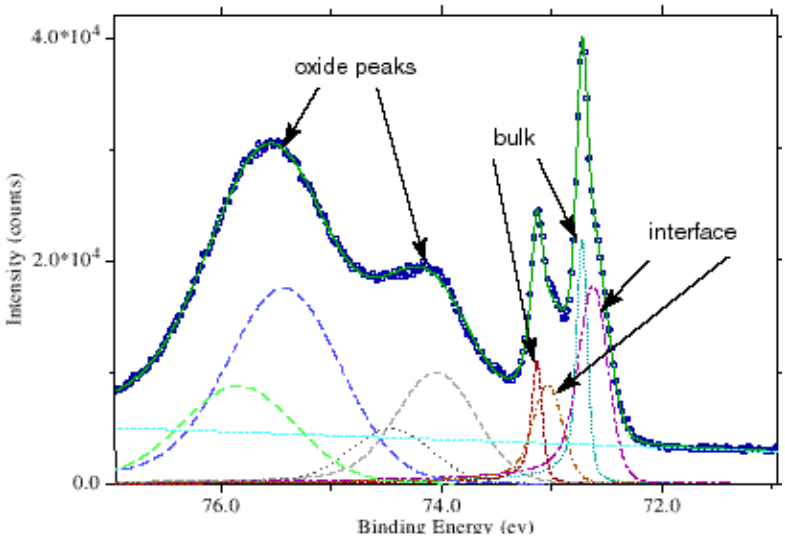

Al-2p spectrum measured after exposure of a clean Al(100) surface to 400L of oxygen.

component at lower binding energies in the Al-2p spectrum (see figure). This peak, previously observed for the oxidized Al(111) surface, can be ascribed to Al in the interface between the oxidized surface and the clean bulk.

It is well known that pre-adsorption of alkali metals promotes the oxidation of metals. In the case of Al(100) we have studied oxidation with Li coverage ranging from 0.05 ML to 1 ML pre-adsorbed and find that the oxidation is promoted in the sense that the initial uptake rate is raised by 2 orders of magnitude but the total amount of oxygen adsorbed is only slightly increased.

References:

[1]C Berg, S Raaen, A Borg, J N Andersen, E Lundgren and R Nyholm, Phys. Rev. B **47** (1993) 13 063

Co-adsorption of Li and Na on Al(100).

J H Petersen, C Søndergaard, and D L Adams
Institute of Physics and Astronomy, University of Aarhus

The co-adsorption of Li and Na on Al(100) has been studied by high-resolution core-level spectroscopy and low-energy electron diffraction at the SGM/SCIENTA beamline. Adsorption of ½ ML of Li at room temperature followed by the adsorption of ½ ML of Na leads to the formation of a sandwich-structure consisting of an ordered c(2x2) Al-Li composite layer and an outermost Na-layer. A similar, but not identical sandwich-structure is formed when adsorbing the Na at 120K on the c(2x2) Al-Li composite layer.

Reversing the adsorption sequence leads to identical structures as illustrated in the figure. Upon Li adsorption the Na atoms, sitting in c(2x2) substitutional sites, are completely substituted by Li even at temperatures as low as 120K.

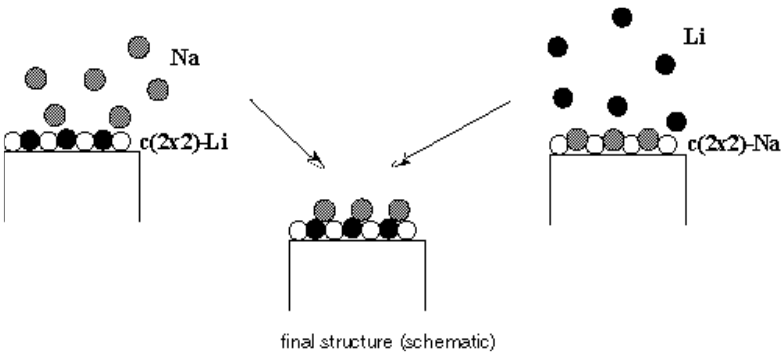

Schematic illustration of the co-adsorption process.

Dissociation of CO on K-modified Cu(115)

J. Onsgaard[1], S.V. Hoffmann[2], P.J. Godowski[3] and P. Møller[1]
[1]*Fysisk Institut, Odense University, DK-5230 Odense M*
[2]*Institute for Storage Ring Facilities, University of Aarhus, DK-8000 Århus*
[3]*Institute of Experimental Physics, University of Wroclaw, Poland*

Chemisorption of CO on potassium modified low-index copper surfaces like Cu(100) and Cu(110) have been extensively investigated [1-3]. It has been found that a moderate attractive interaction between CO and K is responsible for a weakening of the C-O bond, but no dissociation of CO has been reported. At high CO coverages a weak CO-CO interaction is deduced from small changes in the binding energy separation between the 4α and the 5α/1α orbitals. In order to study the combined effect of alkali modification and the influence of structure on the internal C-O bond a high-index surface was chosen. It is demonstrated that CO dissociates on a potassium-modified Cu(115) surface.

Adsorption of CO on a potassium-modified Cu(115) surface at 120 K gives rise to two CO sites dependent on the K-coverage. If Σ_K < 0.4 ML (monolayers) the 4α and 5α/1α orbital-derived features in the valence band have some similarities with the CO/Cu(115) surface and CO desorbs at 200 K. However for 0.4 < Σ_K < 1.0 ML new, extra sites are occupied already at 120 K. These sites are characterized by an extinguished yield from the 4α-derived orbitals and splitting of the 5α/1α complex into two peaks with a 1.3 eV energy difference at 223 K, centre curve in Fig.1. A pronounced rehybridization has taken place and there is bonding between K and O. The binding energies of the peaks at 8.0 eV and 9.3 eV increases with heating and at a temperature of 325 K a third peak appears at 7.3 eV binding energy, upper curve. These new observations are explained by three adsorption states representing (i) CO adsorbed on terraces, (ii) a new, strongly perturbed CO state at the steps with a higher adsorption energy and (iii) a dissociation state where oxygen is bonded to both potassium and copper. The dissociation is thermally activated and conditioned by the presence of steps.

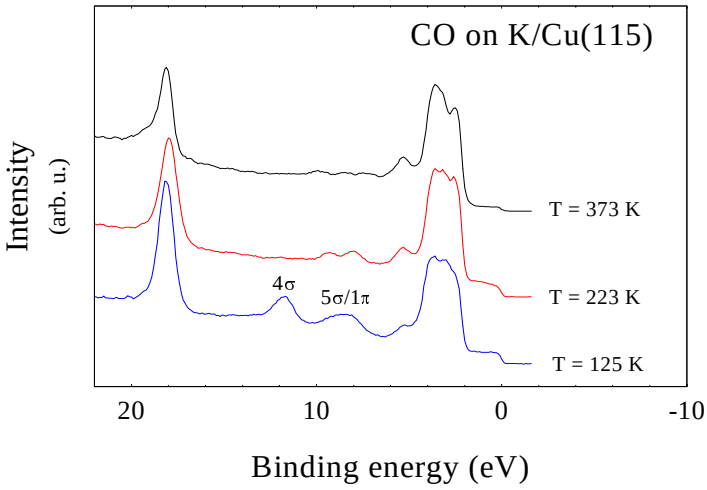

Figure1:. Valence band spectra of the 0.6ML K/Cu(115) interface exposed to 1.5 L CO at 125 K, lower curve. With heating the 4σ orbital disappears and new features represent dissociated CO.

References:

4. "*Chemical and Electrostatic Interactions between Alkali Metals and Carbon Monoxide on Metal Single-crystal Surfaces*", D. Lackey and D.A. King, *J. Chem. Soc. Faraday Trans. 1*, **83**, 2001(1987).
4. *"Photoemission and electron-energy-loss spectroscopy investigation of CO+K/Cu(100)"*, D. Heskett, I. Strathy, E.W. Plummer and R.A. de Paola, Phys. Rev. B **32**, 6222 (1985).
4. *"Photoemission and high resolution electron energy loss spectroscopy study of CO/K/Cu(110)"*, S.V. Christensen, J. Nerlov, P.J. Godowski and J. Onsgaard, J. Chem. Phys. **104**, 9613 (1996).

A RAS and Photoemission Study of the Surface State Contribution to the Optical Anisotropy of Ag(110) Surfaces

K. Stahrenberg[1], T. Herrmann[1], N. Esser[1], J. Sahm[1] and W. Richter[1],
S. V. Hoffmann[2], and Ph. Hofmann[2]
[1]*Institut für Festkörperphysik der TU Berlin, Hardenbergstrasse 36, 10623 Berlin, Germany*
[2]*Institute for Storage Ring Facilities, University of Aarhus*

Clean and oxygen covered Ag(110) surfaces were investigated with reflectance anisotropy spectroscopy (RAS) and photo emission spectroscopy at the SX-700 beamline at ASTRID. The clean surface shows a strong resonance in the reflectance anisotropy spectra at 1.7 eV which we assign to a transition between surface states at the $\overline{Y}$-point of the surface Brillouin zone. The accompanying photo emission spectra show the occupied surface state.

Reflectance anisotropy spectroscopy (RAS) is an optical method which allows the investigation of surface optical properties of semiconductors[1] and metals[2]. It measures the difference of the complex reflectivity along two perpendicular axes in the surface. In case of optically isotropic bulk materials signals are related to anisotropies induced by the surface[1]. The RAS signal consists of the real and the imaginary part of the reflectance anisotropy: $\alpha r = 2(r_{1\bar{1}0}-r_{001})/(r_{1\bar{1}0}+r_{001})$.

The only example for surface state contributions to the reflectance anisotropy on a metal surface so far is Cu(110). Here a sharp peak in the spectrum at an energy of 2.1 eV was assigned to transitions involving surface states at the $\overline{Y}$-point of the surface Brillouin zone[3]. However, since in Cu the transition energies of bulk d-electrons to the Fermi level are also located in this energy range, the observed feature in the Cu(110) spectra might as well also contain contributions arising from near surface bulk states.

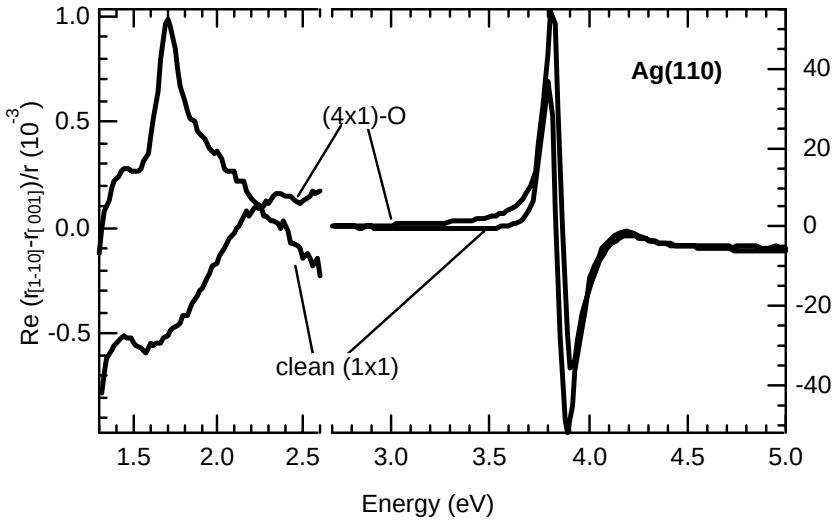

Real part of the RAS spectra for the clean Ag(110)-(1x1) and the oxygen covered Ag(110)-(4x1) surface at T=300 K.

Silver, on the other hand, has a similar surface electronic structure as Cu. However, contributions from the d-band transitions to the optical spectra are expected at much higher energies (above 4 eV) than the surface state transition energies. An anisotropic contribution from surface state transitions to the RAS spectra of the Ag(110) surface thus would be expected in the near infrared region, energetically separated from the d-bands.

RAS spectra of the clean Ag(110)-(1x1) and the oxygen induced (4x1) reconstructed surface are shown in fig. 1. The dominant feature in both spectra is a peak with a derivative like lineshape around 3.9 eV. Similar results had been already obtained in previous measurements[4,5]. These structures have been described by Tarriba and Mochan[6] using a phenomenological surface local

field model. The new feature is a much smaller peak occurring at an energy of 1.7 eV. It is assigned to a transition between an occupied surface state 0.1 eV below (see fig. 2) and an unoccupied surface state 1.6 eV above the Fermi level[7], both located at the $\overline{Y}$-point of the surface Brillouin zone. This transition is absent on the oxygen covered surface.

The anisotropy in the optical reflection spectra of the clean Ag(110) and Cu(110) surfaces was predicted by Jiang and co-workers[8]. They discussed the dipole selection rules of the surface states involved. It follows that the surface state transition is only allowed for light polarized along [001]. Since RAS probes the difference in reflectivity for light polarized along [001] and $[1\bar{1}0]$ one expects to observe this surface state transition due to the absorption for light polarized along [001][8].

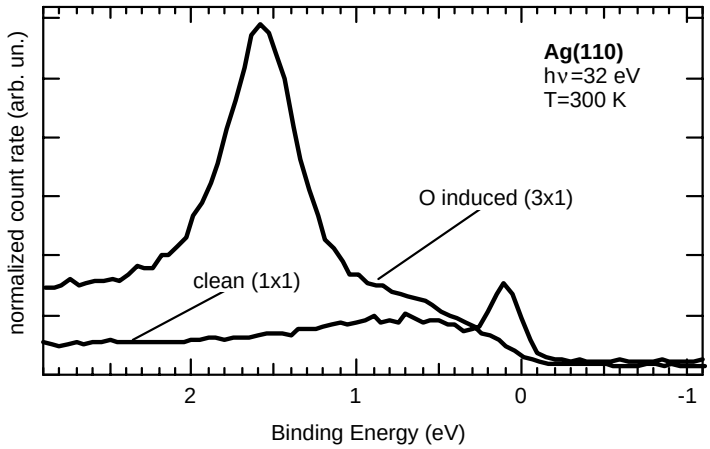

Photo emission spectra for the clean and oxygen induced (3x1)surface taken at ϑ=16.5 ° off-normal emission.

We used photo emission spectroscopy to verify the presence of the occupied surface state and its disappearance upon oxygen adsorption (fig. 2). The spectrum of the clean surface shows the surface state at $\overline{Y}$ 0.1 eV below the Fermi level[9]. On the oxygen covered surface, this peak is absent and a new prominent feature appears at ~1.6 eV below the Fermi level which has been previously been assigned to an antibonding oxygen induced *p*-state[10].

This work has been supported by the Deutsche Forschungsgemeinschaft through the Sonderforschungsbereich 290.

References:

1 D. E. Aspnes, J. P. Harbison, A. A. Studna, and L. T. Florez, J. Vac. Sci. Technol. A **6**, 1327 (1988).
2 A. Borg, O. Hunderi, W. Richter, J. Rumberg, and H. J. Venvik, phys. stat. sol. (a) **152**, 77 (1995).
3 Ph. Hofmann, K. C. Rose, V. Fernandez, A. M. Bradshaw, and W. Richter, Phys. Rev. Lett. **75**, 2039 (1995).
4 Y Borensztein, W. L Mochan, J. Tarriba, R. G. Barrera, and A. Tadjeddine, Phys. Rev. Lett. **71**, 2334 (1993).
5 V. Fernandez, D. Pahlke, N. Esser, K. Stahrenberg, O. Hunderi, A. M. Bradshaw, and W. Richter, Surf. Sci. **377**, 388 (1997).
6 J. Tarriba and W. L. Mochan, Phys. Rev. B **46**, 12902 (1992).
7 A. Goldmann, V. Dose, and G. Borstel, Phys. Rev. B **32**, 1971 (1985).
8 M. J. Jiang, G. Pajer, and E. Burstein, Surf. Sci. **242**, 306 (1991).
9 R. A. Bartynski and T. Gustafsson, Phys. Rev. B **33**, 6588 (1986).
10 R. Courths, S. Huefner, P. Kemkes, and G. Wiesen, Surf. Sci. **376**, 43 (1997).

This work has been published Phys. Rev. B **58**, R10207 (1998).

Synchrotron-radiation related work Sept.1996-Aug. 1998 by the Copenhagen Surfaces Group.

Preben Juul Møller and The Copenhagen Surfaces group
Department of Chemistry, Copenhagen University

During the above period the Copenhagen group has carried out photoemission, and electron and photoelectron diffraction research primarily on clean metal-oxide crystal surfaces and on adsorption and coadsorption of metal clusters (copper, sodium and potassium) and small-molecule active gases (O_2, CO, CO_2, NO and H_2S) onto metal-oxide (rutile titanium dioxide TiO_2, haematite Fe_2O_3, cassiterite tin dioxide SnO_2 , strontium dioxide $SrTiO_3$ and yttrium-stabilised zirconium dioxide $Zr(Y)O_2$) single-crystal surfaces. We have also carried out research on III-V semiconductor crystal surfaces (InP) and reactivity of these toward H_2S.We have primarily used the UHV chamber at ASTRID equipped with the SX700 monochromator, supported by both preliminary and subsequent studies at our Copenhagen University laboratories. The SGM-1 monochromator was found to be unsuitable for oxide crystal studies.

On the metal-oxide crystal surfaces we have carried out primarily fundamental chemistry and physics studies, but several of the above crystal surfaces systems have led to investigations of high relevance for both heterogeneous catalysis and chemical sensing of gases.
In the following is the work described briefly.

Our work has also in this period been primarily focussed on metal-oxide single crystal surfaces and their electronic and geometric structures and their reactivity.
The majority of the publications are concerned with the electronic structure and reactivity of TiO_2(110), Fe_2O_3(0001) and SnO_2(110) surfaces. We have used resonance photoemission spectroscopy (ResPES), valence band and core level photoemission and photoelectron spectroscopy (PED or XPED) supported by low-energy electron diffraction measurements.

The highlights have been the first observation of a site-specific activation process in a metal and gas coadsorption on a metal-oxide (in this case on the Fe_3O_4(111) termination of á-Fe_2O_3(0001) and its relation between structure and activation. The resulting adsorbate is identified as carbonate species. This is of particular interest in heterogeneous catalysis

Another more recent highlight is an investigation of a metal-to-semiconductor phase transition in VO and VO_2 thin films on TiO_2(110) of similar high interest in catalysis. The results were presented on the above International conference hosted in Copenhagen this summer in cooperation with an Italian group (Padova University).

Another focus has been on characterization of in situ synthesized ultrathin-film chemical sensors based upon copper oxide films deposited upon SnO_2 crystal surfaces. We have succeeded in showing and characterizing the sensitivity of this system to oxygen gas and been able to recommend the best suitable crystal surface in this system. This work has been carried out partly in cooperation with an UK group (Manchester University).

The work on synthesising and characterising metal-oxide thin film structures was in focus in the last year in which we obtained support from the European Commission Brite-EuRam materials science program to pursue this research in a larger scale. Finally we have worked on the sulphur passivation of a III-V semiconductor surfaces in continuation of joint work with a Japanese group (Shizuoka University).

The following 8 papers describes some of the projects in more detail.

A Photoemission and Resonant Photoemission study of Ba deposition at the TiO_2 (110) surface

Zheshen Li[1,2], J. Hoffmann Jørgensen[2], P. J. Møller[2], M. Sambi[3] and G. Granozzi[3]
[1]*Institute for Storage Ring Facilities, University of Aarhus, DK-8000 Aarhus C*
[2]*Department of Chemistry, University of Copenhagen, DK-2100 Copenhagen*
[3]*University of Padova, I-35131 Padova, Italy*

Results are reported on photoemission and resonant photoemission measurements performed on a Ba-deposited TiO_2 (110) single crystal surface using synchrotron radiation. An analysis of Ba 4d core levels shows that no metallic Ba exists in the deposition range corresponding to less than 1 monolayer (ML): only Ba oxide states are detected at this stage. Meanwhile, a new gap state centred at 0.8 eV below Fermi edge forms in valence band spectra, which may be attributed to reduced Ti^{3+} states [1]. Resonant photoemission experiments on this gap state show a strong resonance at a photon energy around 47.5 eV, which is the characteristic resonant transition from occupied Ti 3p to unoccupied Ti 3d levels in TiO_2(110) [2]. No resonance is detectable in the photon energy range between 95 and 115 eV, where a Ba resonant state is located [3]. On the other hand, when the Ba thickness on the TiO_2 (110) substrate exceeds 1 ML, a resonance of the near-Fermi-edge bandgap state appears, with maximum intensity found at approximately 106 eV and is a transition from $Ba(4d^{10}5s^25p^6) \approx Ba(4d^94f^15s^25p^6)$[3]. The metallic nature of the layer thicker than 1 ML is confirmed by Ba 4d line shapes, which become asymmetric. Work function is also recorded at each step of the Ba deposition. A drastic change from oxide to metal barium is detected when the Ba thickness exceeds 1 ML, which is consistent with the above reported results.

References

[1] Z. Zhang and V. Henrich, Surf. Sci. **277**, (1992) 263.
[2] J. Nerlov, Q. Ge, and P. J. Møller, Surf. Sci. **348**, (1996) 348.
[3] V. G. Devyatov, S. V. Koshcheev, A. E. Chercashin, E. S. Gluskin, A. V Dudnikov, V. G. Dudnikov, A. K. Sood, V. S. Sahnie and G. Ventkatararnan, Nuclear Instruments and Methods in Physics Research, **A282**, (1989) 688.

Coadsorption of Na and CO_2 on the Fe_3O_4(111) termination of α-Fe_2O_3(0001): relations between structure and activation

Jesper Nerlov[a], Søren V. Hoffmann[b], Masaru Shimomura[c], Preben J. Møller[a]
[a] *Department of Chemistry, University of Copenhagen, DK-2100 Copenhagen Ø, Denmark*
[b] *Institute for Storage Ring Facilities, University of Aarhus, DK-8000 Aarhus C, Denmark*
[c] *Research Institute of Electronics, Shizuoka University, Hamamatsu 432, Japan*

The coadsorption of CO_2 and Na on the Fe_3O_4(111) termination of α-Fe_2O_3 (0001) has been investigated by synchrotron-radiation-based core-level and valence band photoemission and low-energy electron diffraction. We find that a 1×1 structure ideally is formed at ¼ ML Na coverage. Based on a simple adsorption model, Na adsorption in a 3-fold hollow sites equivalent to bulk octahedral intersites is proposed. A perfect structure is not obtained owing to occupancy of an additional adsorption site above $\alpha_{Na} \leq 0.16$ML. The Na adsorption below 0.25 ML is accompanied by a substantial Na-to-substrate charge transfer leading to reduction of the uppermost ¼ ML Fe^{3+} ions. The Na-induced valence band emission observed in the submonolayer region is characteristic of alkali-oxygen compounds.

Occupancy of the second adsorption site also marks the onset of reactivity towards CO_2 of the Na/Fe_3O_4(111) interface at room temperature. This is believed to be the first observation of

site-specific activation in this type of systems. The resulting adsorbate is identified as a carbonate species. Especially near the threshold of activation both types of Na are involved in bonding which is attributed to the existence of Na_2CO_3 units on the surface. The close connections between electronic and geometric structure and reactivity are discussed and general aspects of the observed activation and bonding mechanisms are suggested.

Adsorption of H_2S on InP(001) studied by photoemission spectroscopy

M. Shimomura[a,b] , P. J. Møller[a], J. Nerlov [a], S. V. Hoffmann[c], Q. Guo[a], N. Sanada[b], Y. Fukuda[b]

[a] *Department of Chemistry, University of Copenhagen, DK-2100 Copenhagen Ø, Denmark*
[b] *Research Institute of Electronics, Shizuoka University, Hamamatsu 432, Japan*
[c] *Institute for Storage Ring Facilities, University of Aarhus, DK-8000 Aarhus C, Denmark*

Adsorption of H_2S on InP(001) at 140 K has been studied by valence-band and core-level synchrotron-radiation-induced photoemission spectroscopy (SRPES). Peaks were found in the SRPES spectra after the H_2S exposure at E_F −6.7, −9.4, and −12.4 eV upon adsorption of H_2S. This indicates that H_2S adsorbs molecularly on the surface at 140 K. We find two kinds of chemical state for the sulfur: S2p at 162.0 and 160.8 eV for H_2S strong interaction with surface In atoms and physisorption, respectively. This is consistent with the changes in S2p and In4d spectra upon adsorption of H_2S. Phosphorus atoms on the surface are scarcely interacting with H_2S.

Electronic properties of Cu clusters and islands and their reaction with O_2 on SnO_2(110) surfaces

Zheshen Li[1,2], Qinlin Guo[2] and Preben J. Møller[2]

[1] *Institute for Storage Ring Facilities, University of Aarhus, DK-8000 Aarhus C*
[2]*Institute of Chemistry, University of Copenhagen, DK-2100 Copenhagen*

A number of experimental studies of both polycrystalline and single crystal SnO_2 have been undertaken[1-5]. Among these, the studies on single crystal surfaces are very important for understanding the mechanism of its sensing. To have higher selectivity and sensitivity, metals such as Pt and Pd are commonly used as additives to grains in polycrystalline surfaces of SnO_2[6]. But there are fewer studies of metal clusters on single crystal SnO_2, which is quite important for understanding the microcatalytic properties of SnO_2 gas sensors.

The deposition of Cu on SnO_2(110) surfaces, and its oxidation to Cu_xO, have been studied by low-energy electron diffraction (LEED) and angle-integrated photoemission using synchrotron radiation photoemission spectroscopy (SRPES) at ASTRID.

With the growth of copper on SnO_2(110), which was found to follow the Volmer-Weber ("islanding") growth mode, a small amount of metal-phase Sn segregates to the surface, and even when the copper thickness reaches several tens of Å, Sn metal still is seen at the surface. However, when this surface is annealed at 523≈C in 5×10^{-6} mbar O_2 for 20 min, the Sn atoms are totally converted to SnO_2. Simultaneously, the deposited Cu atoms become oxidized. The surface charges up both during LEED and SRPES data acquisition. The clean SnO_2(110) surface shows a 1×1 structure. With Cu deposition, the substrate LEED pattern gradually became weaker. With even more copper deposited, a Cu(111)-1×1-oriented particle structure appears, indicating coalescence of the Cu islands to 3-dimensional Cu(111) epitaxy. After subsequent heating to 200≈C, the substrate signal appears again, and we see the SnO_2 1×1 pattern. In conclusion, the Cu atoms quite easily form clusters on the SnO_2(110) surface already after a slight heat treatment.

The results show that this system is quite active towards O_2 gas exposure, and that the surface conductivity changes during O_2 exposure.

References

1. D. F. Cox, T. B. Fryferger and S. Semancik, Phys. Rev. B 38 (1988) 2072.
2. K. D. Schierbaum, U. Weimar and W. Göpel, Sensors and Actuators B 7 (1992) 709.
3. J. M. Themlin, R. Sporken, J. Darville, R. Caudano, J. M. Gilles and R. L. Johnson, Phys. Rev. B 42, (1990) 11914.
4. J. W. Erickson and S. Semancik, Surf. Sci. 187 (1987) L658.
5. G. L. Shen, R. Casanova, G. Thornton and I. Colera, J. Phys: Condens. Matter 3 (1991) S291.
6. P. Dutronc, C. Lucat, F. Menil, M. Leosch, M. C. Horrillo, I. Sayago, J. Gutierrez and J. A. de Agapito, Sensors and Actuators B 15-16 (1993) 384.

A photoemission study of the coadsorption of CO_2 and Na on TiO_2(110)-(1×1) and -(1×2) surfaces: adsorption geometry and reactivity

Jesper Nerlov[a], Søren V. Hoffmann[b], Steen Weichel[a], Eddie H. Pedersen[a], Preben J. Møller[a]

[a] *Department of Chemistry, University of Copenhagen, DK-2100 Copenhagen Ø, Denmark*

[b] *Institute for Storage Ring Facilities, University of Aarhus, DK-8000 Aarhus C, Denmark*

The adsorption of CO_2 and Na on TiO_2(110)-(1×1) and -(1×2) surfaces have been investigated by synchrotron-radiation based core-level and valence band photoemission. We find that the initially adsorbed Na exhibits a core-level shift of 1.15 eV when the two surfaces are compared. From a simple adsorption model this binding energy shift is understood in terms a difference in initial Na adsorption site on these surfaces. While the (1×1) surface seems to favour Na adsorption in a hollow site "between" bridging surface oxygen atoms, it is found that the (1×2) surface facilitates a chemically more advantageous Na adsorption "adjacent to" the bridging oxygen atoms. Valence band measurements support this model since Na adsorption on the (1×2) surface leads to emission characteristic of alkali-oxygen-like compounds while this is not the case for the Na/TiO_2(110)-(1×1) system. Finally, the relatively high resolution of the core-level emission allows in a direct way the various features contributing to the Na 2p core-level emission to be determined. With respect to adsorption of CO_2 we find for the (1×2) surface that CO_2 uptake saturates around 0.5 ML Na coverage compared to 1 ML for the (1×1) surface, indicating that the Na coverage required for saturation of CO_2 uptake is proportional to the density of protruded oxygen rows present at the surface. The CO_2 uptake, however, increases as the density of the oxygen rows decreases. Valence band photoemission data obtained from both interfaces show that a surface carbonate species is formed. At lower coverages/exposures there are, however, indications of the presence of a CO_2^- species rather than carbonate, thereby suggesting that the carbonates species is formed through the surface reaction: $2\ CO_2^- \approx CO_3^{2-} + CO$.

Synthesis and characterization of a model CuO/SnO_2 oxygen sensor

Preben. J. Møller[1], Zheshen Li[1,2] and Qinlin Guo[1]
[1]*Department of Chemistry, University of Copenhagen, DK-2100 Copenhagen, Denmark*
[2] *Institute for Storage Ring Facilities, University of Aarhus, DK-8000 Aarhus C*

Tin dioxide (SnO_2) is a very promising material for gas sensor application because of its very good chemical stability and good surface conductivity. It is generally agreed that the gas absorption on the material surface modifies the density of free electrons close to the surface that changes the resistance. But relatively little is known about the mechanism of the surface reactions. So it is quite important to study the microstructure and electronic properties of the surface.

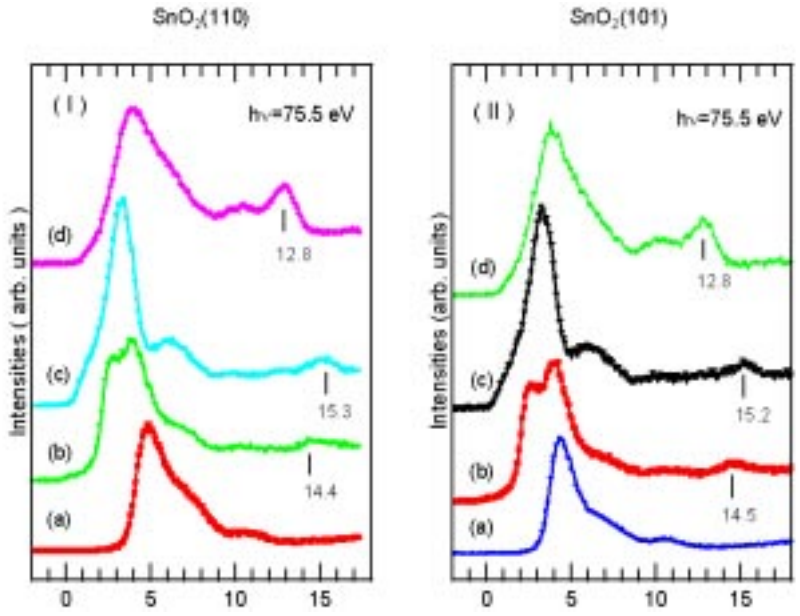

SR PES spectra from SnO_2 surfaces from the (110) surface (I) and the (101) surface (II). (a) clean surface, (b) Cu-covered surface (0.7 monolayer), (c) the sample annealed to 500K in 1×10^{-6} mbar O_2 for 20 min., and (d) the sample annealed to 600K in 1×10^{-6} mbar O_2 for 20 min.

In this paper, we will discuss the structural and electronic properties of interfaces formed by Cu deposits on the (110) and the (101) surfaces of SnO_2, and the subsequent formation of a CuO overlayer by oxidation. Due to the lattice mismatch, epitaxial growth of CuO on the SnO_2 single crystal is not expected. We will therefore deposit nanoscale small particles of Cu in small steps, and oxidize these at each step to CuO, gradually increasing the size of the particles of this material in order to obtain a stronger bonding to the SnO_2 surface. With this in mind, we have studied two low-index SnO_2 surfaces in order to see the influence of SnO_2 crystal structure in the interfacial region on sensor properties.

Synchrotron-radiation-induced photoemission study of VO_2 ultrathin films deposited on TiO_2 (110)

P. J. Møller[1], Z. S. Li[1,2] , T. Egebjerg[1], M. Sambi[3] and G. Granozzi[3]
[1]*University of Copenhagen, DK-2100 Copenhagen, Denmark*
[2] *Institute for Storage Ring Facilities, University of Aarhus, DK-8000 Aarhus C, Denmark*
[3]*University of Padova, I-35131 Padova, Italy.*

Synchrotron-radiation-induced photoemission spectroscopy (SRPES) measurements were carried out on clean and VO_2-deposited TiO_2 (110) surfaces. Metal V was deposited at room temperature (RT) onto the TiO_2 surface and then oxidized to VO_2 at 473K. At a V coverage of 0.2 ML on TiO_2(110), both metallic and oxidized states of V3d are clearly seen near E_F, indicating a strong interaction of metal V with O even at RT. After oxidation of V, a clear (1×1) VO_2 superstructure appears. A semiconductor-to-metal phase transition occurs when the VO_2 film is heated. The energy shift near E_F is 0.1 eV over the RT to 394 K temperature range. This process for the ultrathin film was found to be reversible in that temperature range.

An ARPEFS Study of the Structure of an Epitaxial VO_2 Monolayer at the TiO_2(110) Surface

M. Sambi[a], M. Della Negra[a] ,G. Granozzi[a], Z.S. Li[b,c], J. Hoffmann Jørgensen[c] and P.J. Møller[c]
[a] *University of Padova, I-35131 Padova, Italy.*
[b] *Institute for Storage Ring Facilities, University of Aarhus, DK-8000 Aarhus C, Denmark*
[c] *Department of Chemistry, University of Copenhagen ,DK- 2100 Copenhagen, Denmark*

In the present communication we discuss the results of an angle resolved photoemission extended fine structure (ARPEFS) study of a VO_2 monolayer (ML) grown on the TiO_2 (110) surface by successive cycles of sub-ML vanadium metal deposition followed by annealing at 473 K in 2×10^{-6} mbar O_2. The V 3p photoemission peak shows two distinct components chemically shifted by 1.3 eV. While the higher binding energy (BE) component produces a rather flat ARPEFS curve, the lower BE signal, associated with the VO_2 phase, shows well defined intensity modulations whose main features are similar to the ARPEFS scan on the Ti 3p signal of the substrate. This observation demonstrates that the ordered VO_2 phase grows epitaxially to the substrate, with a rutile type structure. However, some oxide is present in a more highly oxidized and less-ordered phase. In order to investigate the actual arrangement of the ML with respect to the question related to the possible formation of an intermixed VO_2/TiO_2 layer, the ARPEFS data have been interpreted by means of single-scattering spherical wave (SSC-SW) simulations. They are compatible with the hypothesis that the deposited ML evolves toward an intermixed VO_2/TiO_2 double layer where the vanadium atoms occupy the six-fold oxygen-coordinated sites. In addition, our data are in good agreement with a surface relaxation similar to that found by surface XRD on the stochiometric TiO_2(110) surface.

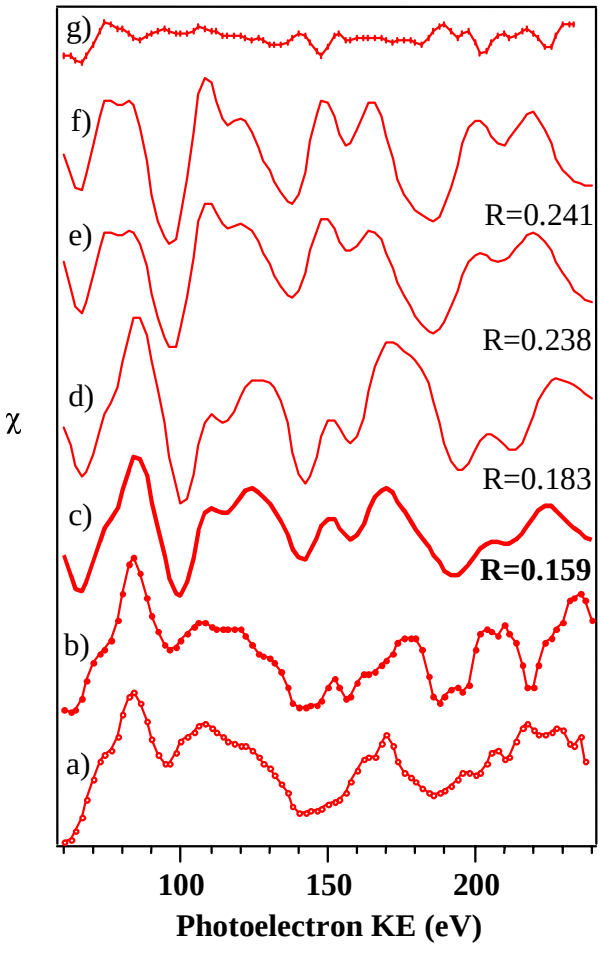

ARPEFS α-functions of (a) the Ti 3p core level of the substrate and (b) the V 3p (I) peak of the overlayer, corresponding to the VO_2 ordered phase; single-scattering-cluster spherical-wave simulations of the V 3p (I) ARPEFS scan from (c) the relaxed mixed-oxide bilayer model, (d) the relaxed VO_2 ML arrangement, (e) the bulk-terminated mixed-oxide bilayer model and (f) the bulk-terminated VO_2 ML arrangement. Curve (g) shows the experimental ARPEFS scan for the V 3p (II) photoelectron component. R-factor values between the theoretical scans and curve (b) are reported

Adsorption of hydrogen on alkali-modified copper surfaces

S.V. Hoffmann[1], L. Thomsen[2], P.J. Godowski[3], and J. Onsgaard[2]
[1]*Institute of Physics and Astronomy, University of Aarhus, DK-8000 ÅrhusC*
[2]*Fysisk Institut, Odense University, DK-5230 Odense M*
[3]*Institute of Experimental Physics, University of Wroclaw, Poland*

Adsorption of an alkali metal on a copper surface causes a substantial decrease in the work function. This change in the electronic structure of the surface has strong consequences for the adsorption and reactive properties. Reactions between CO_2, CO and H on copper surfaces play important roles in catalytical processes like the water-gas shift reaction and the synthesis of methanol. Synthesis of formate, HCOO, by coadsorption of H and CO_2 on an K-modified Cu(110) surface has been demonstrated[1].
Adsorption of H on clean and K-modified Cu(110) and Cu(100) surfaces has been investigated at the ASTRID storage ring. The beam line consists of an SX-700 monochromator and an UHV-chamber.

***H/Cu(110)*:** Adsorption of atomic hydrogen on the Cu(110) surfaces, carried out at a temperature of 140K, results in two hydrogen induced states in the valence band region. The states, α and α, with binding energies at 7.1 eV and 8.6 eV, are characterized by FWHM equal 1.2 eV and around 2 eV, respectively. These states reflect population of two different adsorption sites, which are ascribed to a subsurface state, α, with the high binding energy, and an on-top state, α. Heating causes binding energy shifts, Σα = +0.9 eV and Σα = +0.5 eV, and an intensity increase of the α-state while the α-state is depopulated. Annealing to 330K results in a hydrogen-free surface.

H/K/Cu(110) and H/K/Cu(100): The effects of modifying the Cu surfaces with K before adsorption of H are (i) the hydrogen-potassium induced α-states become more intense; there is no α-state present on the K/Cu(100) surface at 120K for K-coverages below 1 ML, (ii) the α-shift is +0.6 eV for both surfaces and the α-shift is −1.1 eV for the Cu(110) surface, and (ii) they desorb around 500K. As demonstrated in Fig.1, the two potassium-hydrogen states in the valence band behave differently with annealing temperature. Whereas the α-state is weakly or not populated at low temperature and grows significantly, then the α-state decreases in intensity with temperature. Adsorption of 200L H on a K/Cu(110) interface at 130K in the sub-monolayer regime results in a 0.2 eV chemical shift of the K-3p peak towards lower binding energy. When the intensities of the two hydrogen-potassium induced peaks start to decrease, an increase in binding energy of the K-3p peak is observed. The α-state with a binding energy close to the high binding energy state at the H/Cu(110) interface is assigned to H-K bond formation. The α-state with a binding energy markedly different from the Cu-H state is assigned to H-Cu bond formation.

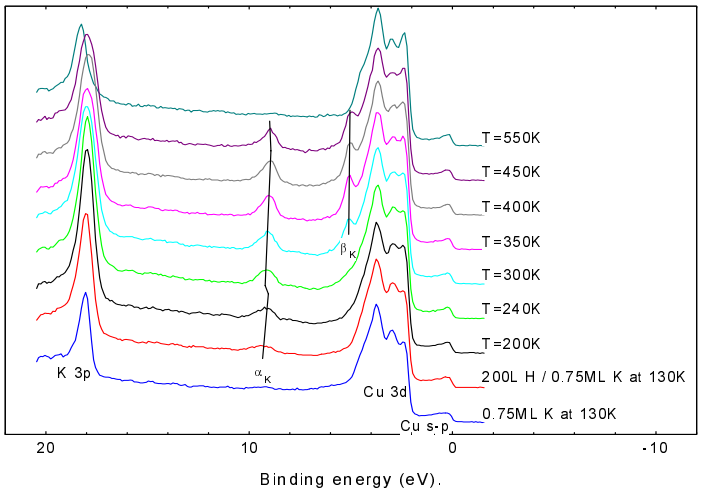

Figure 1: Valence band spectra from a 0.75ML K/Cu(110) interface exposed to 200L H-H_2. The two hydrogen-potassium associated states are labeled α_K and β_K.

4. *"Synthesis of formate on K-modified Cu(110) based on coadsorption of H and CO_2"*, J. Onsgaard, S.V. Christensen, P.J. Godowski, J. Nerlov and S. Quist, Surface Science **370**, L137(1997).

Ultrathin oxides on Si(111) and Si(100)

Per Morgen[1], Flemming K. Dam[1], Lars-Bo Tækker[1],
Kjeld Pedersen[2] and Søren V. Hoffmann[3].
[1]*Institute of Physics, Odense University, DK-5230 Odense M*
[2]*Aalborg University, DK-9100 Aalborg*
[3]*Institute for Storage Ring Facilities, University of Aarhus, DK-8000 Aarhus C*

Introduction

Future generations of microelectronics need gate oxides in MOSFETs to be between 50 and 100Å thick. Traditional growth methods have been unable to meet such requirements. The path to homogeneous, thin oxides with the necessary silicon – oxide interface quality is one with low maximum process temperature, uniform reaction and good control of the amount of - and penetration of oxygen atoms.

The current approach

The control of the growth is achieved in a novel approach using Cs as a catalyst. The clean, perfectly ordered Si(111) and Si(100) surfaces first receive a saturating coverage of atomically inserted oxygen at room temperature under UHV conditions. A monolayer of Cs atoms is made to cover the surfaces after which a new dose of oxygen is given. The chamber is then evacuated and heating the samples until the Cs is desorbed does the oxidising. In further steps the process is repeated with a new monolayer of Cs deposited followed by oxygen and heating. Thus a controlled growth of layers of oxide is possible. Our experiments at ASTRID are done at the SX-700 beamline and at the SGM beamline. In parallel experiments in Odense and Aalborg the reaction kinetics and the role of Cs is studied in more detail, while the measurements at ASTRID focus on the Si 2p core levels and the valence bands during the steps. A program written by D. Adams fits and decomposes the different oxidised Si 2p components in the experimental spectra

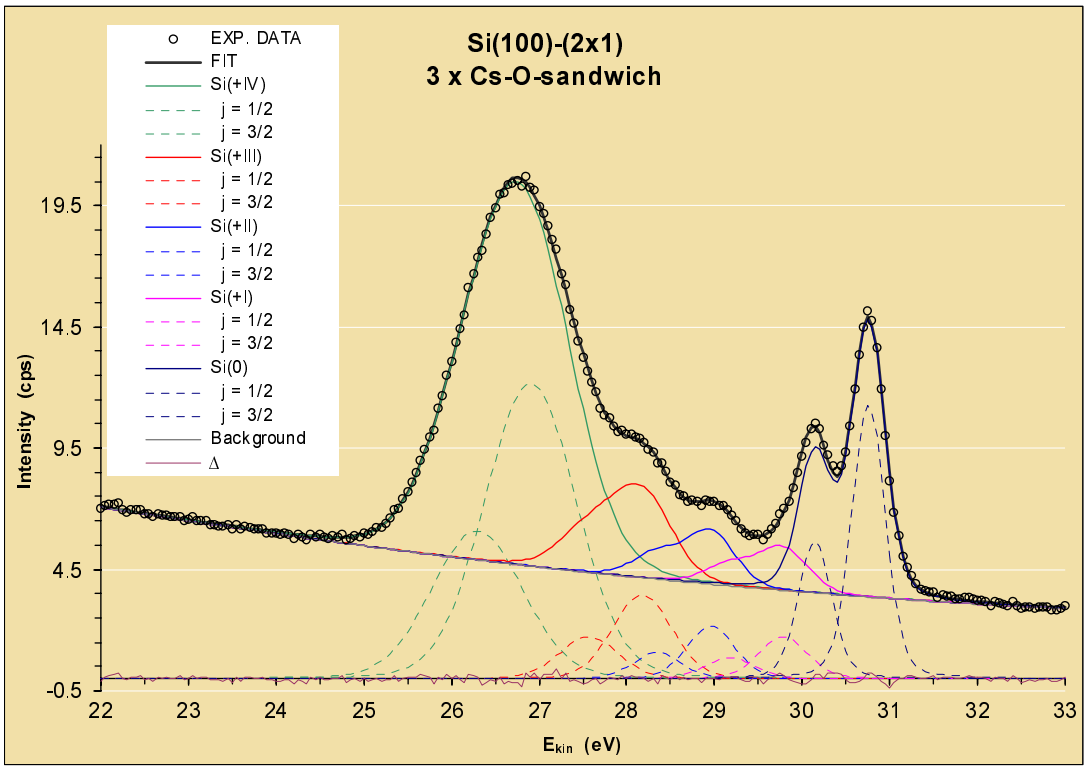

with Lorentzian and Gaussian shapes.

The results are analysed to discuss the sites for the initial oxygen bonding, the structure of the silicon – oxide network building up with insertion of oxygen, the interface co-ordination, and the morphology of the oxide layer. At the same time the studies of both surfaces under identical conditions could give clues to the interface co-ordination differences between them, so crucial to the industry's choice of the Si(100) orientation for this purpose.

Results

We have found that as with all other oxidation mechanisms based on a supply of molecular or atomic gases to the surface the oxide grows by oxygen atom penetration through the forming oxide layer with a lowered mobility compared to clean silicon. Thus the annealing and Cs desorption step is carried out at gradually higher temperatures, but still below the temperature of liberation of SiO. This also increases the chances of keeping the oxide contiguous and uniform. The uniformity of the oxidation is controlled by the uniform adsorption of Cs on these surfaces. The oxygen then sticks uniformly with atoms under the Cs before the thermally induced reaction. It remains to be proven that the oxide layer is totally uniform, however, but experiments are underway using the STM for this.

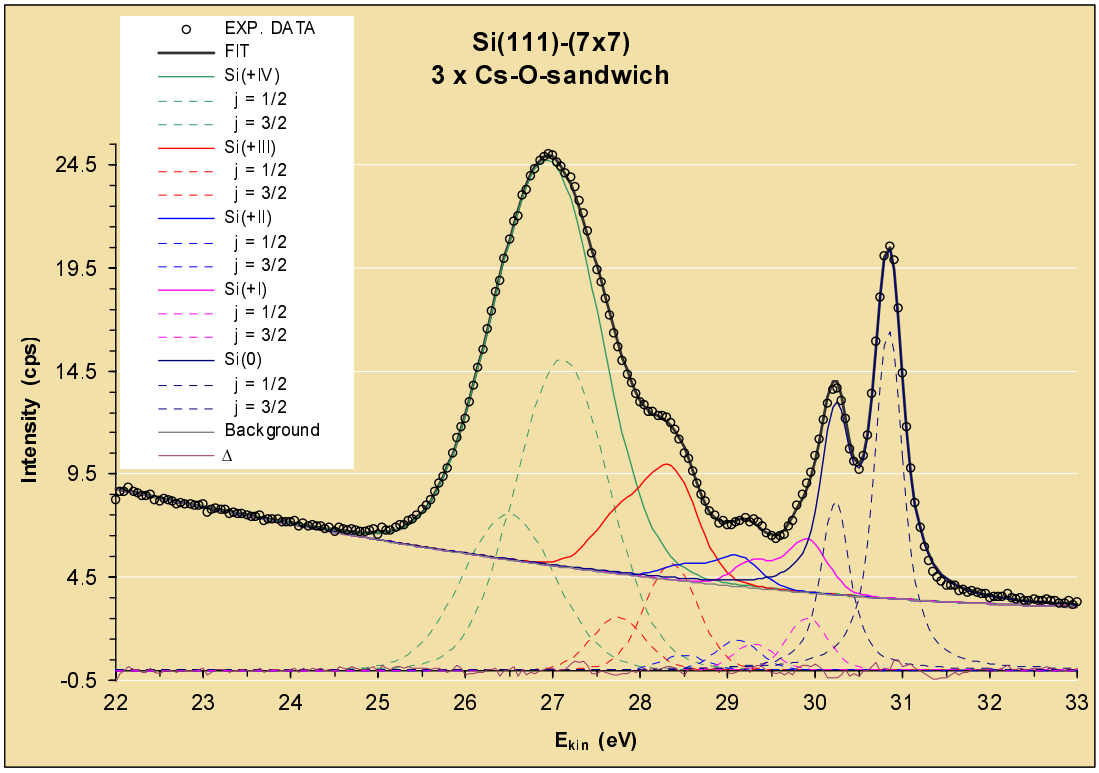

The two graphs compare the structures of a thin oxide on Si(111) and Si(100) after 3 cycles of the oxide growth procedure, through the Si 2p spectra taken at 130eV photon energy. At this thickness the top surface, the silicon – oxygen network and the silicon – oxide interface are all contributing to the spectra. It can be directly seen how the overall Si-O co-ordination differs.

Botanical studies by soft X-ray microscopy

J.V. Abraham-Peskir[1], R. Medenwaldt[1] R. Searle[2], I. Thom[3], M. Grote[4], and R. Wiermann[3]
[1]*Institute for Storage Ring Facilities, University of Aarhus, Aarhus*
[2]*Department of Botany, University of Reading, UK*
[3] *Institut für Botanik der Westfälischen Wilhelms-Universität, Münster, Germany*
[4] *Institut für medizinische Physik und Biophyik der Westfälischen Wilhelms-Universität,Münster, Germany*

Viscin threads are a unique kind of pollen-connecting thread thought to aid pollen dispersal. We used X-ray microscopy (XM) to make a detailed comparative study of the existing literature describing morphology of these threads. Nine plant species (7 Onagraceae and 2 Ericaceae) were investigated and compared to previous electron microscopy studies (Abraham-Peskir et al 1998).

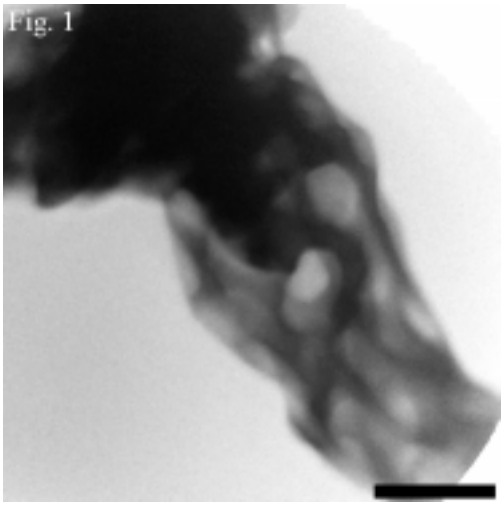

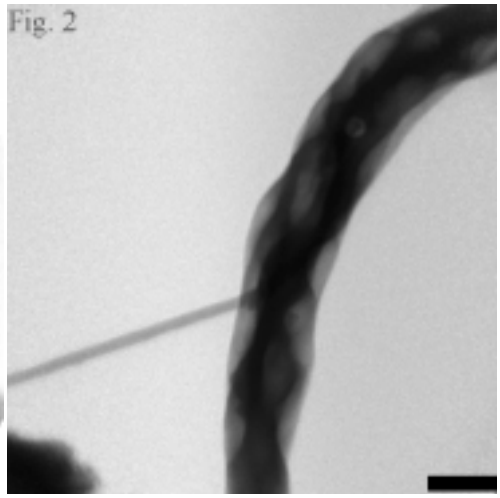

Figures 1 & 2 show X-ray micrographs of compound viscin threads of *Boisduvalia subulata* and *Clarkia tenella*, respectively.

Highly purified exines from Typha angustifolia L. pollen were solubilised by Professor Wiermann and workers at Westfälische Wilhelms-Universität, Münster. The solubilisate was fractionated and re-aggregated sporopollenin-like materials were obtained. As part of a comparative study the re-aggregated materials were analysed by SEM, TEM and X-ray microscopy. High structural congruence to the initial material was shown and additionally distinct substructures were revealed (Thom et al. 1998).

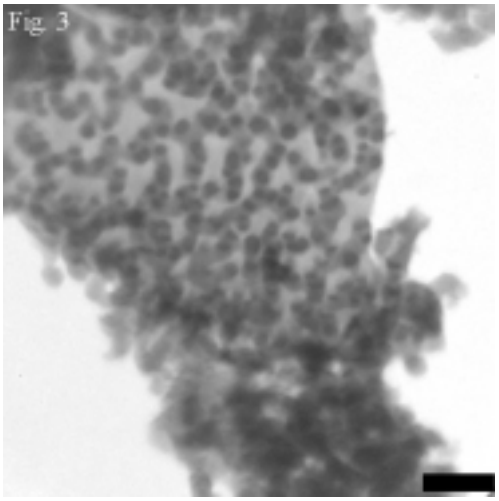

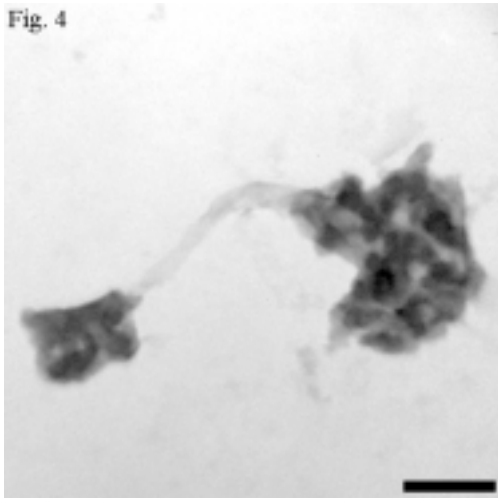

Figures 3 & 4 show X-ray micrographs of two of the sporopollenin fractions.

References:

J.V. Abraham-Peskir, R. Searle, and R. Medenwaldt (1998). A new technique of examining pollen-connecting threads. Grana, 36, 343-346.

I. Thom, M. Grote, J. Abraham-Peskir, and R. Wiermann (1998). Electron and X-ray microscopic analyses of reaggregated materials obtained after fractionation of dissolved sporopollenin, Protoplasma, 203.

Ion and X-ray sensitivity of the human sperm plasmalemma examined using light and X-ray microscopy

J Abraham Peskir[1], R Medenwaldt[1], and E Chantler[2]
[1]*Institute for Storage Ring Facilities, University of Aarhus, Denmark*
[2]*Department of Obstetrics and Gynaecology, University of Manchester, UK*

Freshly ejaculated human sperm lack the ability to fuse with and fertilize the ovum until a series of post-ejaculatory changes have taken place which normally occur during their passage through the cervix, uterus and fallopian tube. These changes can also occur *in vitro*, in a time dependent manner though there is also a dependence on calcium ions for several steps: this whole process is termed capacitation. Many of these changes involve the membranes of the sperm including unmasking of receptor sites and ultimately the exocytosis of the acrosomal membranes.

We have shown for the first time, using the X-ray microscope, that the plasmalemma of the sperm frequently (the membrane that encloses the spermatozoon) expands away from the sperm in the head, mid-piece and tail regions forming clear vesicles that enclose these areas of the sperm[1] (see image). We have also visualised this process using DIC light microscopy, though the mid-piece vesicles are more easy to resolve than those seen at other areas of the sperm. In the mid-piece region the vesicles are 0.7 to 5.0 µm in diameter but are distinct from the cytoplasmic granules which are the same size but have granular rather than clear contents. These latter have long been recognised and contain redundant cytoplasmic elements of the sperm that have been associated with spermiogenesis and are usually, though not inevitably, shed before ejaculation. The occurrence of the clear vesicles has been shown to be greater in sperm that have been visualised by XM than LM suggesting that x-ray exposure may stimulate their formation.

The production of vesicles as a result of x-ray associated damage may be discounted as the vesicles are also visualised by LM. Similarly, their presence as part of the process of apoptosis of sperm (programmed cell death) is also unlikely as vesicles are present on 0 - 76% of the sperm (varying between ejaculates), which is much greater than estimates of the incidence of apoptotic sperm (0.1%).[2]

Recently we have shown that manipulation of the levels of calcium ions within or surrounding the sperm plays a central role in the formation of these vesicles. This observation suggests that formation of vesicles that surround the sperm head may represent part of the calcium-dependent capacitation of sperm. The vesicles that surround the head have an expansion distance from the head of 0.1 to 2.6 µm, which significantly increases the space occupied by the sperm head. Examination of sperm motility using computer assisted image analysis, however, does not suggest that the presence of the vesicle affects the motility of the sperm.

In conclusion, the XM is being used to give superior resolution of sperm allowing the examination of the functional capacity of sperm in both normal and infertile men, as well as the investigation of basic processes in sperm maturation.

References

J. Abraham Peskir, E. Chantler, C. McCann, R. Medenwaldt, and E. Ernst. Med. Sci. Res. Vol.26, no.10, 663 (1998).

B. Baccetti, G. Collodel,, and P. Piomboni . J. Submicrosc. Cytol. Pathol. **28**, 587 (1997)

Metal-induced structural changes in whole cells in solution

J.V. Abraham-Peskir[1], R. Medenwaldt[1] and J. Wendt-Larsen[2]
[1]*Institute for Storage Ring Facilities, University of Aarhus, Aarhus*
[2]*Department of Physics, University of Odense, Odense*

It was found that the flagellated protozoon *Chilomonas paramecium* was sensitive to elevated levels of copper in the external medium (Abraham-Peskir, 1998). This study combined light and soft X-ray microscopy (XM) to determine structural changes in whole cells in solution. Cells rapidly rounded up on exposure to copper and were spherical with 20 minutes. Soft XM studies, revealed further ultrastructural detail of whole cells in solution, compartments had formed and ejectosomes were released in response to toxic levels of the free metal ion of copper. Changes in the pellicle thickness were quantified. Figure 1 shows an X-ray micrograph of a control cell (Bar = 2 ≈m).

This work was extended by Jette Wendt-Larsen in her diploma thesis to study the toxic effects of aluminium and zinc. Jette obtained interesting results by combining conventional LM, XM and confocal LM techniques. The fluorescent dye Newport Green was used to localise the metals after uptake and accumulation within the cell. This new dye had not been used previously to study the uptake of metals in protozoa. It showed that the metals had been compartmentalised, a tolerance mechanism used by some microbes in response to toxic levels of certain metals. The pattern of localisation was different for aluminium and zinc. X-ray microscopy studies gave additional information on the nature of the compartments and further ultrastructural details not seen by LM.

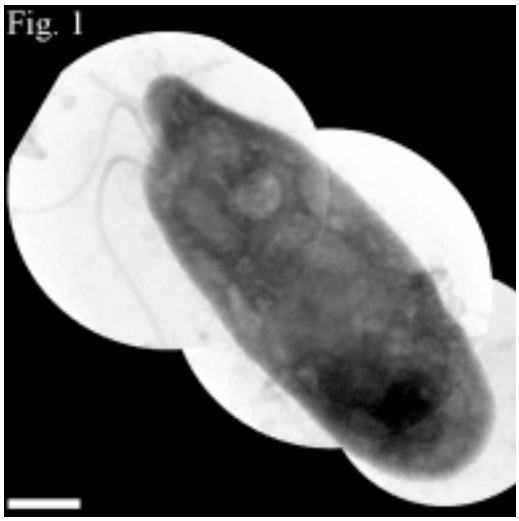

Experiments have now been extended to study the effects of nickel and lead by LM and XM. Fig. 2 shows a cell loaded with the fluorescent dyes Propidium Iodide (PI) and Newport Green (NG) and then exposed to nickel. Green pseudo-colour shows NG fluorescence representative of nickel localisation and yellow represents PI staining (nucleus). See this figure in colour on the inside back cover. Fig. 3 shows an X-ray micrograph of a nickel-treated cell (Bar = 2 ≈m). Quantified levels of the metals after uptake and/or accumulation will be determined by SEM-electron-probe microanalysis of cells exposed to aluminium, copper, lead, nickel and zinc. LM and XM studies are on-going.

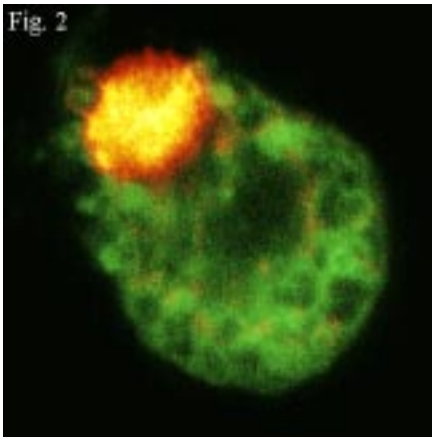

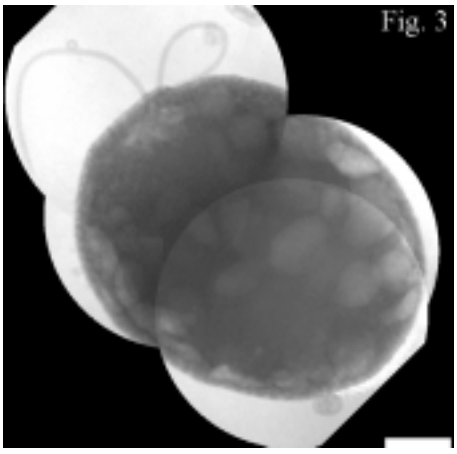

References:

J.V. Abraham-Peskir (1998). Structural changes in fully hydrated *Chilomonas paramecium* exposed to copper. Europ. J. Protistol., **34**, 51-57.

Iron Precipitation in Danish Fresh Water Plants

E.Søgaard[1], J.Abraham-Peskir[2], and R.Medenwaldt[2]
[1]*Department of Chemistry, Aalborg University Esbjerg, Denmark*
[2]*Institute for Storage Ring Facilities, University of Aarhus, Denmark*

The iron and manganese content in Danish groundwater is generally high, so that precipitation is necessary before the water enters the fresh water supply. Especially, the so-called Ribe formation in the south western parts of Jutland, Denmark, has a high content of iron in the ground waters. The precipitation of the excess iron can be chemical (oxidation by air) or biological (oxidation by bacteria). By a variety of methods, we have investigated the sludge of different fresh-water plants around Ribe with the aim to study the effect of chemical or biological precipitation techniques on the sludge morphology. From the data of the freshwater plants, it was obvious that the biological precipitation resulted in far less sludge than the chemical precipitation, which makes the biological method economically more favourable.

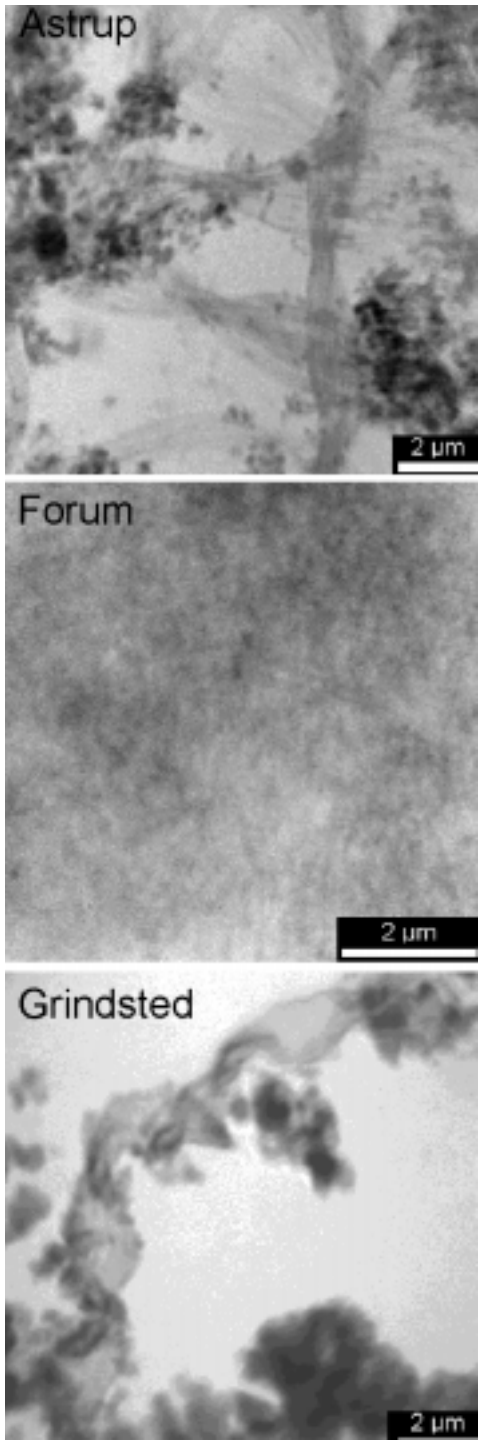

Sludge containing iron oxide precipitates was obtained from three freshwater plants, Astrup, Forum and Grindsted. The fresh water plant in Astrup is the only fresh water plant in Denmark where iron is planned to precipitate biologically. In Forum, the iron is precipitated chemically in the traditional way. The plant at Grindsted was planned to precipitate iron chemically, however, this study shows surprisingly that the iron in the prefilters of Grindsted II is precipitated mainly biologically.

The results will be presented in an article which is currently under preparation and which is aimed to be published in *Water Research*. Here, we present X-ray micrographs of sludge from the three different water plants. The image of the sample from Astrup clearly shows the network of exopolymers to which particles with iron content are attached. Forum has a sludge that appears much more homogeneous in the X-ray microscope, though the colloidal nature of the sample is easily recognised. The sludge from the Grindsted water plant contains a number of different exopolymers that are shaped tube-like (as *Leptothrix*), twisted (as the *Gallionella* type seen in the Astrup sludge), or generally irregular. One of the irregular exopolymers is shown in the third X-ray micrograph.

Morphology Changes During Capacitation in Human Spermatozoa studied with X-ray Microscopy

T.Vorup Jensen[1], T.Hjort[1], J.Abraham-Peskir[2], P.Guttmann[3], J.C.Jensenius[1], E.Uggerhøj[2], and R.Medenwaldt[2]

[1]*Department of Medical Microbiology & Immunology, University of Aarhus*

[2]*ISA, University of Aarhus*

[3]*Forschungseinrichtung Röntgenphysik, Georg-August-Universität Göttingen, Germany and BESSY, Berlin, Germany*

Human spermatozoa are known to undergo changes in the female genital tract from the time of the ejaculate until the act of fertilisation. These changes, called capacitation, are complex involving the motility of the spermatozoa, membrane properties and intracellular metal ion concentrations. One of the characteristics of capacitation is a hyperactivation of the sperm in connection with motility. Capacitated spermatozoa swim more vigorously than freshly ejaculated ones. In microscopic studies, however, the forward progression of capacitated spermatozoa, however, seems to be smaller in spite of the hypermotility, as many spermatozoa tend to swim in circles rather than linearly. An explanation has not yet been given for this phenomenon and no morphological characteristics for the state of capacitation has so far been found.

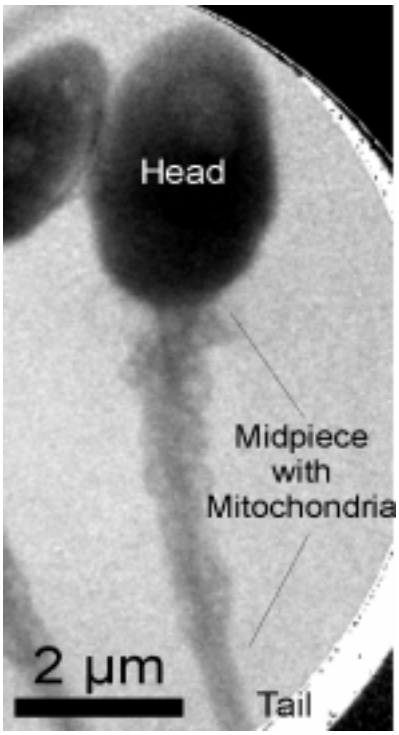

At ISA, we have been studying the morphology of spermatozoa just after ejaculation and in the state of chemically-induced capacitation. A manuscript on this work has been submitted for publication[1].

References:

1 T.Vorup Jensen, T.Hjort, J.Abraham-Peskir, P.Guttmann, J.C.Jensenius, E.Uggerhøj, and R.Medenwaldt, "X-ray Microscopy of Human Spermatozoa Shows Change of Mitochondrial Morphology During Capacitation", accepted for publication in *Human Reproduction.*

Iron and bacteria in Danish soils

Susan Glasauer[1], Christian Koch[2], Per Nørnberg[1], Erik Uggerhøj[3]
[1]*Department of Earth Sciences, University of Århus*
[2]*Department of Chemistry, The Royal Veterinary and Agricultural University*
[3]*Institute for Storage Ring Facilities, University of Århus*

Iron is the most abundant element in the earth as a whole, and the fourth most abundant element in the earth's crust. It is found in many minerals in rocks, sediments and soils; for example, some soils near Silkeborg contain such high concentrations of iron[1] that they were mined for ore a few centuries ago. Iron-bearing springs appear throughout Denmark carrying chemically reduced, mobile Fe to the surface, where it oxidizes and precipitates as reddish, poorly crystalline Fe-hydoxide. Such precipitates have been found to contain high numbers of bacteria that increase the rates of mineral deposition[2]. In soils in general, Fe is found mainly in the form of oxides and hydroxides; these are strong colouring agents (mainly red and yellow) and have a high chemical reactivity[3].

Soil is the major habitat of terrestrial microorganisms, which not only occupy a diversity of phylogenetic and physiological niches there, but also have a high level of activity. This makes microbes critical agents in biogeochemical cycling, and we are just beginning to understand their roles, in particular those of bacteria, in mediating the iron cycle. Traditional methods have generally limited observations to either the microbes or the inorganic mineral substrate with which they appear to associate. Studies combining the two often use destructive preparation and imaging techniques, or have too poor of a resolution for observing the nm-scale changes.

The X-ray microscrope does not have these limitations; furthermore, the ability to image materials in suspensions opens up several possibilities for studying microbe-mineral dynamics. This is because in natural environments, water is essential for growth and dissolution of minerals, and is also a prerequisite for bacterial growth. We will take advantage of this capability to track in-situ transformation of several iron compounds found in the soils near Silkeborg, processes both abiotic and mediated by bacteria. A relatively unexplored aspect of microbially-mediated iron transformation is determining the sites where bacteria attack the minerals. Dissolution studies have been made for abiotic dissolution of iron oxides[4], but little work has been done investigating how bacteria may mediate these reactions. In one study, it was inferred from bacteria-shaped pits on the surface of magnetite, a magnetic iron oxide, that the microbes had etched their way into the mineral[5]. With the realization that microorganisms can dramatically influence mineral weathering processes and thereby affect global element cycling, these kinds of studies are receiving more attention.

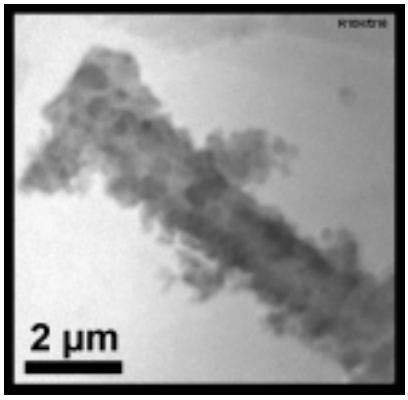

X-ray micrograph of a shell from bacteria involved in iron precipitation in Danish wetlands. The shell is covered with iron containing aggregates.

References

1 Nørnberg, P.; T. Andersen, C. B. Koch and U. Schwertmann. Iron minerals in reddish Danish soils. In prep.
2 Emerson, D. and N. P. Revsbech. Investigation of an iron-oxidizing microbial mat community located near Aarhus, Denmark: Field studies. Appl. Environ. Microbiol. **60/11**, 4022 (1994).
3 Cornell, R. M. and U. Schwertmann: The Iron Oxides. VCH Publishers, Weinheim (1996)
4 Glasauer, S.; J. Friedl and U. Schwertmann:. Properties of goethites prepared under acid and basic conditions in the presence of silicate. In prep.
5 Brown, D. A.; B. L. Sherriff, and J. A. Sawicki:. Microbial transformation of magnetite to hematite. Geochim. Cosmochim. Acta, **61**, 3341 (1997).

Phase contrast studies with the X-ray Microscope

R.Medenwaldt
Institute for Storage Ring Facilities, University of Aarhus, Denmark

In the soft X-ray wavelength region between the absorption K-edges of oxygen (2.4 nm) and carbon (4.4 nm), which is usually called the "water window", there is a large difference between the linear absorption coefficient of water and that of organic matter. Therefore, these wavelengths are suited for imaging of aqueous, biological specimens. Transmission images of this kind of samples have a natural high contrast due to the strong absorption by the carbon and nitrogen containing molecules.

The dominating process in the interaction between soft X rays and matter, however, is not the absorption, but the phase shift. So, use of phase contrast in soft X-ray microscopy has the potential of enhancing the contrast for small features. The method, introduced to light microscopy by Fritz Zernike in the beginning of this century, was applied successfully to X-ray microscopy by G.Schmahl et al. in 1993 [1].

The set-up that is used in phase contrast X-ray microscopy is shown in figure 1. It differs from the absorption contrast configuration by having an annular diaphragm in front of the condenser to define a narrow cone of radiation that is phase shifted in a corresponding ring in the Fourier plane of the objective [2]. The phase shifter is a Ni ring on a 100 nm thick Si_3N_4 membrane [3]. The thickness of the ring is 0.45 µm, which causes a 3.3α/2phase shift. A 3α/2 phase shift is usually used for negative phase contrast. I our case the 10% extra phase shift takes into account the absorption in the specimen and optimises the system for phase shifts by 50 nm thick biological structures in water.

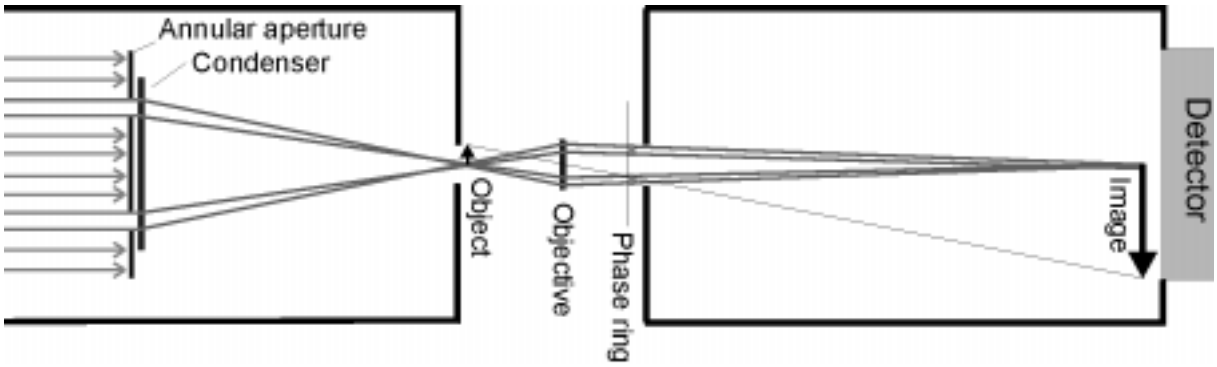

Figure 1: Ray diagram of the X-ray microscope in phase contrast mode.

First tests have been performed with phase contrast and an example is shown in figure 2 showing exopolymers of bacteria in sludge from a water plant in Denmark [4]. It is obvious from the images that the contrast is enhanced in the phase contrast case. The apparent lower resolution in the phase contrast image as compared to the absorption contrast image is partly due to the fact that the 2.5 times longer exposure time causes blurring of the image, because the set-up is drifting slightly. The longer exposure time is needed, because the annular diaphragm in front of the condenser reduces the incoming flux. Due to the reduced flux, the longer exposure time in the phase contrast mode does not lead to a higher dose load on the object as compared to amplitude contrast.

These first studies indicate the effect of phase contrast for structures that have low amplitude contrast in X-ray micrographs. Further investigations are planned to clarify the usefulness of this method in our present and future microscopy projects.

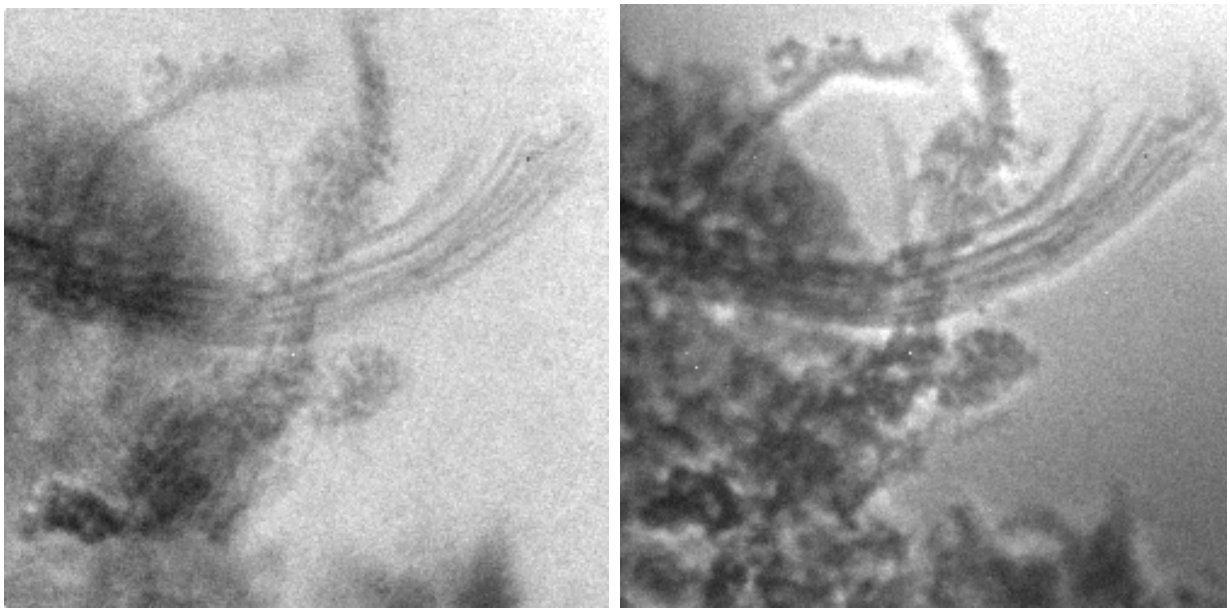

Figure 2: Amplitude contrast (left) and phase contrast (right) image of exopolymers in sludge from a fresh water plant. Imaging times were 2 min. and 5 min. at a wavelength of 2.4 nm.

References:

[1] G.Schmahl et al. pp.196-206 in V.V.Aristov and E.Erko (Eds.), X-Ray Microscopy IV, Proceedings of the 4th International Conference on X-Ray Microscopy XRM'93, Sept. 20-24 1993, Chernogolovka, Russia, (1994).
[2] The micro zone plate has been fabricated by S.J.Spector from SUNY at Stony Brook and D.M.Tennant from Lucent Technologies, USA.
[3] The phase ring has been fabricated by FASTEC (Peter Anastasi), England.
[4] E.Søgaard, J.Abraham-Peskir, and R.Medenwaldt: *Iron Precipitation in Danish Fresh Water Plants*, see contribution elsewhere in this activity report.

Added September 1999:

X-ray microscopy group activities since publication of ISA activity report No. 2. November 1998

1) Activities

The Aarhus X-ray microscopy (XRM) is now a busy multi-user facility and is used for many different scientific investigations, in a diversity of areas: algae, biopolymers, colloidal chemistry, food industry, human sperm, iron-precipitating bacteria, pollen-connecting threads, protozoa and metal toxicity.

Human Spermatozoa

Spermatozoa are proving to be an ideal specimen for study by XRM. Not only do they suit the machine working parameters in terms of thickness, size, and abundance, but they are relatively radiation resistant, showing very little damage after multiple exposures. Surface membranes can be imaged on whole intact cells in seminal plasma or synthetic media. The changes in sperm biochemistry and morphology following ejaculation, but before fusion with the egg, are still being elucidated. XRM investigation of this area has provided an exciting insight into this process.

a Morphological changes of mitochondria with capacitation

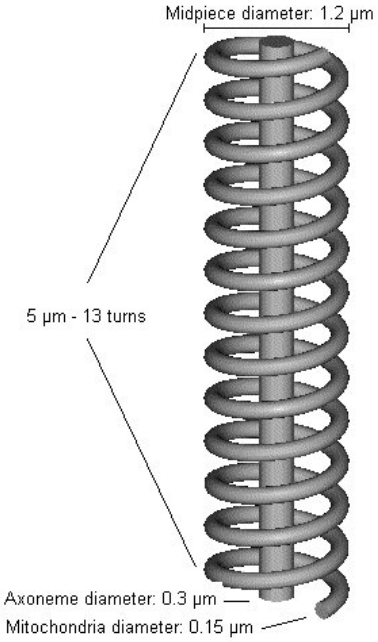

The paper resulting from this work (activity report p65) was published in Human Reproduction and selected out of around 40 papers as the "Outstanding Contribution" Vorup-Jensen et al. 1999.

Figure 1: Model of loosely-wrapped mitochondria and approximate dimensions

b Vesicular bodies and fertilisation process

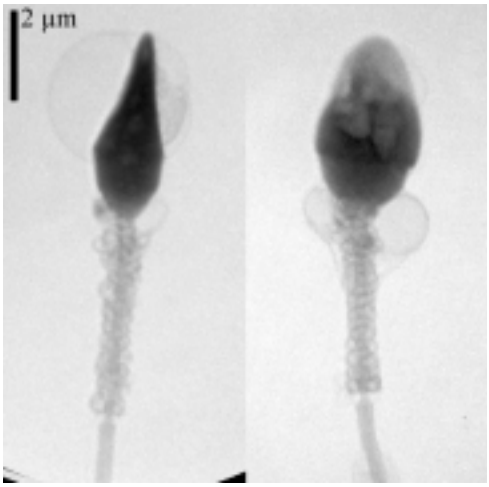

Figure 2: Aarhus XRM image of human sperm in medium

In collaboration with Eric Chantler's group (Academic Unit of Obstetrics & Gynaecology, University of Manchester) we are continuing our study into the function of vesicular structures associated with specific membrane domains of human spermatozoa (Abraham-Peskir et al., 1998). On closer inspection by light microscopy (LM) using high magnification and Nomarski optics the vesicles associated with the mid-piece are clearly visible. Furthermore, the frequency of occurrence is found to be subject dependent and may be of diagnostic significance in conditions that affect the male reproductive tract. Even more exciting is the discovery of vesicular structures associated with the acrosomal region. Biochemical investigations in combination with fluorescence LM and XRM, are being used to determine the physiological function of these vesicular bodies that we think play a central role in fertilisation.

c Sperm binding to zona pellucida

In collaboration with Eric Chantler's group we have made preliminary LM and XRM studies of human sperm binding to human zona pellucida fragments (fragments of the egg's extracellular matrix). The preliminary results obtained support our proposition that the head vesicles seen on human sperm by XRM play an important role in the containment of acrosomal enzymes and/or binding to the zona pellucida of the oocyte. The theory that we have proposed is wholly novel and is a refinement on current dogma that, if substantiated will be of fundamental significance both in the understanding of sperm binding to the egg and in the treatment of infertility.

d Sperm motility and chilling

The fact that sperm are still motile up until the moment the external medium freezes is a fascinating observation considering the sensitivity of the axoneme to low temperature. Here at ISA we have collected data from 5 different donors with known fertility. The Percoll separated samples were cooled in 5 degree increments down to 5 degrees using a Peltier cooling stage and recorded onto video. These video recordings were sent to Eric Chantler's group for CASA (computer-aided sperm analysis) which tracks individual sperm cells and then calculates a number of parameters characterising the kinematics (time-dependent geometry) of sperm motion. Preliminary findings show an unexpected complete recovery of motion parameters following stepwise chilling to 5 degrees. This work is being extended to include studies of function in Eric Chantler's laboratory and will have significance in processing of sperm in IVF.

e Effect of acute and chronic exposure to ionising radiation on human sperm

We have recently begun a 6 month collaboration (in the first instance) with Prof. V Grieschinka from the Institute for Cryobiology and Cryomedicine at the Ukrainian Academy of Science, Kharkov, Ukraine. He will send samples of cryopreserved sperm from a group of liquidators who lived in Kharkov and worked at Chernobyl, men evacuated from Chernobyl but who had remained there for one week after the accident and men rescued from the polluted areas after five years. Access to such material is extremely rare making this is a very privileged and exciting opportunity.

f Effects of electromagnetic radiation emitted from cellular phones on male fertility potential

We have recently applied for EU funding within the Framework 5 program with Eric Chantler, University of Manchester; Prof. Benjamin Bartoov, Faculty of Life Sciences, Bar-Ilan University (BIU), Ramat-Gan, ISRAEL and CRYOS International Sperm Bank, Aarhus, Denmark. ISA's budget is for 524 160 ecu over a three-year period.
This three-year study seeks to evaluate the effect of a regular and quantified exposure of both human males and rams to UHF radiation at those frequencies, radiated power and method of modulation that are used by mobile telephones. The study will be directed to the evaluation of changes that may occur as a result of such exposure on male reproductive function. The whole of the pituitary-testicular axis can be sensitive to UHF radiation, consequently pituitary gonadotrophins, testicular steroid production and sperm output and function will be measured. X-ray microscopy will form a large portion of the project.

Figure 3: DIC light microscopy image of a bovine sperm. Bar = 4µm.

g Bull sperm

As part of the work with Eric Chantler's group we have made useful contact with Taurus Syd, Randers which is a bull farm used specifically for collection of bull sperm for breeding programs. They have over 500 bulls and have agreed to provide free samples of bull semen. In contrast to EM findings, which report that cryopreservation of bovine sperm causes severe disruption of the plasma lemma, we have found using XRM that fresh bovine sperm also display plasmalemma disruption. We have already studied a number of different bull semen samples and found similar levels of plasmalemma disruption using both LM and XRM. This work is on-going and will be especially interesting to the veterinary community and will therefore be submitted to a veterinary journal. It supports the hypothesis that the presence of vesicles on sperm is a normal occurrence and not restricted to humans. Bull sperm is a useful model as, unlike its human counterpart, it shows a low level of morphological variation and has high quality with good fertility.

Myeloid Stem Cell Apoptosis

The growth factor dependent FDCP-mix cell line is a non-leukaemic, karyotypically normal, multipotential myeloid stem cell with the capacity to undergo in vitro differentiation into all the myeloid lineages including erythrocytes. Furthermore, it has been shown that withdrawal of haemopoietic growth factors (Interleukin-3) induces >80% of these cells to undergo apoptosis within 24 hours. This phenomenom has been studied by the use of light and electron microscopy which has indicated that alterations in mitochondrial numbers/mass are early changes in the apoptotic process. X-ray microscopy has provided a new method for the investigation of this phenomenom giving high resolution images of living rather than fixed cells. In the preliminary studies of Run 13 we imaged normal FDCP-Mix cells. The cells were washed, re-suspended in the medium minus IL3, and incubated for 24 hours. Samples of cells were withdrawn for X-ray microscope imaging at various time points during this incubation.

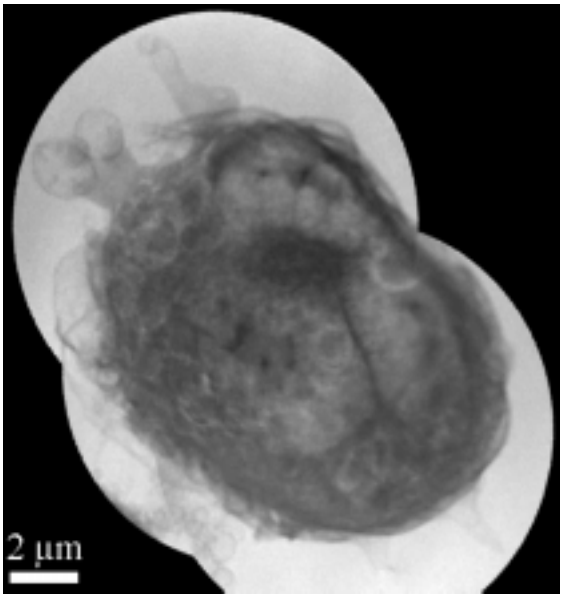

Figure 4: XRM image of a myeloid stem cell undergoing apoptosis, No fixation, no staining.

Micro-organisms

a Algae

Together with the School of Biological Sciences, University of Manchester, UK, we are conducting structural studies on a variety of blue-green algae. We are particularly interested in the effects of nutrient conditions, such as phosphorus and nitrogen. The project includes the association of bacteria with the algae and the role of algal mucilage in bacterial adhesion processes. The blue-green algae play an important role in nutrient recycling in the fresh water environment. Fluctuations in species composition and population densities can have far reaching effects, with sporadic toxic algal blooms causing extensive destruction of ecosystems resulting in the death of many higher organisms such as fish.

b Protozoa

In recent years, research using protozoa has flourished because biologists have recognised that these organisms provide excellent subjects for studying biological phenomena at the cellular level. So far, ultrastructural studies of micro-organisms have been limited to the EM. Despite the high resolution obtained with conventional EM, shrinkage is unavoidable during the preparation of many samples. With XM, the sample can remain free-swimming in solution throughout imaging, thus reducing artefact caused by dehydration of the sample. Here at ISA, we are studying metal toxicity in the flagellated protozoon, *Chilomonas paramecium* commonly found in polluted water (Abraham-Peskir, 1998).

Soil Science

The influence of modern agriculture on the soil structure was being investigated with The Royal Veterinary & Agricultural University in Copenhagen. We studied different soils (alfisols and vertisols from Denmark and India) at the colloidal level.

Material Science

We have made preliminary studies of cement in collaboration with the Industrial Materials Group, Department of Crystallography, Birkbeck College, London. During the preliminary stages of cement hardening, needle-like crystalline growth of the mineral ettringite is seen to occur rapidly. Ettringite is implicated in the setting properties of cement but not its final strength. This is mainly determined by a much slower growth of amorphous hydrates. Studies of cement hydration with and without retarders have clearly shown differing behaviour in crystalline growth.

Iron-precipitating bacteria

In collaboration with the Department of Earth Sciences, University of Aarhus, a project has been started on iron-precipitating bacteria (activity report p66). In many Danish wetlands, deposits with a large content of iron - in Danish called "myremalm" - can be found. Melting iron out of these deposits went on from the Iron Age until the last century. The natural precipitation process is thought to be connected with the occurrence of bacteria. This work is also linked to the Mars project, a joint collaboration between the Universities of Aarhus and Copenhagen who plan to analyse soil collected from Mars.

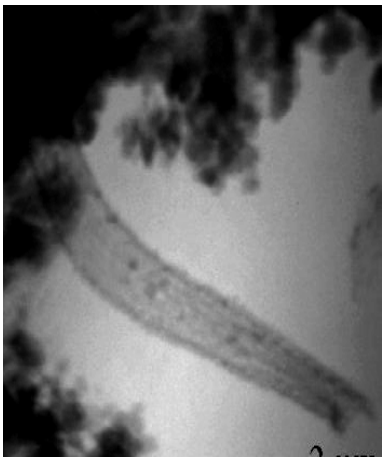

Iron sludge
Around Esbjerg, Denmark, there are high levels of iron in the ground water. The iron has to be removed before distribution for drinking water. The biological treatment of drinking water is more efficient than chemical treatment. With the Department of Chemistry, Aalborg University, Esbjerg, we have characterised the morphology of the different types of precipitated sludge and determined the kinds of bacteria involved in the oxidation of iron (Søgaard et al., 1999).

Figure 5: XRM image of exopolymer sheath left by an iron-precipitating bacteria

Industrial-based projects

Danisco Ingredients have been using the XRM at Aarhus for 18 months as part of an investigative project of substances used in the manufacture of their food stuffs. More recently Unilever Research of Lever Brothers Ltd. have expressed an interest in using the XRM.

2) Student Projects
Jette Wendt-Larsen Diploma Student
Title 'Metal Induced Changes in *Chilomonas paramecium* Investigated by X-ray and Light Microscopy'. Graded 11
The research involved both physics and biology and incorporated a variety of imaging techniques. Jette located sites of metal uptake and accumulation and quantified the associated ultrastructural changes in *Chilomonas paramecium*, without altering the environment of the cells or introducing artefact-inducing procedures. Therefore, cells were fully-hydrated throughout the study which used a combination of DIC LM, confocal LM and transmission XRM. For confocalmicroscopy the relatively new fluorochrome Newport Green was used. This made fluorescent complexes with excess levels of intracellular Zn^{2+} and Al^{3+}, allowing localisation of metal-containing granules. The results gave new information about the toxicity response to Zn^{2+} and Al^{3+} in otherwise untreated cells. A manuscript on some of the work has been submitted for publication (Wendt-Larsen et al., 1999).

Ion Storage Activities

High-resolution VUV spectroscopy of H^- in the region near the H(n=2) threshold

P. Balling, H. H. Andersen, P. Kristensen, U. V. Pedersen, V. V. Petrunin,
M. K. Raarup, P. Steiner, and T. Andersen.
Institute of Physics and Astronomy, University of Aarhus, DK-8000 Aarhus C, Denmark

The attachment of an additional electron to a neutral atom is normally characterized by the short-range force acting on the electron. The associated potential can only hold a finite number of bound states, which means that the structure of negative ions is very different from that of neutral atoms or positive ions, where the Coulomb potential gives rise to an infinite Rydberg series. Laser spectroscopy of negative ions is devoted to the observation of excited states that are located in the continuum of the system and that give rise to resonances in the photodetachment cross section.

The negative hydrogen ion is an interesting system due to its three-body nature and the study of the system has been closely linked to the understanding of negative ions. In addition, the unique properties of the hydrogen atom give rise to an infinite series of resonances for this particular negative ion: the mixing of degenerate angular-momentum states by the electric field of a distant electron results in an asymptotic long-range dipole tail of the potential seen by the electron. This potential holds a series of resonances that converge exponentially to the neutral atom threshold and their positions and widths satisfy very specific recurrence relations.

The photodetachment cross section of H^- has been measured in the region near the H(n=2) threshold, located approximately 11 eV above the ground state of the negative ion [1,2]. A comparatively high resolution in this region was achieved by applying a narrow-bandwidth fixed-frequency vacuum-ultraviolet laser beam (118 nm) collinearly overlapped with a ~1 MeV H^- beam stored in ASTRID. Tunability was achieved through the Doppler effect by tuning the velocity of the stored ions. The resulting resolution of 180 ΣeV was determined by the velocity spread of the accelerated ion beam, $\Delta v/v = 4 \approx 10^{-4}$, and represented an improvement in resolution of almost two orders of magnitude compared to previous studies.

The relative photodetachment cross section measured [2] for D^- is shown in figure 1, together with a recent calculation [3]. (The same structures in the cross section were observed for H^-.) The data show two narrow resonances below the H(n=2) threshold and one broad resonance above. The two narrow resonances are the first two members of a dipole-like series converging to H(n=2) (denoted by the collective quantum numbers ${}_2\{0\}_m^- {}^1P^0$,m=3,4,...) The present technique allowed the first observation of the second of these resonances and therefore enabled predictions about the remaining part of the series.

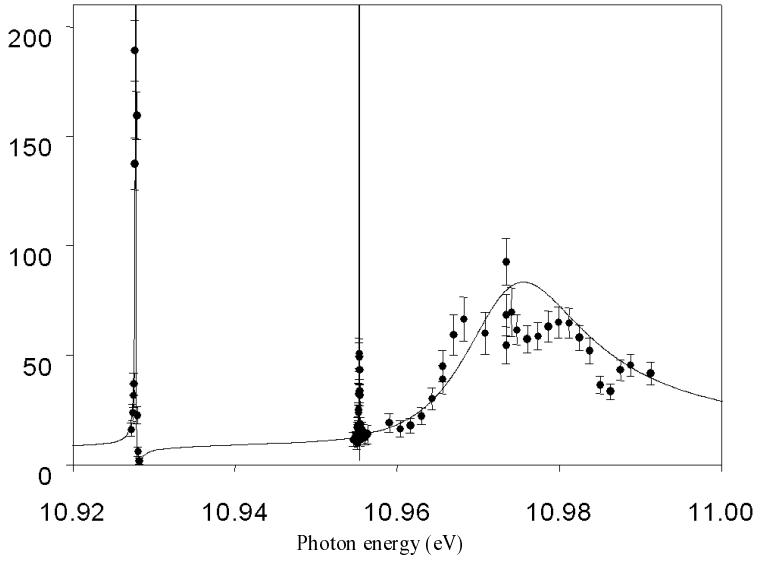

Figure 1: Relative photodetachment cross section (see text)

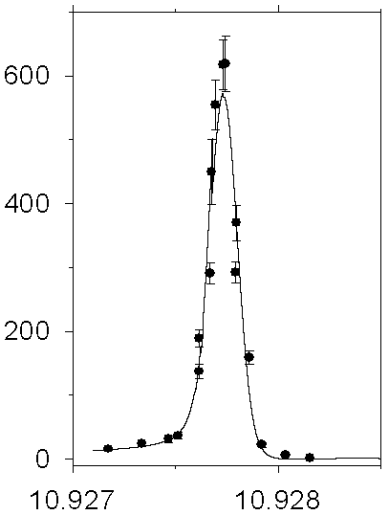

Figure 2

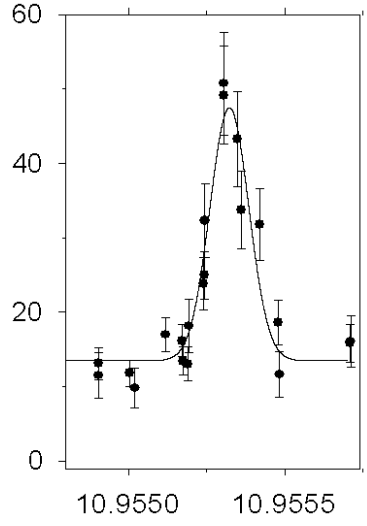

Figure 3

In fact, theoretical investigations predict that only one more member should exist, since the series is truncated by the relativistic splittings of the of the H(n=2) state (Ref. 2 and references therein). Blow-ups of the two resonances are shown in figures 2 and 3. The $_2\{0\}_4^-$ resonance (fig. 3) is predicted to be as narrow as ~2 ΣeV, which is consistent with the observation that the measured data are fit well by a Gaussian function, representing the velocity distribution of the ions. On the other hand, although the predicted width of the $_2\{0\}_3^-$ resonance (fig. 2) is lower than the present resolution, the asymmetry of the resonance (Fano profile) is clearly visible in the experimental data. A fit to a convolution between a Fano profile and the Gaussian resolution provides constraints on the resonance parameters [2].

The accurate position measurements of the two resonances obtained by this study has allowed a critical test of current theoretical developments (see Ref. 2). In particular, the ability to perform the experiment with both H^- and D^- has permitted a study of the isotope shift of the resonances. The observed shift in resonance positions could be reproduced by accounting for the proper reduced mass, which is consistent with calculations of a very small mass polarization for the resonances.

Since the resolution in the experiment is limited by the Doppler spread, the present development of the technique is closely linked to technical developments at ASTRID. In order to achieve the upcoming scientific goals, which comprise an identification of the third member in the series and a measurement of the true width of the $_2\{0\}_3^-$ resonance, it is necessary to reduce the velocity spread. Applying electron cooling of the negative ion beam can do this, but this development has been challenging and only recently successful, primarily due to the short storage times of the negative ions.

In summary, the application of Doppler-tuned collinear laser spectroscopy has allowed the observation of the first two members of the $_2\{0\}_m^-\ ^1P^0$ series. The measured isotope shift of resonance positions between H^- and D^- evidence a small specific mass shift. An improved resolution will allow a future study of the $_2\{0\}_5^-$ resonance, which is predicted to terminate the dipole series.

VUV laser spectroscopy of the H^- ion.

The negative hydrogen ion H^- plays a special role in the investigation of atomic systems as one of the few available three-body systems. The study of structural and dynamic properties of H^- can lead to an improved understanding of the strong electron correlation which governs the behaviour of many negative ions, including H^-, and also to a useful nomenclature of features which cannot be described within the independent electron model The structure of the H^- ion is revealed as resonances in the photo-detachment cross section, corresponding to doubly excited states of the negative ion, where both electrons are promoted to spatially extended orbits. Previous studies have been limited to the broad shape-type resonances, whereas the present ones focus on the narrow Feshbach-type resonances, the spectroscipic properties of which position, width, and shape are the ideal properties to test and guide the ongoing theoretical development.

Research goals:
Observation and characterisation (position, width, and shape parameters) of the ^{1}P resonances, located below or just above the H(n=2) threshold by means of a new spectroscopic technique based on Doppler-tuned spectroscopy in a collinear geometry.

Results:
This project has involved development of an intense VUV radiation laser source (118 nm), which is overlapped collinearly with the H^- ions in ASTRID over a distance of 8 m. The photo-detachment cross section has exhibited a rich spectrum of doubly excited ^{1}P resonances near the H(n=2) threshold. The position of the resonances has been determined with an accuracy that challenges the current theoretical developments. The observations are used to predict the behaviour of a dipole series below H(n=2). Measurements on both hydrogen and deuterium facilitated a study of isotope effects. By means of momentum-spread-reduction technique (electron cooling) it has just been possible to resolve the natural linewidth of the narrow dipole resonances. The results obtained have stimulated new theoretical activity in the H^- ion.

[1] P. Balling *et al.*, Phys. Rev. Lett. **77**, 2905 (1996).
[2] H. H. Andersen *et al.*, Phys. Rev. Lett. **79**, 4770 (1997).
[3] E. Lindroth, Phys. Rev. A **52**, 2737 (1995).

Clusters in storage rings

J.U. Andersen, K. Hansen, P. Hvelplund, T.J.D. Jørgensen and M.O. Larsson.
Institute of Physics and Astronomy
University of Aarhus, DK – 8000 Aarhus C, Denmark

Anions of fullerenes and small metal clusters have been stored in the storage rings ASTRID and ELISA. Decays on a millisecond time scale are due to electron emission from metastable excited states. For the fullerenes the decay curves have been interpreted in terms of thermionic emission quenched by radiative cooling.

The negative clusters were produced in a plasma source or in a sputter source and were accelerated and mass selected before injection into the ring at an energy around 50 keV. The rate of neutral particles detected behind one of the dipole magnets was then recorded as a function of time after injection and a so-called lifetime spectrum was obtained. The clusters are normally "born" in the ion source with a broad distribution in internal excitation ('temperature') and the decay of hot clusters by electron emission is observed. The injected clusters can also be heated in the ring in one of the straight sections with the beam from a Nd:YAG laser or an OPO pumped by this laser. At present, the first test experiments have been performed on ELISA with C_{60}^- and improved short time ($\approx$ 1 ms) information has been obtained as compared to similar measurements at ASTRID. We are currently testing an electro-spray ion source[1] for production of multiply charged biomolecules and plan in the near future to install this ion source on ELISA in order to study free protein molecules. Both the spontaneous decay of hot, metastable molecules and decay induced by laser excitation can be measured, in analogy to the cluster studies.

Statistical description of the decay and cooling of stored ions

Only if the injected cluster ions are stable against all forms of spontaneous particle decay will the evolution of the number of stores particles be described by a simple exponential time dependence due to destruction in collisions with the rest gas. If clusters possess internal energy, decay channels such as unimolecular fragmentation and thermionic emission open up.[2] Figure 1 shows the decay of stored C_{60}^- ions in the millisecond range after subtraction of the nearly constant contribution from rest-gas collisions. The rapid decay on the millisecond time scale is caused by electron emission, since the electron affinity of C_{60} (2.7 eV) is much smaller[3,4] than

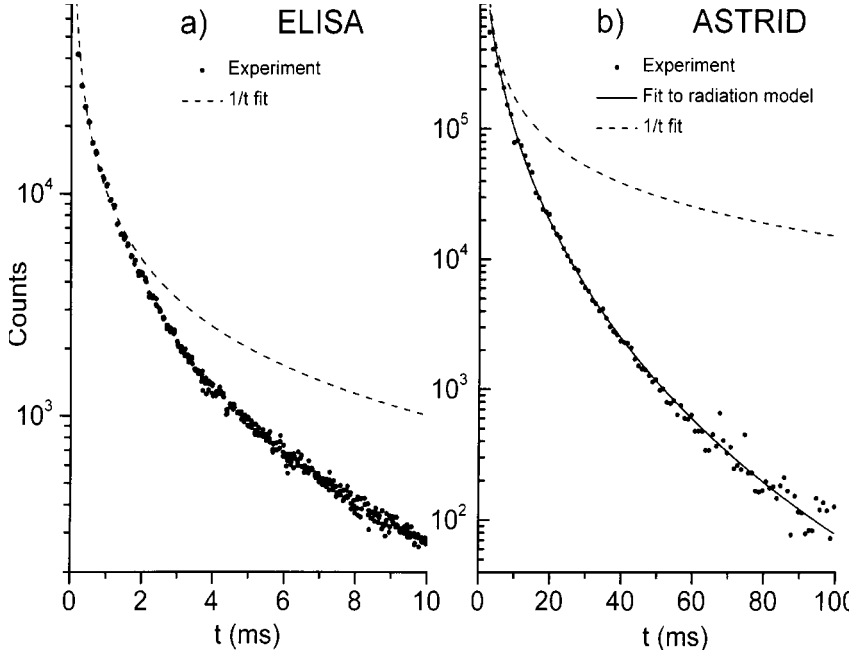

Figure 1. *Rate of decay by thermionic emission of a stored C_{60}^- beam. A contribution from collisions with the rest gas has been subtracted.*

the activation energy for unimolecular fragmentation ≈ 10 eV.[5]
The functional form of the decay rate at short times carries information about the internal state of the clusters and the development of that state over time. In the atomic case, when all or a fraction of the ions are in a well-defined metastable state, the decay is described by a single exponential. If several metastable states are populated, the decay function will be more complicated, containing exponentials with different lifetimes. However, in the limit, where many states are populated, with a broad distribution of lifetimes, the decay function again becomes simple and the decay is described approximately by a t^{-1} law.[2,6]

This description may be expected to apply to negative fullerene ions stored in ASTRID or ELISA. In the ion source, the clusters are bombarded with electrons, and the extracted negative ions have a broad distribution in excitation energy. Furthermore, even at moderate excitation energies, the vibrational level density is enormous. With the new storage ring ELISA we have extended our earlier measurements at ASTRID to shorter times, as seen in Fig. 1a. In the range 0.2 – 1 ms, the expected t^{-1} law is seen to describe the decay quite well, while the signal decreases faster at longer times. The results from ASTRID in Fig. 1b illustrate the nearly exponential decrease in the millisecond range. We have interpreted this as evidence for radiative cooling of the hot clusters.[2]

The curve through the data points in Fig.1b is a fit calculated from a statistical model of the competition between electron emission and cooling. The radiation intensity is about 190 eV/s

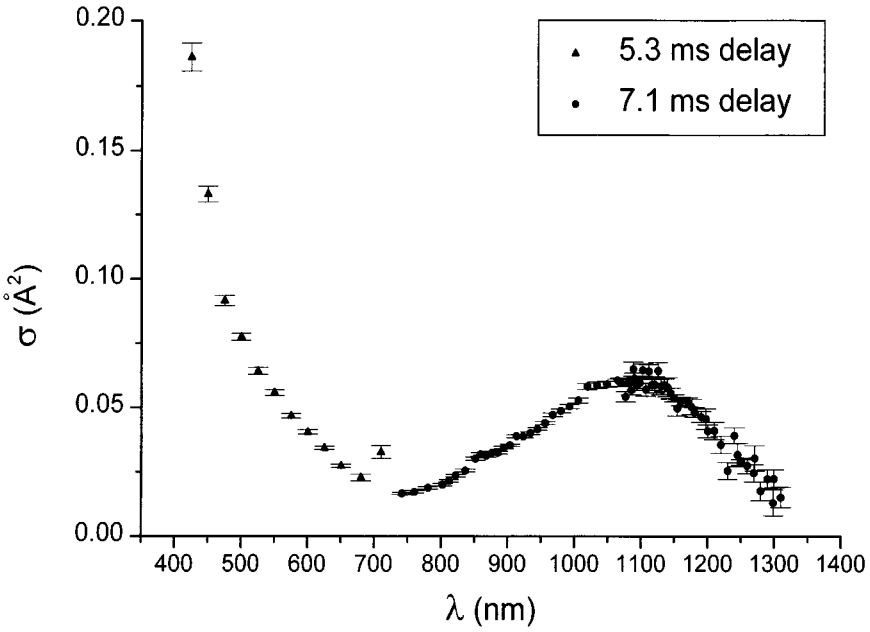

Figure 2. *Photon absorption cross section as a function of laser light wavelength at a laser firing time around 5–7 ms.*

at an internal temperature of 1500 K and is approximately proportional to T^7. The major contribution to the radiative cooling comes from a thermally stimulated transition at 1.16 eV of the electron attached to C_{60} to form the anion[7,8] In the following, we describe a spectroscopic study of absorption of radiation by this transition in hot C_{60}^- molecules.

Thermionic emission laser spectroscopy of C_{60}^-

Thermionic emission of electrons from clusters is enhanced by absorption of photons. The process can therefore be used to monitor the wavelength dependence of the photo-absorption cross sections of hot molecules and clusters.[9] A stored C_{60}^- beam can at a preselected time be irradiated with a pulse from a tunable, Nd:YAG pumped OPO laser. The resulting enhanced electron emission, measured with a ≈ 200 μs delay, reflects the photon absorption cross section. The absorption strength decreases with photon wavelength up to 700 nm, followed by a broad absorption peak around 1070 nm (Fig. 2). This absorption peak has been studied extensively for

C_{60}^- ions at lower temperature, for example for C_{60}^- in solution[7,8] and the data in Fig. 2 have been normalized to give the same peak area as obtained in those experiments. The peak is ascribed to the lowest transition ($t_{1u} \rightarrow t_{1g}$) of the additional electron in the anion. Strong sidebands at shorter wavelengths have been observed, corresponding to vibrational excitation. At the high temperatures of the stored ions (≈ 1400 K according to the analysis illustrated in Fig. 1b), such excitations should be stronger because dipole matrix elements increase with excitation of an oscillator, $|<n+1|x|n>|^2 \leq n+1$, and also hot bands with vibrational deexcitation should be observed. These expectations are consistent with the observed, very broad absorption peak. We had hoped to be able to deduce a temperature from the asymmetry between the sidebands corresponding to vibrational excitation and deexcitation, respectively, but since the sidebands are not resolved there is a large uncertainty in the analysis from the broadening and a possible shift of the central electronic transition.

References:

1 Fenn, J. B., Mann, M., Meng, C. K., Wong, S. F. and Whitehouse, C.M., Mass. Spec. Rev. **9**, 37 (1990).

2 Andersen, J. U., Brink, C., Hvelplund, P., Larsson, M. O., Bech Nielsen, B., and Shen, H., Phys. Rev. Lett. **77**, 3991 (1996).

3 Wang, L.-S., Conceicao, J., Jin, C., and Smalley, R. E., Chem. Phys. Lett. **182**, 5 (1991).

4 Brink, C. Andersen, L. H., Hvelplund, P., Mathur, D., and Voldstad, J. D., Chem. Phys. Lett. **233**, 52 (1995).

5 Hansen, K. and Echt, O., Phys. Rev. Lett. **78**, 2337 (1997).

6 Hansen, K. and Campbell, E. E. B., J. Chem. Phys. **104**, 5012 (1996).

7 Greaney, M. A. and Gorun, S. M., J. Phys. Chem. **95**, 7142 (1991).

8 Lawson, D. R., Feldheim, D. L., Foss, C. A., Dorhout, P. K., Elliott, C. M., Martin, C. R., and Parkinson, B., J. Electrochem. Soc. **139**, L68 (1992).

9 Hansen, K., Andersen, J. U., Cederquist, H., Gottrup, C., Hvelplund, P., Larsson, M.O., Petrunin, V. V. and Schmidt, H. T.: Thermionic emission laser spectroscopy of stored C_{60}^-. To be published.

Laser Cooling of a Stored Ion Beam

N. Kjærgaard[1], N. Madsen[1] , J. S. Nielsen[2], P. Bowe[1],
M. Drewsen[1], L. Hornekær[1], A. Labrador[1] and J. Hangst[1].
[1]*Institute of Physics and Astronomy, University of Aarhus*
[2]*Institute for Storage Ring Facilities, University of Aarhus*

Recent work [1,2] has been devoted to the studies of longitudinal to transverse coupling of a laser cooled beam of 100 keV $^{24}Mg^{+}$ ions stored in ASTRID. The experiment utilizes an ultraviolet optical transition at 280nm in $^{24}Mg^{+}$ to obtain interaction between the ion beam and a continuous wave (CW) laser beam. Ultraviolet laser light is made by second harmonic generation (SHG) in KDP crystals of tunable 560nm dye lasers pumped by Argon ion lasers. The KDP crystals are placed in specially designed external cavities for power enhancement [3].

For a coasting ion beam the cooling can be achieved by merging it coaxially with a co- and counterpropagating laser beam in a straight section in ASTRID (fig. 1).
Both lasers are detuned a little towards red from the resonance frequency of an ion with the ideal longitudinal momentum. Slower and faster ions will scatter photons from the co- and counterpropagating lasers respectively due to the Doppler shift and hence their longitudinal momentum is corrected towards the ideal one. In this so-called *Doppler cooling* scheme longitudinal beam temperatures of a few Kelvin are routinely obtained [4].

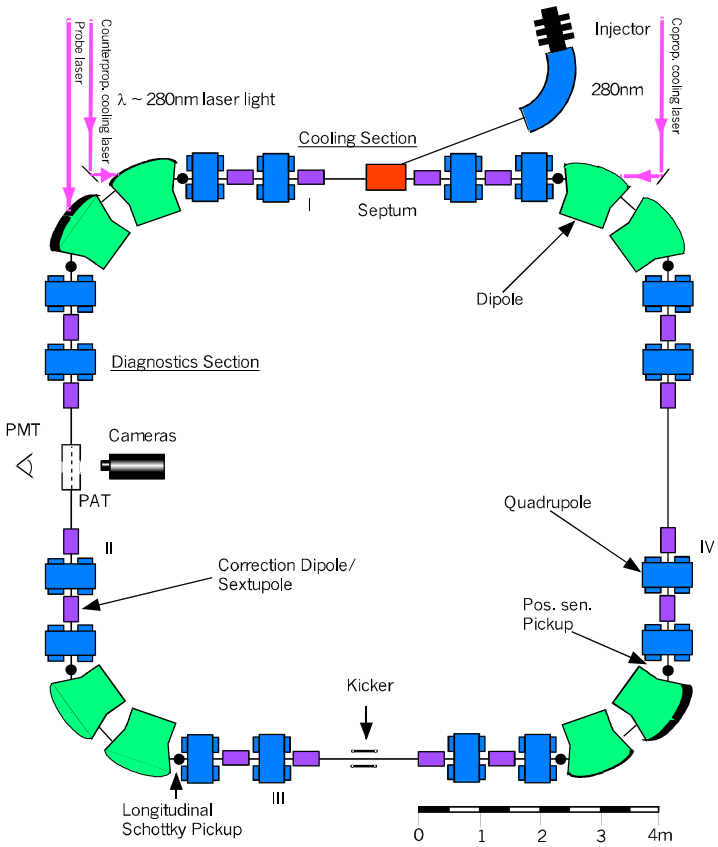

***Figure 1**: Schematic drawing of the experimental setup used for laser cooling of a coasting beam in ASTRID.*

Doppler cooling only affects the longitudinal momentum distribution of the ion beam directly. However, due to the Coulomb interactions between the ions, momentum can be transferred from the transverse dimensions of the beam to the longitudinal one, where the Doppler cooling mechanism works. This coupling leads to so-called *sympathetic cooling* of the transverse dimensions, which can be characterized by the emittance of the beam (it is not very meaningful to assign a transverse temperature in terms of the transverse mean kinetic energy of the ions, since this changes around the ring due to the varying focusing). If knowledge of the local beta function is assumed, the emittance can be found by either monitoring the transverse velocity distribution or the transverse beam size, and in the experiments so far we have used the latter method. The transverse beam size is measured fully nondestructively in a diagnostics section (fig. 1) by actually taking pictures of the ion beam, illuminating it with resonant light from a probe laser. This is done both in the horizontal and vertical dimensions by means of two high resolution, low noise CCD cameras described in detail in a previous ISA activity report [5]. An example of measured transverse profiles in the case of cooled and uncooled beams of about $6 \cdot 10^{7}$ particles is shown in fig. 2.

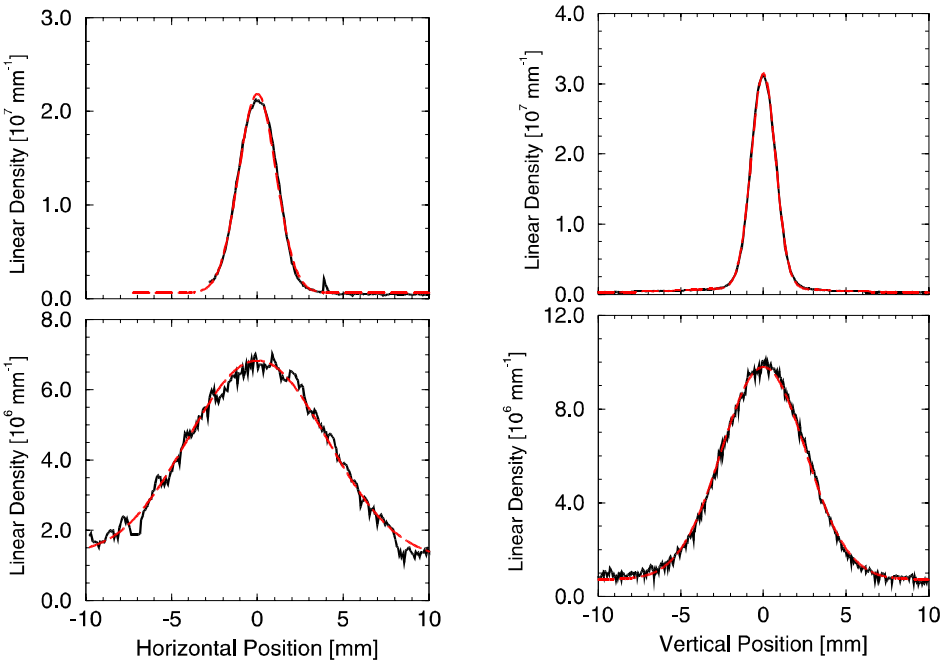

Figure 2: *The horizontal/vertical transverse profiles in case of a cooled (upper left/right) and an uncooled beam (lower left/right).*

The probe laser induced fluorescence is furthermore used for longitudinal velocity diagnostics by measuring the scattered photon yield inside a post acceleration tube (PAT) excited by a DC voltage. This PAT shifts the ions locally in velocity and the longitudinal velocity distribution is readily observed when sweeping the voltage of the PAT and bringing different velocity classes into resonance with the probe laser.

The longitudinal beam temperature can be chosen by the detuning of the cooling lasers. Fig. 3 shows the development in transverse beam sizes as functions of the number of particles circulating in the ring for a fixed longitudinal momentum spread (relative) of $\alpha p/p \sim 5 \cdot 10^{-5}$.

It is seen from fig. 3, that the scaling behaviour is well described by a square root

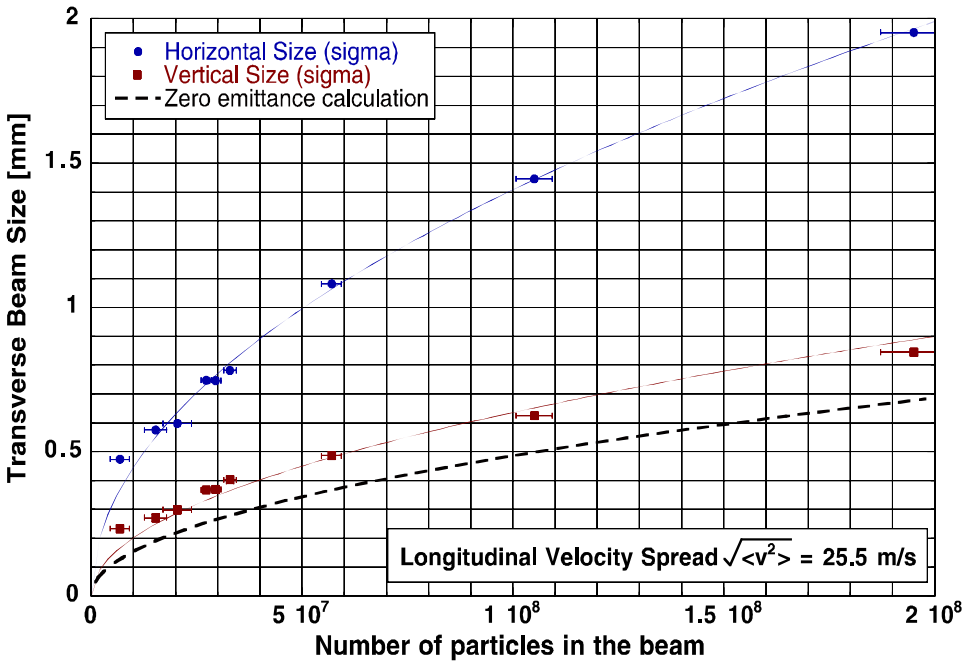

Figure 3: *Transverse beam sizes for a laser cooled ion beam as functions of the number of stored ions. The solid curves are square root fits. The dashed curve shows the calculated size of a zero emittance beam.*

dependency on the number of particles. The figure also shows the result of a calculation of the transverse size for a zero emittance, uniform density beam using a ring averaged focussing force. This zero emittance beam is clearly seen to be smaller than the measured beams.

The reason that a zero emittance beam is not reached in the experiment is believed to be due to the fact that the laser cooled beam is in a highly space charged dominated state leading to a *space charge tune shift* towards a resonance in the pseudo-sinusoidal oscillations (*betatron-oscillations*) of the ions in the magnetic lattice of the storage ring. Hence pertubations from field imperfections can add coherently giving rise to heating of the beam. The apparent limits on the ion beam size/density observed, are then likely to be interpreted as an equilibrium between this heating mechanism and the sympathetic cooling of the beam. Whether or not it is possible to cross such a resonance is not known at present, and the answer to this question is of crucial importance when trying to take further steps towards a crystalline beam [6]- the ultimate in density.

The sympathetic cooling has turned out to depend strongly on the position of the cooling lasers in the ion beam, and so it is possible to have good cooling in one transverse dimension while the other remains hot. Therefore, the ability to monitor both transverse dimensions *simultaneously* has proven to be of vital importance for this experiment. This position dependency imposes severe demands to both the lasers and the operation of the ring. The laser system is about to be upgraded with servo controlled mirrors for positioning and stabilization of the cooling lasers. Moreover new cavities based on the Bow Tie scheme are constructed for SHG using BBO-crystals, which are expected to provide nicer laser beam profiles than the presently used. With these improvements in the laser setup, it should be possible to follow the theoretical [7] and experimental trend [8] towards studies of dispersion effects.

Added September 1999:

For a fixed injected current we have observed that the transverse beam sizes develop plateaus as the cooling lasers are detuned blue and the beam gets longitudinally colder. Fig. 4 shows the transverse sizes and the corresponding longitudinal beam temperatures for different detunings measured 4 s after injection. The occurrence of plateaus supports the interpretation of the previously observed current scaling behaviour of transverse sizes as a result of resonant heating from the magnetic lattice of the storage ring. A strong resonant heating as a result of a space-charge tune shift may prevent the beam from being sympathetically cooled transversely even though the beam is effectively cooled longitudinally. Evidently, the sympathetic cooling mecha-

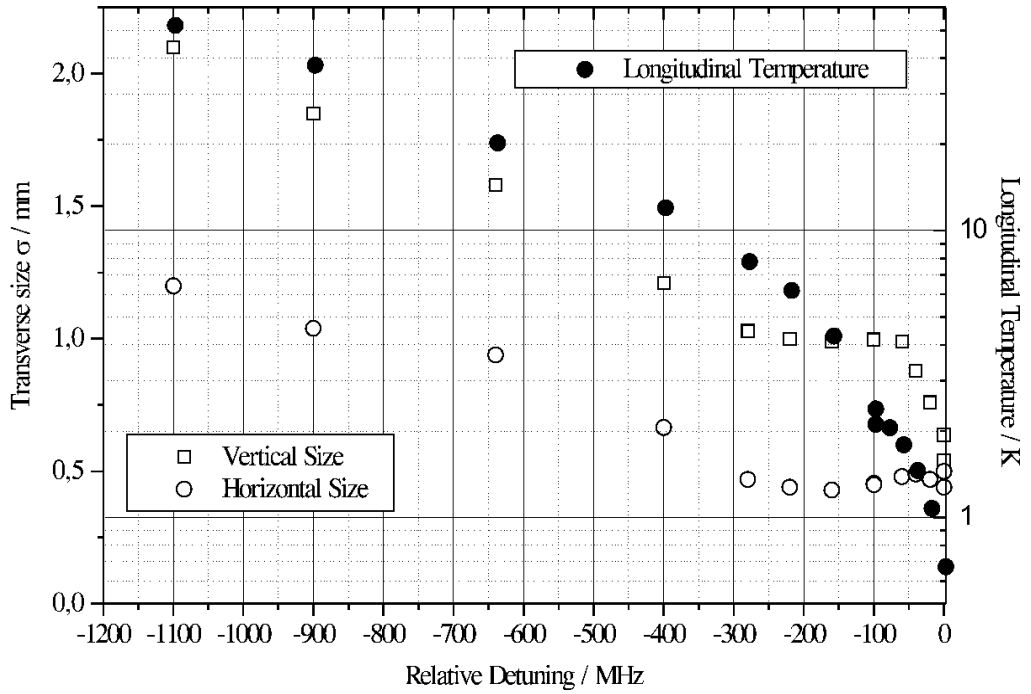

Figure 4: The transverse beam sizes 4s after injection as function of cooling laser detuning for an injected current of 400 nA. Also shown is the corresponding longitudial temperature.

nism is too weak to couple heat into the cold longitudinal dimension at an appreciable amount at the onset of the resonance. The apparant drop in horizontal beam size after the plateau is caused by the loss of particles from a narrow velocity distribution when the two cooling lasers get too close in frequency, and is not to be attributed to a sudden reduction in the total beam emittance.

As something completely new, we have recently implemented real time monitoring of the transverse dimensions of the laser cooled ion beam using a fast digital camera with a high resolution image intensifier. Real time diagnostics of an ion beam done in this way represents a major step forward, and has already given rise to exciting discoveries. Fig 5 shows the development in transverse sizes for a laser cooled ion beam of injected current ~ 40 nA as the beam decays due to collisions with the residual gas in the storage ring. At a time ~ 110s after injection, we notice a blow up in the vertical size of the ion beam whereas the horizontal size stays small. This might be explained by the fact, that as the number of beam particles is reduced, the sympathetic cooling of the transverse dimensions looses its significance. The reason that the beam stays horizontally small can be attributed to a dispersive cooling mechanism (see ref. [7,8]) working only the horizontal plane where so-called dispersion is present due to the bending of the circulating beam. In the vertical dimension where dispersion is essentially absent, no such cooling mechanism exists, and the emittance will start to grow when the number of particles is too small to effectively couple the spatial dimensions through intra-beam scattering.

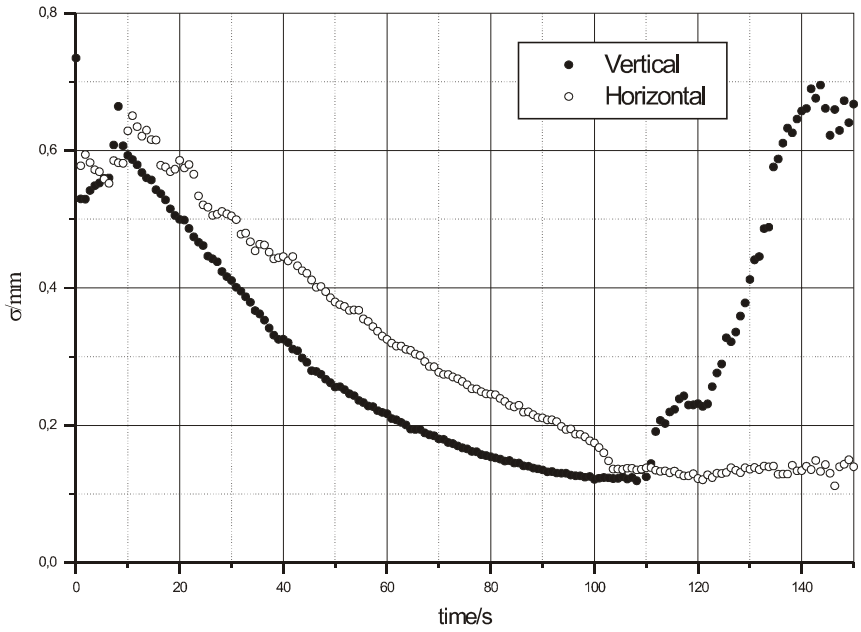

Figure 5: The transverse beam sizes as the ion beam decays. At time ~ 110s after injection the vertical dimension starts to blow up while the horizontal dimension of the beam remains small. The injected current is about 40 nA.

References:

1 N. Madsen, P. Bowe, M. Drewsen, L. Hornekær, N. Kjærgaard, A. Labrador, J.S. Hangst, J.S. Nielsen, P. Shi and J.P. Schiffer, EPAC`98, IOP Publishing, June 1998, p. 1046.

2 N. Madsen, P. Bowe, M. Drewsen, L. Hornekær, N. Kjærgaard, A. Labrador, J.S. Hangst, J.S. Nielsen, P. Shi and J.P. Schiffer, EPAC`98, IOP Publishing, June 1998, p. 1043.

3 J.S. Nielsen, Optics Letters **20**, 840 (1995).

4 J.S. Hangst, A. Labrador, V. Lebedev, N. Madsen, J.S. Nielsen, O. Poulsen, P. Shi and J.P. Schiffer, Phys. Rev. Lett. **74**, 86 (1995).

5 N. Madsen, ISA Activity Report No.1, September 1996, p. 39.

6 A. Rahman and J.P. Schiffer, Phys. Rev. Lett. **57**, 1133 (1986).

7 J. Wei, H. Okamoto, and A. M. Sessler, Phys. Rev Lett. **80**, 2606 (1998)

8 I. Lauer *et al.*, Phys Rev. Lett. **81**, 2052 (1998)

Physics with stored molecular ions in ASTRID & ELISA

M. J. Jensen[1], P. J. Johnson[1], D. Kella[1], H. B. Pedersen[1], C. P. Safvan[1], L. Vejby Søgaard[1], X. Urbain[1], N. Djuric[2], O. Heber[3], D. Zajfman[3], P. H. Mokler[4], H. T. Schmidt[5]and L. H. Andersen[1]

[1]*Institute of Physics and Astronomy, University of Aarhus*
[2]*Jila, University of Colorado and Nat. Inst. of Standards and Tech., Boulder, USA*
[3]*Department of Particle Physics, Weizman Institute of Science, Rehovot, Israel*
[4]*Gesellschaft für Schwerionenforschung (GSI), Darmstadt, Germany*
[5]*Manne Siegbahn Laboratory, University of Stockholm, Stockholm, Sweden*

Since the last ISA activity report, we have continued and further developed our activities at ASTRID with interactions between free electrons and ions. We have studied dissociative recombination and dissociative excitation of several positive molecular ions, determining both branching ratios and the energy dependence of the cross sections. These measurements are of fundamental importance, not only for the understanding of the process itself, but also for modelling plasmas, the chemistry of planetary atmospheres, and the interstellar media. Our studies of electron scattering on negative ions now include a number of different atomic and molecular ions. In electron scattering experiments with C_2^- and B_2^-, the cross sections show structures that can be attributed to a resonance state in C_2^{2-} and B_2^{2-}, respectively. This is presently the only direct evidence for the existence of diatomic, doubly charged negative ions. In addition to these electron-ion interactions, our activities have, just recently, been extended to include lifetime measurements at the new electrostatic ion storage ring, ELISA.

Dissociative recombination

Dissociative recombination of a diatomic molecular ion can be described by the following equation:

$$AB^+(n,v,J) + e^- \approx A(\alpha) + B(\alpha) + E_{kin}$$

The molecular ion AB^+, with electronic, vibrational and rotational quantum numbers n, v and J, recombines with an electron and dissociates into two neutral atoms A and B in electronic states α and α. The excess energy is carried by the fragments as kinetic energy release, E_{kin}. Since dissociative recombination often produces fragments in excited states that subsequently decay by emission of radiation, it is of major importance in, for instance, the physics of planetary atmospheres, where these decays give rise to characteristic lines in the emission spectra.

The molecular ions O_2^+, N_2^+ and NO^+ are of particular interest. They are abundant in planetary atmospheres, and in order to understand the various processes occurring in these media, it is important to know the excited state distribution of the fragments produced by dissociative recombination. We have measured these distributions by an imaging technique, where the kinetic energy release is measured event by event.

Our results for O_2^+ have solved a long-standing puzzle concerning the oxygen chemistry in the earth ionosphere. During the daytime, the ionosphere is exposed to ultraviolet sunlight that creates ionized molecules like O_2^+. At night-time, the molecular ions may undergo dissociative recombination resulting in the production of excited oxygen atoms. A prominent feature in the spectrum of the night sky is a green line at 5577 Å, which is attributed to the $^1S \approx {}^1D$ transition in atomic oxygen. Before our measurement, it was, on the basis of theoretical calculations, believed that only around 0.1 % of the oxygen atoms produced by dissociative recombination were in the ^1S state. This amount of $O(^1S)$ atoms originating from dissociative recombination was inadequate to explain the intensity of the 5577 Å line, which led to speculations about other possible sources for $O(^1S)$ production.

According to our measurement, about 5 % of the oxygen atoms turn out to be produced in the ^1S state, and this solves the long-standing puzzle of the green light emission in the

ionosphere. The result has later been confirmed by a theoretical calculation including the spin-orbit coupling, and new routes of dissociation has been revealed.

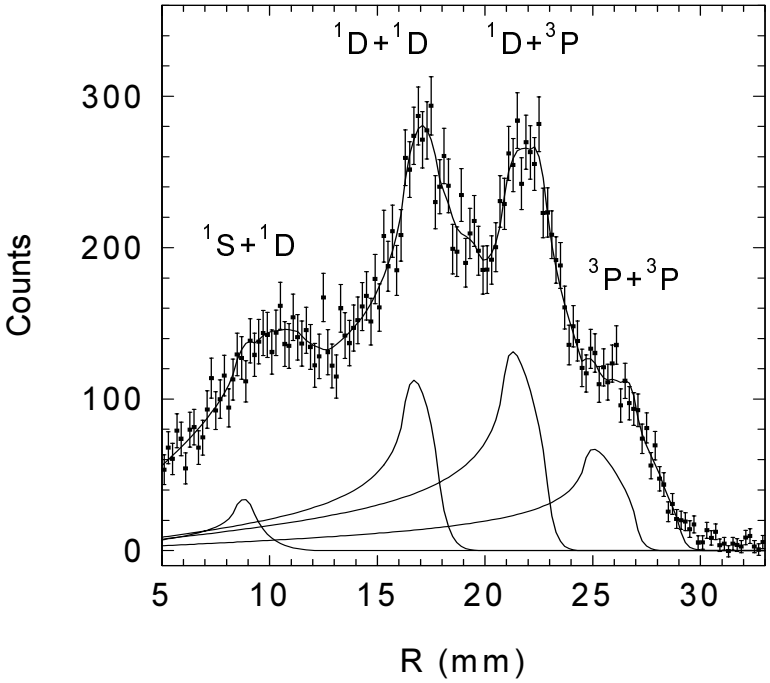

FIG. 1. Distribution of two-dimensional projected distances (on the imaging detector) between to oxygen atoms, reflecting the kinetic energy release and consequently the internal states of the atoms. The solid curve through the data is the fit, including all rovibrational levels. The other solid curves are the v=0 contributions.

Electron scattering on negative atomic and molecular ions

We have performed low-energy scattering of electrons on several atomic and molecular negative ions. In the case of atomic ions, we have measured the electron-impact detachment cross section as a function of energy, whereas cross sections for both detachment and dissociation have been measured in the case of molecular ions. Our experimental results have contributed substantially to the understanding of the dynamics of negative ions, and to the question concerning the existence of doubly charged negative ions (dianions).

Large molecular systems can hold many extra electrons because the electron cloud can spread out over an extensive volume or the excess electrons can stay well separated. This is in marked contrast to smaller systems, such as atoms or diatomic molecules that do not have the advantage of extending over a large volume in space. The physics of dianions in small systems is dominated by the extreme amount of electron correlation, and the stability is determined by the destructive decay modes of autodetachment and dissociation. Over the last few years, there has in our group been an ongoing experimental and theoretical search for these rarely occurring dianions. It seems evident that atomic dianions are not stable, but it is still an open question under which conditions metastable atomic and molecular dianions can exist. Our experimental work sheds light on this question.

According to a recent theoretical prediction, a $(2p^3)$ ^4S state should give rise to a resonance state in H^{2-}. Due to spin conservation, it can not be formed by electron scattering on H^-, however there is no selection rule preventing the isoelectronic state in B^{2-} from being formed by electron scattering on B^-. If the resonance state exists, we expect to observe it as a structure in the detachment cross section due to the formation of an intermediate dianion,

$$B^- + e^- \approx \{B^{2-}\} \approx B + 2e^- .$$

We have measured the cross section for electron-impact detachment from B^-, and observe no sign of a short-lived B^{2-} ($2p^3$) state.

Due to the additional degree of freedom and larger spatial extend, diatomic systems seems to be better candidates for forming dianions. To study resonances belonging to diatomic dianions, we have performed electron scattering experiments with C_2^-, B_2^-, BN^-, O_2^- and OH^-. When scattering electrons on C_2^- and B_2^-, the cross sections show structures that can be related

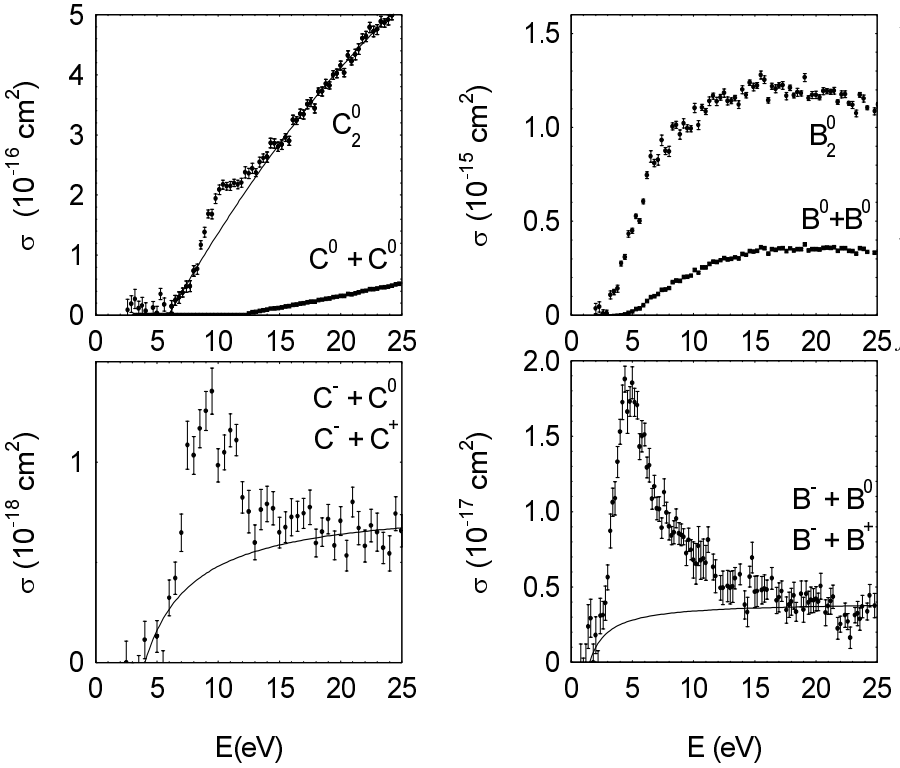

Figure. 2. The upper curves are the cross sections for detachment and detachment+dissociation, and the lower curves are the cross sections for dissociation without and with ionization. The solid curves are the non-resonant backgrounds estimated from a classical calculation.

to a short-lived resonance around 10 eV and 5 eV above the anion ground states, respectively. In the case of C_2^-, the resonance is visible as a structure in cross sections for detachment and dissociation, whereas in the case of B_2^-, the resonance is visible as a structure in the dissociation cross section only. Both resonances have a lifetime of about 10^{-16} s (estimated from the width). The present series of measurements constitute currently the only experimental investigation of diatomic, dianion resonance states.

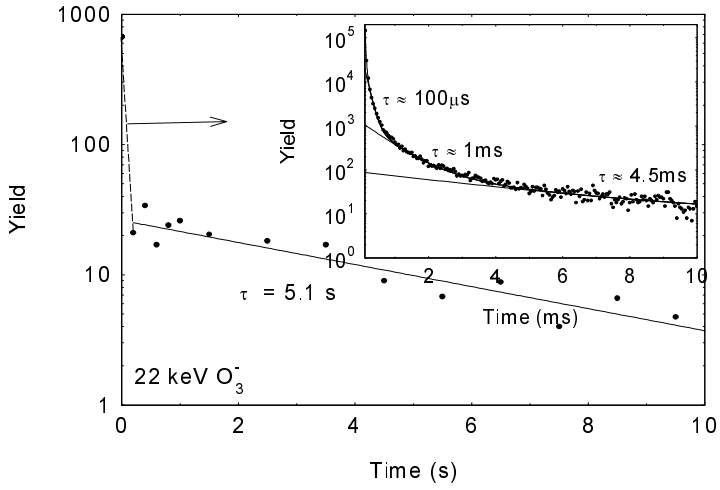

Decay curves for O_3^-. The inset shows the decay of metastable states. The solid curves are exponential decays fitted to the data.

Lifetime measurements at ELISA

Our first experiments at ELISA have been lifetime measurements of molecular anions. We have produced and stored an O_3^- beam in ELISA with a pressure limited lifetime of 5.1 s (at $3\cdot10^{-11}$ mbar). The decay curve consists of a long-lived component corresponding to interactions with the background gas, and some short-lived components corresponding to metastable states of O_3^-. We plan to perform photoelectron spectroscopy studies of O_3^- in order to investigate the nature of these metastable states. In addition, we plan to study electron scattering on O_3^- at ASTRID, and search for structures that can be related to a possible resonance state in O_3^{2-}.

Added September 1999:
We have also started studies of isomerization processes at ELISA and the first system that we investigated was C_2H_2. As a negative ion C_2H_2 has the vinylidene structure, but as a neutral molecule C_2H_2 has the acetylene structure (se the figure below).

It is readily seen that the anion is unstable since it has more energy than the ground state of the

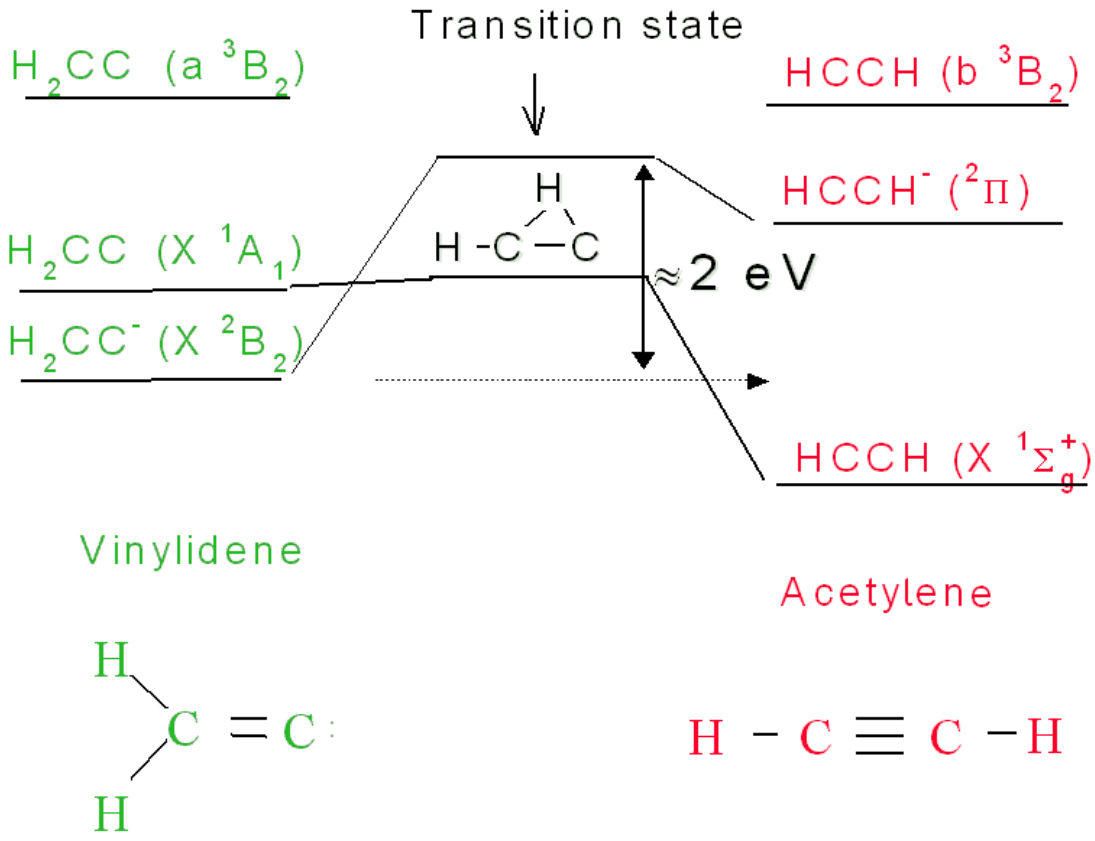

neutral C_2H_2. The decay mode is autodetachment (electron emission). Due to the large energy barrier the decay is however extremely slow. At ELISA we have been able to determine that the lifetime associated with this autodetachment process involving a vinylidene-acetylene conformation change is as long as 110s.

References

D. Kella, L. Vejby-Christensen, P. J. Johnson, H. B. Pedersen, and L. H. Andersen, Science **276**, 1530 (1997).
D. Kella, P. J. Johnson, H. B. Pedersen, L. Vejby-Christensen, and L. H. Andersen, Phys. Rev. Lett. **77**, 2432 (1996).
L. Vejby-Christensen, D. Kella, H. B. Pedersen, and L. H. Andersen, Phys. Rev. A **57**, 3627 (1998).
L. H. Andersen, M. J. Jensen, H. B. Pedersen, and L. Vejby-Christensen, Phys. Rev. A **58**, 2819 (1998).
H. B. Pedersen, N. Djuric, M. J. Jensen, D. Kella, C. P. Safvan, L. Vejby-Christensen, and L. H. Andersen, submitted.

Binding energies and lifetimes of negative ions determined using ASTRID

T. Andersen[1], H. H. Andersen[1], H. K. Haugen[2], U. V. Pedersen[3],
V. V. Petrunin[1], and M. Raarup[1]
[1]*Institute of Physics and Astronomy and Aarhus Centre for Atomic Physics, University of Aarhus*
[2]*Institute of Physics and Astronomy, McMaster University, Hamilton, Canada*
[3]*Institute for Storage Ring Facilities, University of Aarhus*

The studies of binding energies of weakly bound negative atomic ions and of lifetimes of metastable negative atomic or molecular ions have been continued using ASTRID. The influence of the blackbody radiation on a weakly bound negative ion, with a binding energy of less than 150 meV, can be utilized to obtain a fairly accurate estimate of its binding energy, since the ion will photodetach in the storage ring on a time scale ranging from μs to 10ms[1]. This technique has been applied to dismiss the hypothesis that the negative Cs ion should possess a weakly bound excited 6s6p state[2] and to eliminate previous claim for the existence of a very weakly bound negative Yb ion[3].

The use of ASTRID to study lifetimes of metastable negative ions is well established and described in several review articles[4,5]. Within the present period the lifetime technique has been applied to search for longlived metastable negative molecular ions, which could be formed from the atmospheric gases N_2 and CO_2. The very surprising claim that a longlived metastable state of N_2^- may exist[6] has been confirmed and its lifetime determined. Previously, it had only been observed that the negative molecular nitrogen ion could exist as short lived doublet resonances in e - N_2 collisions. Contrary to the expectation[7] the negative molecular nitrogen ion may not belong to the quartet system. The present experiments[8] at ASTRID and at the tandem accelerator indicate that the longlived (200 μs) N_2^- ion belongs to the sextet system.

The CO_2^- ion has previously been reported to exist as a bent molecule with a lifetime of 60-90 μs, bound with respect to the first excited singlet state of CO_2. During experiments[9] to confirm this lifetime it was observed that the CO_2^- ion, formed by charge exchange of the CO_2^+ ion in alkali metal vapour, also exists in a metastable state with a much longer lifetime (7.8(5)ms). This value combined with the technique used to create the ion strongly indicate that the observed CO_2^- ion represents a quartet state of the negative CO_2 ion, bound with respect to the lowest lying triplet state in the neutral molecule. The decay of the strongly bent quartet state can only occur to the linear ground state of the neutral CO_2 molecule, explaining the surprisingly long lifetime.

References:

1. H. K. Haugen et al., Phys. Rev. A**46**, R1 (1992)
2. M. Scheer et al., Phys.Rev. Lett. **80**,684 (1998)
3. H. H. Andersen, T. Andersen, and U. V. Pedersen, J. Phys. B**31**, 2239 (1998)
4. T. Andersen, H. H. Andersen, P. Balling, and V. V. Petrunin, J. Phys. B**30**, 3317 (1997)
5. L. H. Andersen, T. Andersen, and P. Hvelplund, Adv. At. Mol. Opt. Phys. **38**, 155 (1997)
6. H. Gnaser, Phys. Rev. A**56**, R2518 (1997)
7. T. Sommerfeld and L. S. Cederbaum, Phys. Rev. Lett. **80**, 3723 (1998)
8. T. Andersen, J. Heinemeier, M. Raarup, and N. Rud to be published.
9. M. Raarup and T. Andersen to be published.

Added September 1999:

Lifetimes of atomic and molecular negative ions .
Studies of the structural and dynamic properties of negative atomic and molecular ions represent a special niche in the physics of atomic interaction due to the strong electron-electron correlation effects and the short range potential ($\approx r^{-4}$). The existence of many negative ions is due to the

electron-correlation effect, and consequently the elctron affinities are often one to two orders of magnitude lower than the binding energy of neutral atoms. It has also been a challenge to obtain reliable and unambiguos dynamic data for metastable ions with lifetimes in the μs to 100 ms region. ASTRID proved already in 1992-95 to be a suitable facility to obtain accurate lifetime data for metastable negative atomic ions, and the influence of blackbody radiation was utilized to gain information about very weakly bound negative ions, since these will be detached due to the radiation and appear as decay components in a time of flight study.

Research goals:
To further develop and apply ASTRID for studies of weakly bound atomic systems and for selected small molecular ions of atmospheric importance and combine these results with laser spectroscopic measurements at smaller ion accelerators.

Results:
The blackbody radiation technique has been applied to disprove the existence of the predicted excited 6s6p state in Cs^- and of the stable Yb^- ion. The lifetime studies have provided evidence for the existence of high-spin states (sextets) in negative molecular ions of N_2 and CO_2 and the very long lifetimes of these molecular ions have been measured. These results have stimulated several new theoretical studies.

External Activities

Deflection and extraction of multi-TeV Pb^{82+} at CERN

C. Biino[1], M. Clement[1], N. Doble[1], K. Elsener[1], L. Gatignon[1], P. Grafström[1], W. Herr[1], J. Klem[1],U. Mikkelsen[1,2], S.P. Møller[2] and E. Uggerhøj[2]
[1]*CERN, Geneva, Switzerland*
[2]*Institute for Storage Ring Facilities, University of Aarhus*

The correlated scattering off the lattice nuclei in a crystal leads to a guidance of the penetrating particle for small angles of incidence to eg. a crystallographic plane. This effect of channeling persists even if the crystal is slightly bent, such that one may obtain a deflection of those particles that are channeled through the crystal. Since the electric fields in the crystal exceed even super-conducting dipole fields by at least two orders of magnitude, an extremely compact deflection device can be constructed by use of a crystal. This opens for the possibility of extracting high energy particles for parasitic experiments in an environment where standard extraction devices would be too costly or take up too much space.

Since the late 70's the deflection of singly charged, heavy particles of high energy in bent crystals has evolved into a mature discipline where most aspects are understood[1]. This includes for example the deflection efficiency as a function of bend angle, the influence of radiation damage and the effect of higher nuclear charge of the lattice nuclei in the bent crystal[2]. However, with the availability of the fully stripped, relativistic lead nuclei as a beam at the CERN SPS, new possibilities have been opened for. As for the previous tests with protons, the investigations with multi-TeV Pb^{82+} are motivated by the prospects of extracted relativistic nuclei at the future LHC at CERN, as well as by fundamental interests.

Recent experiments[3] show that the deflection of the lead nuclei in a 60 mm bent silicon crystal agrees very well with theoretical estimates and that the efficiency of 14% for an angle of 4 mrad is close to that expected for protons of equal momentum per charge. This indicates that nuclear interactions from close encounters and electromagnetic dissociation play a minor role for the channeled particles. That question is at the time of writing being tested by a comparison of the content of Tl^{81+} in the incident, undeflected and deflected beam from which the probability of proton-loss during deflection can be inferred.

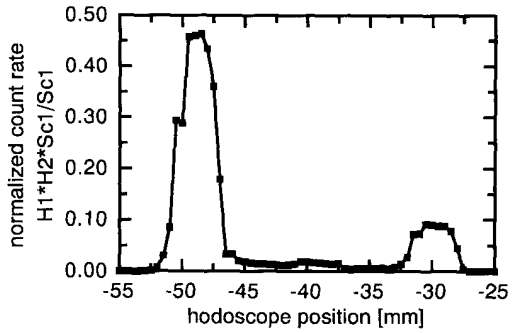

Figure 1 Scan across the undeflected, dechanneled and deflected beam for 33 TeV Pb^{82+}

In figure 1 is shown a scan across the undeflected, dechanneled and deflected beam by use of a scintillator with an effective width of 2 mm. The beams are clearly separable and the deflection efficiency is easily extracted.

On the other hand, extraction of 22 TeV Pb^{82+} through an angle of 8.5 mrad in a U-shaped Si crystal, show very high extraction efficiencies of up to 10%, an encouraging result. However, this is somewhat smaller than that obtained at the SPS with protons of equal momentum per charge, an effect which may be connected to the suppression of so-called multi-turn extraction[4] in the case of composite particles.

In conclusion, the results obtained for the deflection and extraction of relativistic Pb^{82+} are very encouraging, both in terms of application as an extraction device or beam-splitter at eg. RHIC, Brookhaven or at the future LHC at CERN as well as from a fundamental point of view in comparison with theoretical expectations.

Added September 1999:

Deflection and extraction of multi-GeV ions

Following the encouraging outcome of the first experiments with deflection of multi-GeV fully stripped lead ions, a new experiment was performed to investigate the dependence of the

deflection efficiency on the bend angle. As expected, there is only a small difference between highly charged ions and protons of equal momentum per charge. Furthermore, a large suppression of nuclear interactions was indicated by a drastic reduction in secondary particles emitted to a counter outside the beams.

References:

1 A. Baurichter *et al.*, Nucl. Instr. Meth. B **119**, 172 (1996)

2 C. Biino *et al.*, Phys. Lett. B **403**, 163 (1997)

3 G. Arduini *et al.*, Phys. Rev. Lett. **79**, 4182 (1997)

4 X. Altuna *et al.*, Phys. Lett. B **357**, 672 (1995)

Influence of Strong Crystalline Fields on QED Processes – NA43 Results

Erik Uggerhøj
Institute for Storage Ring Facilities, University of Aarhus

When multi-GeV electrons/positrons traverse single crystals close to axial/planar directions, QED processes are strongly influenced by coherent scattering on many target atoms. Channelling is one type of such coherent processes. Along crystal directions the incident ultrarelativistic particles "see" very strong electromagnetic fields (~10^{11} V/cm). These fields in the particle rest frame must be multiplied by the Lorentz Factor α (10^5-10^6). Under such conditions radiation emission processes resemble the well-known synchrotron radiation in very strong fields. Further on, the transverse motion of such high-energy projectiles during photon emission is small because the longitudinal radiation formation length, $\approx_f$, is assumed to be short, so the crystalline fields are nearly constant during the processes – leading to the so-called constant-field approximation (CFA).

The influence of strong fields on QED in the CFA is dependent on the invariant parameter $\chi = \gamma\varepsilon/\varepsilon_0$, where ε is the local field strength, $\varepsilon_0 = mc^2/e\chi_c$ = 1.3 x 10^{16} V/cm. We use standard notation for electron charge, mass, Compton wavelength, and speed of light. For χ«1 classical electrodynamics can be used, whereas for $\chi \geq 1$ a full quantum description is needed – already at χ~0.1 quantum effects begin to appear. In the present experiments $\alpha \leq 1$. In the following some typical experimental results from the CERN NA-43 experiment are presented – for details around NA43 see ref. 1 and ISA Activity Report No. 1.

For radiation emission it was found that the strong crystalline fields lead to enhancements of up to two orders of magnitude with photon multiplicities of 5-10. This means that the main free path for photon emission is reduced around 100 times.
The energy loss for GeV e^+/e^- is practically all due to radiation emission and shown in fig. 1.

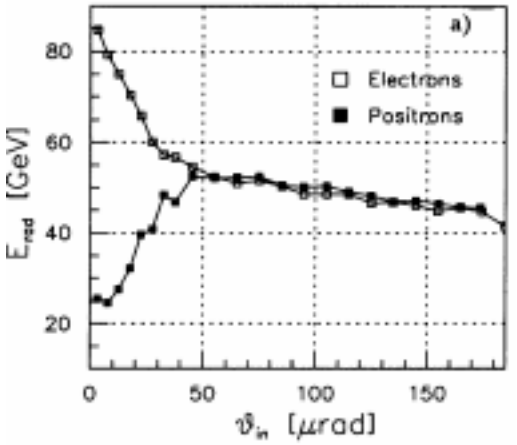

Figure 1a. Radiation energy loss for 150 GeV e^+/e^- traversing a 0.7 mm diamond – as function of angle to ⟨110⟩ axis.

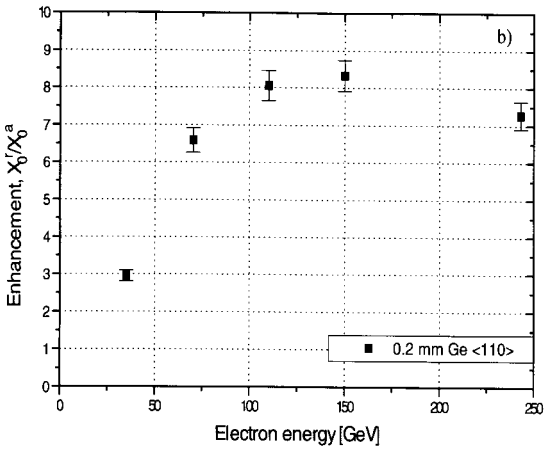

Figure 1b. Radiative energy loss along ⟨110⟩ axis in a Ge crystal – normalized to random values.

For a comparison it should be mentioned that the radiative energy losses for amorphous dia mond is 0.5 GeV. In general, it is seen that inside the channeling regions positrons lose considerably less energy than electrons. Outside the channeling region the energy loss in both cases is (25-30) times the amorphous values, showing the dramatic effect of the strong fields from the axis.

For the $\theta_{in} > \psi_1$ the positrons loose a few GeV more than electrons. This reflects the fact that for the same incident angle the positron velocities are a little smaller than those of electrons in the regions around the axes are. So positrons spend more time in the strong field region and thereby radiate a little more.

Fig. 1b shows radiative energy loss in Ge crystals for increasing electron energy. Due to the strong crystalline field we here have come to a region where the energy loss turns from a γ^2 - dependence to a $\gamma^{2/3}$ dependence as described above. In Schwinger´s original 49-paper on

radiation it was shown that the classical χ^2-dependence is adequate in fields around 1 Tesla, and particle energies $\approx 10^{15}$ eV. The present experiment shows that strong crystalline fields give access to detailed investigations of such effects – but at existing particle energies.

The dramatic enhancements of radiation emission from multi-GeV electrons/positrons traversing single crystals have raised many questions both theoretically and experimentally, like: What is the influence of this strong radiation on the angular distribution of the particles behind the crystal? After the emission of a photon, the transverse energy $E_\perp = \frac{1}{2} m\chi\gamma^2_\perp + U(r)$ decreases. This so-called radiation cooling will counteract the multiple scattering. Furthermore, the reduction in $\varepsilon_\perp$ might result in an increase of the number of channeled particles coming from above-barrier particles, the so-called "feed-in". For electrons, such a situation can lead to "re-channeling" followed by dechanneling. This means that such particles spend a considerable time in the strong field from the atomic axis/plane, leading to strongly enhanced radiation emission.

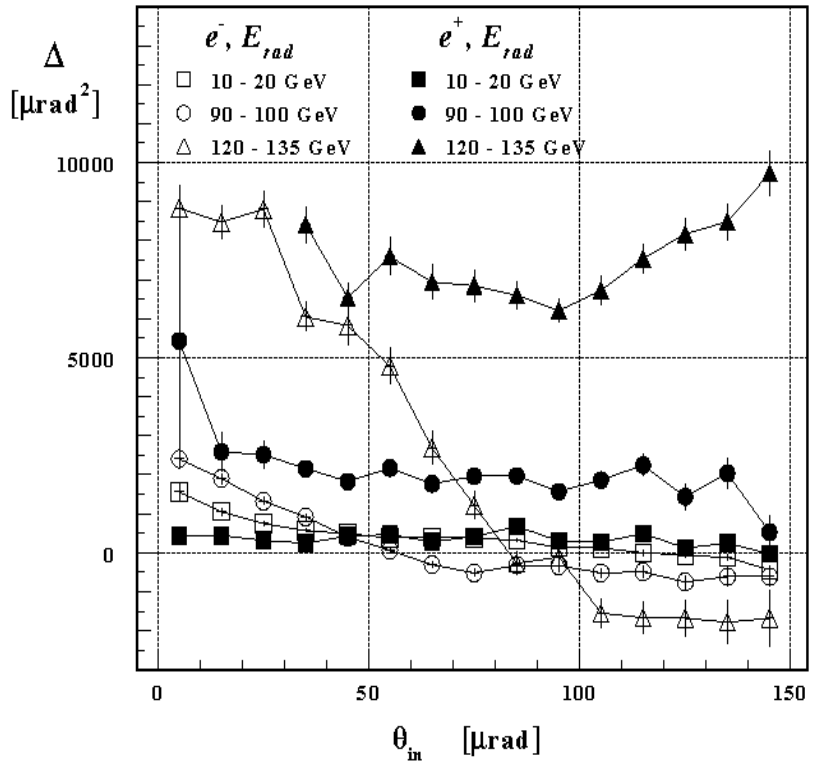

Figure 2. Difference between $\langle\theta^2_{out}\rangle$ and $\langle\theta^2_{in}\rangle$ for 150 GeV e^+/e^- incident on 0.7 mm ⟨110⟩ diamond. Data are given for increasing radiative energy loss.

In Fig. 2 are shown new experimental results on radiation cooling.

Here we present the parameter:

$$\theta \leq \psi^2_{out}\rangle - \psi^2_{in}\rangle$$

for 150 GeV e^+/e^- penetrating a 0.7 mm thick ⟨110⟩ diamond. It is clear that θ is negative (strong cooling) for electrons with $\psi_{in} \geq \psi_1$ but positive for $\psi_{in} \leq \psi_1$.

For normal multiple scattering for 150 GeVe^- in 0.7 mm diamond θ = 110 μrad^2. So for $\psi_{in} > \psi_1$ the radiative cooling is so much stronger than multiple scattering that θ goes negative. For $\psi_{in} \leq \psi_1$ it is found that ψ_{out} is close to the critical angle ψ_1 calculated for exit electron energies. For positrons θ is always positive and large, corresponding to strong angular heating.

Also pair production and shower formation are strongly enhanced in the strong crystalline fields. For details see proceedings from Aarhus Conference. NIMB 119 1-316 (1996).

Added September 1999:

High energy polarized photons

In the spring of 1999, an experiment was performed to verify earlier, indirect evidence for a birefringent effect of multi-GeV photons in single crystals. The method is based on the production of r-mesons by photons in a beryllium target. The r-mesons decay into pion pairs which have specific angular correlations for polarized photons compared to that for non-polarized, such that the polarisation of the photons can be derived from the decay products without introducing theoretical models. Furthermore, the electron-positron pair production method used earlier – which is model-dependent, but fast – was used again to enable a cross-calibration between the two methods. This means that the degree of polarization in the future may be determined by means of pair production in single crystals rather than the much slower process of r-meson production. The analysis of the experiment is underway.

References

1 A. Baurichter et al.: Phys. Rev. Lett. **79** 3415 (1997).

People

ISA Staff members:

Besides ISA employees, this list includes PhD students and externally funded staff

Joanna V. Abraham-Peskir	X-ray microscopy
Jan Creutsberg	Mechanical maintenance & assembly
Erling Dalsgaard	Mechanical maintenance & construction
Peter C. Damm	PC maintenance
David Field	Electron/molecule interactions, astrophysics
Susan Glasauer	X-ray microscopy
Niels Hertel	Acc. physics, acc. operation, microtron, EBIS, radiation safety
Søren Vrønning Hoffmann	Monochromators, surface physics
Philip Hofmann	Surface physics
Kaare Iversen	Mechanical maintenance & construction
John Kenney	Biological imaging
Iouri Kononets	QED, strong fields, CERN
Tonny Korsbjerg	RF, diagnostics, electronics
Peter Lange	Mechanical workshop
Ruth Laursen	ISA secretary
Zheshen Li	Surface physics, monochromators
Stuart Lunt	SR beamlines, acc. operation, electron/molecule interactions
Robin Medenwaldt	X-ray microscopy
Jonathan Merrison	Positron beamline
Ulrik Mikkelsen	Antiproton decelerator, CERN
Søren Pape Møller	Technical director, acc. physics, ELISA, acc. operation
Jørgen S. Nielsen	Acc. physics, control system, acc. operation
Ulrik Vindelev Pedersen	ELISA, EBIS
Lars Præstegaard	Acc. physics
Stefan Stahl	Positron beamline
Christian Schultz	Surface physics
Yuri Senichev	Acc. physics
Christian Skou Søndergaard	Surface Physics
Lars Therkelsen	Mechanical maintenance & construction
Erik Uggerhøj	Director, x-ray microscopy, CERN
Jens Vestergaard	Mechanical maintenance & assembly
René Warthoe	Mechanical maintenance & assembly
Torben Worm	Computer group, control system

In addition to the above, ISA uses an unnamed staff effort from the Institute of Physics corresponding to 2½ persons in the electronics workshop and 1½ persons in the mechanical workshop.

Visiting Scientists: (Staying more than 2 months at ISA)

Eric Chantler, x-ray microscopy,
University of Manchester, Manchester, UK.

Nina Golubeva and Sergei Volin, ASTRID II calculations,
Institute for Nuclear Research, Moscow, Russia

Leonid Ognev, glass capillaries,
Kurchatov Institute, Moscow, Russia

The ISA Board:

Professor, dr.scient Flemming Besenbacher (chairman), Institute of Physics and Astronomy, University of Aarhus.

Professor Jens Ulrik Andersen, Institute of Physics and Astronomy, University of Aarhus.

Afdelingsleder, PhD Bjerne S. Clausen, Haldor Topsøe A/S, Lyngby.

Forskningschef Lene Lange, Novo Nordisk A/S, Bagsværd.

Professor Erik Larsen, The Royal Veterinary and Agricultural University, Copenhagen.

Dr.scient Søren Pape Møller, Institute for Storage Ring Facilities, University of Aarhus.

Professor Fritz Vollrath, Institute of Biology, University of Aarhus.

Dekan Karl Pedersen, Faculty of Science, University of Aarhus.

Direktør, professor, dr. scient Erik Uggerhøj, Institute for Storage Ring Facilities, University of Aarhus.

The ISA Advisory Committee:

Professor Alexander M. Bradshaw, Fritz-Haber-Institut der MPG, Berlin, Germany

Professor Harold K. Haugen, McMaster Univ., Hamilton, Canada

Professor Janos Kirz, SUNY at Stony Brook, NY, USA

Professor Sidney Leach, (Chairman), Observatoire de Paris-Meudon, Meudon, France

Professor Joe Macek, Uni. Tenn., Knoxville, TN, USA

Professor Gerhard Materlik, DESY, Hamburg, Germany

Dr. Daniel-Jean Simon, CERN, Geneva, Switzerland

Dr. Vic P. Suller, Daresbury, Warrington, UK.

ISA Users

Australia

Australian National University, Canberra
Robert Gulley

Belgium

Catholic University of Louvain
Xavier Urbain

Canada

McMaster University
Harold Haugen, C. A. Brodie, R. C. Bilodeau

Denmark

University of Aalborg
Kjeld Pedersen, Erik G. Soegaard

Dept. of Medical Microbiology and Immunology, University of Aarhus
Erik Ernst, Tage Hjort, Thomas Vorup Jensen

Dept. of Earth Sciences, University of Aarhus
Per Nørnberg, J. Tyge Møller

Institute of Biology, University of Aarhus
Xiao Wen Hu, Kjeld Ingvorsen, Volker Loeschcke, Fritz Vollrath

Institute of Genetics and Microbial Ecology, University of Aarhus
Volker Loeschcke

Institute of Physics, University of Aarhus
Dave Adams, Lars Henrik Andersen, Jens Ulrik Andersen, Torkild Andersen, Peter Balling, Henrik Bluhme, Paul Bowe, Michael Drewsen, Finn Folkmann, Christian Gottrup, Jeffrey Hangst, Liv Hornekær, Marie Jensby Jensen, Henrik Kjeldsen, Helge Knudsen, Niels Madsen, Jon Merrison, Anders Mikkelsen, Henrik B. Pedersen, Victor Petrunin, Christian Søndergaard, Lars Henrik Andersen, C.P Safvan, Liv Hornekær, Preben Hvelplund, Niels Kjærgaard, Lise Vejby-Christensen, Dror Kella, Peter J. Johnson, Mårten Larsson, Poul Kristensen, J. H. Petersen, Karen Paludan, Kim Aamund Nielsen, Daniel Walker, Robin Mitchell, H. H. Andersen, M. K. Raarup, P. Steiner

Institute for Storage Ring Facilities, University of Aarhus
Joanna Abraham Peskir, David Field, Niels Hertel, Søren Vrønning Hoffmann, Zheshen Li, Stuart L. Lunt, Robin Medenwaldt, U.V. Pedersen, Jan Van Elp, Søren Pape Møller, Jørgen S. Nielsen, Yuri Senichev, Erik Uggerhøj, Susan Glasauer

Danfysik, Jyllinge
Lars Præstegaard

Danisco, Aarhus
Lisbeth Høj Johansen

The Royal Veterinary and Agricultural University, Copenhagen
Birgitte Neergaard Bearden

Microelectronics Center, Danish Technical University, Lyngby
Peixiong Shi

Institute of Chemistry, University of Copenhagen
Jan Hoffmann Jørgensen, Nanna Meyland Nicolaisen , Preben Juul Møller, T. Egebjerg

Niels Bohr Institute, University of Copenhagen
Ian Bearden, Jens Jørgen Gaardhøje, Erik Jacobsen, Claus Jørgensen, Mads Gammeltoft, Børge Svane

Institute of Physics, University of Odense
Palle Møller, Per Morgen, Jens Onsgaard, Jacob Birkedal Wagner, L. Thomsen, Susanne Quist, Jette Wendt Larsen

France

Observatoire de Paris-Meudon
Sydney Leach, Jean-Louis le Maire

Université Sergy-Pontoise, Paris
Stephan Douin, Francois Dulieu

Université Paul Sabatier, Toulouse
Jean-Pierre Ziesel

Germany

Fritz-Haber-Institut, Technische Universität, Berlin
Martin Polcik, J. Haase

University of Münster
Ina Thom, R. Wiermann, M. Grote

GSI Darmstadt
Paul Mokler

Institut für Festkörperphysik
Wolfgang Richter, Knut Stahrenberg

Westfälische Wilhelms-Universität
Mathias Grote, I. Thom, Rolf Wiermann

Freie Universität Berlin
Hans Werner Jochims

University of Mainz
Stefan Stahl, Richard Ley

Israel

The Weizmann Institute
Daniel Zajfmann, Oded Heber

Bar-Ilan University
Benjamin Bartoov

Italy

University Padova
Michela Della Negra

Laboratorio XPS
Gaetano Granozzi, Mauro Sambi

Japan

NIFS Data and Planning Centre, Nagoya
Hiroyki Tawara

Norway

Dept. of Physics, University of Bergen
Renate Grunner, Dieter Roerich

Poland

University of Wroclaw
Przemyslaw Jan Godowski

Russia

Troitsk University
V. V. Petrunin, S. A. Aseyev

St.-Petersburg Mining Institute
I. V. Makassiouk

Spain

Universitat Autonoma de Barcelona
Ana Labrador

Sweden

MAX-LAB, Lund
Jesper N. Andersen

MSL Laboratory, Stockholm
Henning T. Schmidt, Stefan Schwartz, Håkan Danared

University of Stockholm
Henrik Cederquist

Ukraine

Institute for Cryobiology and Cryomedicine, Kharkov
V. Grieschinka

United Kingdom

Daresbury Laboratories
John B. West

University of Manchester
Eric Chantler, Graham Jones, Christine McCann, David Sigee, Geoff Thornton, Paul Wincott, Thomas Field, Ian Hampson, Lynn Hampson

University of Reading
Rosalind Searle

Birkbeck College, London
Paul Barnes Group

University College London
Lars Jørgensen, Michael Charlton

University of Nottingham
Tom Field

United States of America

Argonne National Laboratory
J. P. Schiffer

Brookhaven National Laboratory
Stephen Spector

Jefferson Laboratory
Valery Lebedev

State University of New York at Stony Brook
Chris Jacobsen

University of Colorado
Nadja Djuric

Publications
1996-1998

Added September 1999:
An updated list can be found in
ISA Activities in the period 1996 to mid-1999.

References to published work 1996-1998:

This list is divided into 5 sections:

Accelerator Physics and Technical developments, including Laser Cooling
Ion Storage
Synchrotron Radiation, Biology, which is x-ray microscopy work
Synchrotron Radiation, Physics
External Activities, which are other activities in which ISA staff has been involved.

Accelerator Physics (AC) and Technical Developments

Refereed Journals

V. A. Lebedev, A. Labrador, N. Madsen, and J.S. Hangst:
Single and multiple scattering in a laser cooled ion beam.
Nucl. Instrum. Methods in Physics Research **A. 391**, 176 (1997)

S.P. Møller:
ELISA, an electrostatic storage ring for atomic physics.
Nucl. Instrum. Methods in Physics Research A **394** (1997) 281.

B. Wanner, R. Grimm, A. Gruber, D. Habs, H.-J. Miesner, J. S. Nielsen and D. Schwalm:
Rapid adiabatic passage in laser cooling of fast stored ion beams.
Phys. Rev. A **58**, 2242 (1998)

Conference (AC)

C. Burggraf, Chr. Burggraf, C. Koenig, P. Siffert, M. Hage-Ali, R. Winfield, P. Kelly, A. Rafferty, G. Crean, E. Uggerhøj, R. Medenwaldt, T. Dunholl, K. Skuse:
Elaboration de capillaires en verre pour focalisation des rayons X. Application des micro-faisceaux X en Cristallographie.
Conf.Proc. of Rayons X et Matiére-RX97, Strasbourg, 14-16 Oct.1997, Publ. J.de Physique Colloque CIV, 1998.

J.S. Hangst:
Bunched Beam Laser Cooling.
Presented at the 1996 European Accelerator Physics Conference in connection with the 1996 European Prize for Accelerator Physics, Sitges, Spain, June 1996.

J. S. Hangst:
Phase space cooling of stored ion beams.
Proc. of the International School of Physics "Enrico Fermi" Course CXXXI, eds.: A. Aspect, W. Barletta and R. Bonifacio. (IOS Press, Amsterdam 1996).

J.S. Hangst, M. Drewsen, A. Labrador, V.A. Lebedev, N. Madsen, J. S. Nielsen, J.P. Schiffer, and P. Shi:
Ion cooling in storage rings.
Invited talk presented at the annual meeting of the European Physical Society, "New trends in physics", Seville Spain, September 1996.

J. S. Hangst, M. Drewsen, A. Labrador, V. Lebedev, N. Madsen, J.S. Nielsen, O. Poulsen, J.P. Schiffer, and P. Shi:
The status of laser cooling experiments in ASTRID.
In Proceedings of the Workshop on Crystalline Beams and Related Issues, J.S. Hangst and A. Ruggiero, editors, World Scientific, 1997.

V.A. Lebedev, A. Labrador, N. Madsen, J.S. Nielsen, and J.S. Hangst:
Anomalous Behaviour of Schottky Noise for Cooled beams.
Invited Talk presented at the 11th Int. Advanced ICFA (International Committee for Future Accelerators) Beam Dynamics Workshop on Beam Cooling and Instability Damping, Moscow, Russia, June 1996.
V
N. Madsen, P. Bowe, M. Drewsen, L.H. Hornekær, N. Kjærgaard, A. Labrador, P. Shi, J.S. Hangst, J.S. Nielsen, and J.P. Schiffer
Limits to bunched beam laser cooling
Proceedings from 6th European Particle Accelerator Conference, EPAC-98, Stockholm 22-26 june 1998

N. Madsen, P. Bowe, M. Drewsen, L. Hornekær, N. Kjærgaard, A. Labrador, P. Shi, J.S. Hangst, J.S. Nielsen, and J.P. Schiffer
Observed limits to laser-cooling of a stored ion beam
Proceedings from 6th European Particle Accelerator Conference, EPAC-98, Stockholm 22-26 june 1998

N. Madsen, M. Drewsen, L.H. Hornekær, A. Labrador, J.S. Nielsen, P. Shi, J.S. Hangst, J.P. Schiffer, V.A. Lebedev:
Lasers and Laser-Cooling used for studies of Beam Dynamics.
To be published in proc. of the 1997 Particle Accelerator Conference, Vancouver 12-16 May 1997.

J.P. Merrison, H. Bluhme, N. Hertel, H. Knudsen, and E. Uggerhøj:
ISA Positron Beam Facility.
Book of Abstracts, XX International Conference on the Physics of Electronic and Atomic Collisions, Vienna, Austria, (1997) FR 210.

S.P. Møller
ELISA – An electrostatic storage ring for atomic physics
Proceedings from 1997 Particle Accelerator Conference, PAC'97, Vancouver, B.C., Canada, 12-16 May 1997.

S.P. Møller, T. Korsbjerg, and E.N. Zaplatine
ASTRID electron cavity study
Proceedings from 1997 Particle Accelerator Conference, PAC'97, Vancouver, B.C., Canada, 12-16 May 1997.

S. P. Møller
Design and first operation of the electrostatic storage ring, ELISA
Proceedings from 6th European Particle Accelerator Conference, EPAC-98, Stockholm 22-26 june 1998

J.S. Nielsen, K.T. Nielsen, and T. Worm
CONSYS – A new control system for ASTRID and ELISA
Proceedings from 6th European Particle Accelerator Conference, EPAC-98, Stockholm 22-26 june 1998

J.S. Nielsen and S.P. Møller
New developments at the ASTRID storage ring
Proceedings from 6th European Particle Accelerator Conference, EPAC-98, Stockholm 22-26 june 1998

Yu. Senichev, N. Hertel, S. Lunt, S.P. Møller and J.S. Nielsen
Increasing the life time of SR sources by RF phase modulation
Proceedings from 6th European Particle Accelerator Conference, EPAC-98, Stockholm 22-26 june 1998

Yu. Senichev
The proposed racetrack lattice for the synchrotron light source ASTRID II.
Proceedings from 6th European Particle Accelerator Conference, EPAC-98, Stockholm 22-26 june 1998

Yu. Senichev, T. Korsbjerg, S.P. Møller, and E.N. Zaplatine
Solving the problem of heating of RF contacts in cavity tuners
Proceedings from 1997 Particle Accelerator Conference, PAC'97, Vancouver, B.C., Canada, 12-16 May 1997.

Thesis (AC)

Niels Madsen:
Laser Cooling of $^{24}Mg^{+}$ ions in ASTRID
M.Sc. Thesis as part of PhD Degree, 1996.

Ion Storage (I)

Refereed Journals

H.H. Andersen, T. Andersen, and U.V. Pedersen:
Search for stable or metastable negative Yb ions.
Subm. to J.Phys.B, January 1998.

H. H. Andersen, P. Balling, P. Kristensen, U. V. Pedersen, S. A. Aseyev, V. V. Petrunin, and T. Andersen*:*
Experimental investigation of the H^- ($^1P^o$) resonance series converging to the H(n=2) threshold
Phys. Rev. Lett. **79**, 4770 (1997)

J.U. Andersen, C. Brink, P. Hvelplund, M.O. Larsson, B. Bech Nielsen and H. Shen:
Radiative cooling of carbon 60.
Phys.Rev.Lett. **77**, 3991 (1996).

J.U. Andersen, C. Brink, P. Hvelplund, M.O. Larsson, and H. Shen:
Carbon clusters in a storage ring.
Z.f.Physik D **40**, 365 (1997).

J.U. Andersen:
News from ASTRID.
Submitted to the Proc. of the 3rd Euroconf. On Atomic Physics with Stored Ions, Ferrara, Italy.

L.H. Andersen:
Electron-impact detachment from Atomic and molecular negative ions.
Comments At.Mol.Phys. **33**, 111 (1996).

L.H. Andersen, H.P. Pedersen, L. Vejlby-Christensen, O. Heber and D. Zajfman:
The production of water from the dissociative recombination of H_3O^+.
Phys.Rev.Lett. **77**, 4891 (1996).

L.H. Andersen, P. Hvelplund, D. Kella, P.H. Mokler, H.B. Pedersen, H.T. Schmidt and L. Vejlby-Christensen:
Resonance structure in the eletron-impact detachment cross section of C_2^-.
J.Phys.B: At.Mol.Phys. **29**, L643 (1996).

L.H. Andersen, P.J. Johnson, D. Kella, H.B. Pedersen, and L. Vejlby-Christensen:
Dissociative recombination and excitation measurement with H_2^+ and HD^+.
Phys.Rev. A **55**, 2799 (1997).

L. H. Andersen, T. Andersen, and P. Hvelplund:
Negative Ion studies at Storage Rings
Adv. At. Mol. Opt. Phys. **38**, 155 (1997)

L.H. Andersen:
Nattehimlens fysik studeret i en lagerring.
To be published in naturens Verden (1998).

L. H. Andersen, M. J. Jensen, H. B. Pedersen, L. Vejby-Christensen, N. Djuric
Electron-impact detachment from B^-
Phys. Rev. A **58**, 2819-2823 (1998).

T. Andersen:
New approaches to negative ions: Resonant ionisation spectroscopy and storage ring.
Nucl.Instr. and Methods in Phys.Research **123** (1997) 508.

T. Andersen :
Structure, dynamics and collisions of negative ions
Photonic, Electronic, and Atomic Collisions (World Scientific, Singapore) p. 401 (1998)

T. Andersen, H.H. Andersen, P. Balling, P. Kristensen, and V.V. Petrunin:
Structure and dynamics of the negative alkaline-earth ions.
J.Phys. B **30**, 3317 (1997).

P. Balling, P. Kristensen, H.H. Andersen, U.V. Pedersen, V.V. Petrunin, L. Præstgaard, H.K. Haugen and T. Andersen:
Vacuum ultraviolet spectroscopy of H^- utilising a heavy ion storage ring: The region near the H(n=2) threshold.
Phys.Rev.Lett. **77**, 2905 (1996).

D. Kella, P.J. Johnson, H.B. Pedersen, L. Vejlby-Christensen and L.H. Andersen:
Branching Ratios for Dissociative Recombinations of $^{15}N^{14}N^+$.
Phys.Rev.Lett. **77,** 2432 (1996).

D. Kella, P.J. Johnson, H.B. Pedersen, L. Vejlby-Christensen, and L.H. Andersen:
Dissociative recombination and excitation of $^{18}O^{16}O^+$, total cross sections and branching ratios.
Phys. Rev. A **57**, 3627 (1998).

D. Kella, L. Vejlby-Christensen, P.J. Johnson, H.B. Pedersen, L.H. Andersen:
The source of green light emission determined from a heavy-ion storage ring experiment.
Science **276**, 1530 (1997).

V.V. Petrunin, and T. Andersen:
New nonlinear laser techniques for studies of negative ions on and off an ion storage ring.
Subm. to Hyperfine Interactions, Nov. 97.

H.T. Schmidt, L. Vejlby-Christensen, H.B. Pedersen, D. Kella, N. Bjerre and L.H. Andersen:
Dissociative recombination from vibrationally excited H_2^+ ions: The effect of laser photo dissociation on the initial vibrational distribution.
J.Phys.B **29**, 2485 (1996).

M.Scheer, J. Thøgersen, R. C. Bilodeau, C. A. Brodie, H. K. Haugen, H. H. Andersen, P. Kristensen, and T. Andersen:
Experimental Evidence that the 6s6p ^3P_J States of Cs^- are Shapes Resonances
Phys. Rev. Lett. **80**, 684 (1998)

H. Shen, P. Hvelplund, D.C. Lorents, and D. Matthur:
On the collisionary induced destruction of short- and long-lived fullerene ions.
Chem.Phys.Lett.**264,** 508 (1997).

L. Vejlby-Christensen, D. Kella, D. Mathur, H.B. Pedersen, H.T. Schmidt, and L.H.Andersen:
Electron-impact detachment from negative ions.
Phys. Rev. A **53** 2371 (1996)

L. Vejlby-Christensen, L.H. Andersen, O. Heber, D. Kella, H.B. Pedersen, H.T. Schmidt, and D. Zajfman:
Complete branching ratios for the dissociative recombination of H_2O^+, H_3O^+, and CH_3^+.
The Astrophys. Journal **483**, 531 (1997).

Conference (I)

J.U. Andersen:
Cooling of C_{60} in ASTRID, derived from observations of thermionic emissions.
Contribution, Workshop "Collision studies involving fullerenes", Stockholm, August 1996.

J.U. Andersen, C. Brinck, P. Hvelplund, M.O. Larsson, and H. Shen:
Fullerenes in a heavy-ion storage ring. Electron emission and radiative cooling
ISSPIC-8 Conference, Copenhagen, June 1996, Poster.

L.H. Andersen:
Electron-negative ion interaction.
Invited lectures, 2nd Euro-study Conf., Stockholm, June 1996.

T. Andersen:
Detachment and lifetimes of negative ions.
Invited lectures, 2nd Euro-study Conference, Stockholm, June 1996.

T. Andersen et al:
New approaches to negative ions: Resonant ionisation spectroscopy and storage rings.
Invited paper, 7th Int.Conf. On Accelerator Mass Spectroscopy, Tuscon, USA, May 1996.

P. Balling, P. Kristensen, H.H. Andersen, U.V. Pedersen, V.V. Petrunin, L. Præstgaard, H.K. Haugen and T. Andersen:
Vacuum ultraviolet spectroscopy of H^-.
Contribution, QELS/CLED Conference, 2-6 June 1996, Los Angeles, USA.

P. Kristensen, P. Balling, H.H. Andersen, U.V. Pedersen, V.V. Petrunin, L. Præstgaard, H.K. Haugen, and T. Andersen:
Vacuum ultraviolet spectroscopy of H^-.
15th Int.Conf. on Atomic Physics, Amsterdam, August 1996. Poster.

Thesis (I)

Carsten Brink:
Fullerenes-investigated by Atomic Collisions and Photon Interactions
Ph.D. Thesis1996.

Peter J. Johnson
Imaging of nuclear fragments applied to dissociative recombination
M.Sc. Thesis 1997

Poul Kristensen:
Laser Spectroscopy of Negative Ions
Ph.D. Thesis 1997.

Henrik B. Pedersen:
Studies of diatomic molecular ions at ASTRID
M.Sc. Thesis as part of PhD Degree, 1996.

L. Vejlby-Christensen:
Electron-Ion Collision Studies at ASTRID
Ph.D. Thesis, 1997.

Synchrotron Radiation, biology (SB)

Refereed Journals

J.V. Abraham-Peskir, R. Searle, R. Medenwaldt and E. Uggerhøj:
A new technique of Examining Pollen-connecting Threads
Grana **36,** 343, 1997.

J.V. Abraham-Peskir
Copper-induced structural changes in fully-hydrated Chilomonas paramecium.
European Journal of Protistology, **34**, 51-57 (1998)

J.V. Abraham-Peskir, E. Chantler, C. McCann, R. Medenwaldt, and E. Ernst (1998).
Ultrastructure of human sperm using X-ray Microscopy,
Medical science Research **26**, 663 (1998)

Thomas Vorup-Jensen, Tage Hjort, Joanna V. Abraham, Peter Guttmann, Jens C. Jensenius, Erik Uggerhøj, Robin Medenwaldt:
X-ray Microscopy of Human Spermatozoa Shows Change of Mithochondrial Morphology During Capacitation
Subm. to Human Reproduction.

R. Medenwaldt and E. Uggerhøj:
Description of an X-ray Microscope with 30 nm resolution.
Review of Scientific Instruments **69**/**8**, 2974 (1998

R. Medenwaldt, J.V. Abraham-Peskir & E. Uggerhøj
X-ray microscopy in Aarhus with 30 nm resolution.
Synchrotron Radiation News 11, 37-40. (1998)

I. Thom, M. Grote, J.V. Abraham-Peskir and R. Wiermann
Electron and X-ray microscopic analyses of reaggregated materials obtained after fractionation of dissolved sporopollenin. Protoplasma (in press). (1998)

Conference (SB)

J. Abraham, R. Medenwaldt, E.Uggerhøj, P. Guttmann, T. Hjort, J. Jensenius, T. Vorup-Jensen, Fritz Vollrath, E. Søgaard, J. Tyge Møller:
X-ray Microscopy in Aarhus
(Eds J. Thieme, G. Schmahl, E. Umbach, D. Rudolph) X-ray Microscopy and Spectromicroscopy, Springer Verlag, Heidelberg, pp 13-23 (1998).

C. Jacobsen, R. Medenwaldt and S. Williams:
A comparison between electron and X-raymicroscopy: theoretical considerations.
To be published in (Eds. J. Thieme, G. Schmahl, E. Umbach, D. Rudolph) X-ray Microscopy and Spectromicroscopy, Springer Verlag, Heidelberg (1998).

R. Medenwaldt. J. Abraham, and Erik Uggerhøj:
X-ray Microscopy in Aarhus.
pp. 184-185 in A.B. Mausbach (ed.), Extended abstracts of the 48th Annual Meeting of the Scandinavian Society for Electron Microscopy. Scandem-96.

R. Medenwaldt, J. Abraham, E. Uggerhøj:
Projects and Results on the Aarhus X-ray Microscope.
pp. 54-55 in A.B. Mausbach (ed.), Extended abstracts of the 48th Annual Meeting of the Scandinavian Society for Electron Microscopy, Scandem-96.

R. Medenwaldt, J. Abraham, E. Uggerhøj, F. Vollrath, E. Søgaard:
X-ray Microscopy Projects in Aarhus.
pp. 907-908 in G. Bailey et al. (eds.), Proceedings Microscopy and microanalysis 1997, Cleveland, Ohio, August 10-14, 1997, Springer 1997.

Thesis (SB)

Jette Wendt-Larsen
Metal Induced Changes in Chilomonas Paramecium *Investigated by X-ray and Light* Microscopy
M.Sc. Thesis, 1998

Synchrotron Radiation, physics (SP)

Refereed Journals

D.L. Adams:
New Phenomena in the adsorption of alkali metals on Al surfaces (sect.7)
Appl.Phys. A **62** (1996). 123-142.

S. V. Christensen, J. Nerlov, P. J. Godowski, and J. Onsgaard:
Photoemission and high resolution electron energy loss spectroscopystudy of CO/K/Cu(110)
J. Chem. Phys. **104** (1996).

S. V. Christensen, J. Nerlov, K. Nielsen, J. Burchhardt, M. M. Nielsen, and D. L. Adams:
Formation of Surface Ternary Alloys by Coadsorption of Alkali Metals on Al(111)
Phys. Rev. Lett. **76** 1892 (1996)

P. J. Godowski, J. Onsgaard, S. V. Christensen, and J. Nerlov:
Photoemission study of CO adsorbed on K/Cu(110). Analysis of adsorbate induced structures
Acta Physica Polonica A **89** 657 (1996).

R. J. Gulley, S. L. Lunt, J-P Ziesel and D. Field:
Very low energy electron scattering from benzene and deuterated benzenes
J. Phys. B: At. Mol. Opt. Phys **31** 2735 (1998)

Q. Guo and P.J. Møller,
CO and residual H adsorption on Cu/ZnO(10-10),
Applied Surface Science **115** (1997) 39-45.

Z. Li and P.J. Møller,
Electronic properties of Cu clusters and islands and their reaction with O_2 on SnO_2(110) surfaces,
Zeitschrift für Physik D: Atoms Molecules and Clusters **40** (1997) 550-553.

E. Lundgren, R. Nyholm, M. Qvarford, J.N. Andersen, D. Heskett, and S.V. Christensen:
Unified behavior of alkali core-level binding-energy shifts induced by sp metals.
Phys.Rev. **B 56**, (1997) 12560-12565.

P. Morgen, P.-E. Hansen, K. Pedersen:
Experiments with extrinsic Si(111)surfaces: Cs adsorption at room temperature on Si(111) terminated with hydrogen and oxygen.
Appl.Surf.Sci. **117/118** (1997) 72-76.

P.J. Møller, Z.S. Li and Q. Guo,
Synthesis and characterization of a model CuO/SnO_2 oxygen sensor
in *Functional Graded Materials*, I. Shiota & M.Y. Miyamoto, eds., 707-712, Elsevier Science 1997.

P.J. Møller, Z.S. Li, T. Egebjerg, M. Sambi and G. Granozzi,
Synchrotron-radiation-induced photoemission study of VO_2 ultrathin films deposited on TiO_2(110),
Surface Science **402** (1998) 719-723.

P.J. Møller, Q. Guo and L. Gui,
Ultrathin film of Cu on á-Fe_2O_3(0001) surfaces,
Thin Solid Films **281** (1996) 76-79.

J. Nerlov, Qingfeng, Q. Gea and P.J. Møller:
Resonant photoemission from TiO_2(110) surfaces : Implications on surface bonding and hybridization.
Surf. Sci. **348,** 28-38. (1996).

J. Nerlov, S.V. Christensen, S. Weichel, E.H. Pedersen, P.J. Møller:
A photoemission study of the coadsorption of CO_2 and Na on TiO2(110)-(1x1) and -(1x2) surfaces: Adsorption geometry and reactivity.
Surf. Sci. **371** (1997) 321-336.

J. Nerlov, S.V. Hoffmann, M. Shimoura and P.J. Moller:
Co-adsoprtion of Na and CO_2 on the Fe_30_4(111) termination of alpha-Fe203(0001): relations between structure and Activation.
Surf.Sci. **401** (1998) 56-71.

J. Onsgaard, S.V. Christensen, P.J. Godowski, J. Nerlov and S. Quist:
Synthesis of formate on K-modified Cu(110) based on coadsorption of H and CO_2.
Surf.Sci.lett. **370** (1997) L137-L143.

J. Onsgaard, P.J. Godowski, J. Nerlov, S. Quist and S.V. Hoffmann:
Interactions between H, CO, CO_2 on a K-modified Cu(110) surface.
Surf.Sci. **398** (1998) 318-331.

K. Pedersen and P. Morgen*:*
Room temperature deposition and growth of Au on Si(111) investigated by optical second-harmonic generation.
Accepted for publication in J.Phys.C.

M. Shimomura, P.J. Møller, J. Nerlov, S.V. Christensen, Q. Guo, N. Sanada, and Y. Fukuda:
Adsorption of H2S on In(001) studied by photoemission spectroscopy.
Appl. Surf. Sci. **121/122** (1997) 237-240.

K. Stahrenberg, T. Herrmann, N. Esser, J. Sahm, W. Richter, S.V. Hoffmann and Ph. Hofmann:
Surface state contribution to the optical anisotropy of Ag(110) surfaces:A RAS and photoemission study
Phys. Rev. B **58**, R10207 (1998).

Conference (SP)

D.Field, S.L.Lunt, S.V.Hoffmann, J.P.Ziesel
Do PAHs soak up electrons in the interstellar medium?
Proc. 3rd Cologne-Zermatt Symposium: The Physics and Chemistry of the Interstellar Medium. 1998 Ed. V.Ossenkopf.

R.J. Gulley, D.Field, S.V.Hoffmann, S.L.Lunt and J-P Ziesel.
Very low energy electron scattering from polycyclic aromatic hydrocarbons and substituted benzene molecules
Abstracts of the International Symposium on Electron-Molecule Collisions and Ion and Electron Swarms, Engelberg, Switzerland, (1997).

R.J.Gulley, S.L.Lunt, D.Field and J-P. Ziesel
Very low energy electron scattering from C_6H_6 and C_6D_6
Abstracts of contributed papers, XX International Conference on the Physics of Electronic and Atomic Collisions, eds. F.Aumayr, G.Betz and H.P.Winter. Vienna, Austria. (1997)

R.J.Gulley, S.L.Lunt, D.Field and J-P. Ziesel
Very low energy electron attachment and scattering from the CH_3NO_2, $C_2H_5NO_2$ and $C_6H_5NO_2$
Abstracts of contributed papers, XX International Conference on the Physics of Electronic and Atomic Collisions, eds. F.Aumayr, G.Betz and H.P.Winter. Vienna, Austria. (1997)

Z.S. Li, J. Hoffmann Jørgensen, P.J. Møller, M. Sambi and G. Granozzi,
A photoemission and resonant photoemission study of Ba deposition at the TiO_2(110) surface,
Applied Surface Science, in press, presented at ICSFS-9.

Z.S. Li,
Resonant photoemission spectroscopy on SnO_2(101) surfaces,
Nordic Conference on Surface Science, Ålesund, Norway, 1997.

P.J. Møller, Z.S. Li, J. Hoffmann Jørgensen, M. Sambi and G. Granozzi,
A photoemission study of the oxidation of Ba ultrathin layers deposited on TiO_2(110),
presented at ICSFS-9.

P.J. Møller:
Co-adsorption on metal-oxide crystal surfaces.
Invited in Chemisorption and reactivity on supported clusters and thin films: Toward understanding heterogeneous catalysis, eds. RM Lambert and G. Pacchioni (Kluwer Academic Publ. 1997) p. 267.

P.J. Møller, S.A. Komolov, E.F. Lazneva and T. Egebjerg,
Oxygen effect on the conductivity of the Cu_xO/ZnO(0001) and (000-1) systems,
Applied Surface Science, in press, presented at ICSFS-9.

M. Sambi, M. Della Negra, G. Granozzi, Z.S. Li, J.Hoffmann Jørgensen and P. J. Møller:
An ARPEFS study of the structure of an epitaxial VO_2 monolayer at the TiO_2(110) surface,
Applied Surface Science, in press, presented at ICSFS-**9**

H.N. Waltenburg and P.J. Møller,
Growth of ultrathin Pd films on Zr(Y)O_2(100),
Applied Surface Science, in press, presented at ICSFS-9.

Thesis (SP)

S.V. Christensen:
Some geometrical and Catalytic Aspects of alkali metal Adsorption.
PhD. Thesis, 1996.

Jesper Nerlov:
Structure and reactivity studies of alkali metal adsorption on metal and metal oxide surfaces.
PhD. Thesis, 1996.

Eddie Hjelm Pedersen:
Studier af ZnO(0001) ig TiO2(110) overfladerne og deres reaktivitet overfor film af henholdsvis Cu og na.
Kemisk Institut, Kemisk Laboratorium IV, Københavns Universitet, April 1996.

Christa Larsen Theil:
Indkøring af SGM monokromatoren ved ASTRID of efterfølgende undersøgelser af $L_{21,3}$-kanterne i krom i forskellige forbindelser vha. synkrotronstråling.
M.Sc. Thesis, 1996.

Lars Thomsen:
Adsorption of hydrogen and carbon dioxide on alkali-modified copper surfaces
M.Sc. Thesis, 1998.

Steen Weichel:
Den elektroniske og geometriske struktur af CoO(100) og Cu/CoO(100) undersøgt med elektron spektroskopi, elektron diffraktion og skanning tunnel mikroskopi.
Københavns Universitet, Oktober 1996.

Susanne Quist:
Adsorption of H_2, CO_2 and HCOOH on an alkali-modified Cu(110) surface.
M.Sc. Thesis, 1997.

External Activities

Refereed journals

G. Arduini, C. Biino, M. Clément, K. Cornelis, N. Doble, K. Elsener, G. Ferioli, G. Fidecaro, L. Gatignon, P. Grafström, M. Gyr, W. Herr, J. Klem, U. Mikkelsen, and E. Weisse
Deflection and extraction of Pb ions up to 33 TeV/c by a bent silicon crystal
Phys. Rev. Lett. **79** (1997) 4182

A. Baurichter, U. Mikkelsen, K. Kirsebom, R. Medenwaldt, S.P. Møller, E. Uggerhøj, T. Worm, K. Elsener, S. Ballestrero, P. Sona, J. Romano, C. Biino, R. Moore, and Z.Z. Vilakazi
Enhancement of electromagnetic showers initiated by ultrarelativistic electrons in aligned thick germanium crystals
Nucl. Instrum. Methods in Phys. Research **B 119** (1996) 143

A. Baurichter, K. Kirsebom, R. Medenwaldt, S.P. Møller, T. Worm, E. Uggerhøj, C. Biino, M. Clément, N. Doble, K. Elsener, L. Gatignon, P. Grafström, U. Mikkelsen, A. Freund, Z. Vilakazi, P. Siffert, and M. Hage-Ali
New results from the CERN-SPS beam deflection experiments with bent crystals
Nucl. Instrum. Methods in Phys. Research **B 119** (1996) 172

A. Baurichter, K. Kirsebom, Yu.V. Kononets, R. Medenwaldt, U. Mikkelsen, S.P. Møller, E. Uggerhøj, T. Worm, K. Elsener, S. Ballestrero, P. Sona, J. Romano, S.H. Connell, J.P.F. Sellschop, R.O. Avakian, A.E. Avetisian, S.P. Taroian:
Radiation Emission and Its Influence on Motion of Multi-GeV Electrons and Positrons in Strong Crystalline Fields.
Phys. Rev. Lett. **79** (1997) 3415.

C. Biino, M. Clément, N. Doble, K. Elsener, A. Freund, L. Gatignon, P. Grafström, K. Kirsebom, U. Mikkelsen, S.P. Møller, E. Uggerhøj, and T. Worm
Deflection of 200 GeV/c and 450 GeV/c positively charged particles in a bent germanium crystal
Phys. Lett. **B 403** (1997) 163

H. Bluhme, H. Knudsen, U. Mikkelsen, E. Morenzoni, K. Paludan, S.P. Møller, and E. Uggerhøj
Non-dissociative and dissociative ionization of O2 molecules by impact of 40-1000 keV antiprotons
J. Phys. B: At. Mol. Opt. Phys. **30** (1997) 3417

K. Elsener, G. Fidecaro, M. Gyr, W. Herr, J. Klem, U. Mikkelsen, S.P. Møller, E. Uggerhøj, G. Vuagnin, and E. Weisse
Proton Extraction from the CERN SPS using bent silicon crystals
Nucl. Instrum. Methods in Phys. Research **B 119** (1996) 215

M.H. Holzscheiter, E. Uggerhøj... (54 authors):
Antihydrogen Production and Precision Experiments.
Int.Workshop on Antimatter Gravity and Antihydrogen Spectroscopy, Molise, Italy (1996), Hyperfine Interactions **109**, 1 (1997).

K. Kirsebom, Yu.V. Kononets, U. Mikkelsen, S.P. Møller, E. Uggerhøj, T. Worm, C. Biino, K. Elsener, S. Ballestrero, P. Sona, S.H. Connell, J.F.P. Sellschop, Z.Z. Vilakazi, A. Apyan, R.O. Avakian, and K. Ispirian
Pair Production by 5-150 GeV photons in the strong crystalline fields of germanium, tungsten and iridium
Nucl. Instrum. Methods in Phys. Research **B 135** (1998) 143

K. Kirsebom, R. Medenwaldt, U. Mikkelsen, S.P. Møller, K. Paludan, E. Uggerhøj, T. Worm, K. Elsener, S. Ballestrero, P. Sona, J. Romano, S.H. Connell, J.P.F. Sellschop, R.O. Avakian, A.E. Avetisian, and S.P. Taroian
Experimental investigations of photon multiplicity and radiation cooling for 150 GeV electrons/positrons traversing diamond and Si crystals
Nucl. Instrum. Methods in Phys. Research **B 119** (1996) 79.

K. Khayyat et al:
Differential Cross Sections in Antiproton- and Proton – Helium Collisions.
Submitted to Phys.Rev.Letters (1998).

R. Moore, M.A. Parker, A. Baurichter, U. Mikkelsen, K. Kirsebom, R. Medenwaldt, S.P.Møller, E. Uggerhøj, T. Worm, N. Doble, K. Elsener, S. Ballestrero, P. Sona, V.M. Strakhovenko, C. Biino, and Z.Z. Vilakazi
Measurement of pair-production by high energy photons in an aligned tungsten crystal
Nucl. Instrum. Methods in Phys. Research **B 119** (1996) 149

S.P. Møller, E. Uggerhøj, H. Bluhme, H. Knudsen, U. Mikkelsen, K. Paludan, and E. Morenzoni
Measurement of the Barkas effect around the stopping power maximum for light and heavy targets
Nucl. Instrum. Methods in Phys. Research **B 122** (1997) 162

S.P. Møller, E. Uggerhøj, H. Bluhme, H. Knudsen, U. Mikkelsen, K. Paludan, and E. Morenzoni

Direct measurement of the stopping power for antiprotons of light and heavy targets
Phys. Rev. **A 56** (1997) 2930

K. Paludan, M. Charlston, K. Kirsebom, H. Knudsen, U. Mikkelsen, E. Morenzoni, S.P. Møller, J. Slevin, and E. Uggerhøj:

Ionization collisions between 30-1000 keV antiprotons and atomic hydrogen.
Can.J. Physics, **74** 490 (1996).

E. Uggerhøj:

Atomic Collisions with Antiprotons.
Nucl. Instruments and Methods in Physics Research **B 135** (1998) 35-39.

Conference (EA)

H. Bach, D. Einfeld, N. Hertel, S. P. Møller, B. R. Nielsen, F. Perez, L. Præstegaard, U. Ristau, and R. Rossmanith

The ANKA injector
Proceedings from 6th European Particle Accelerator Conference, EPAC-98, Stockholm 22-26 june 1998

C. Biino, M. Clément, N. Doble, E. Elsener, L. Gatignon, P. Grafström, U. Mikkelsen, A. Freund, K. Kirsebom, S. P. Møller, E. Uggerhøj, and T. Worm

Record deflection efficiencies measures for high energy protons in a bent Germanium crystal
Proceedings from 1997 Particle Accelerator Conference, PAC'97, Vancouver, B.C., Canada, 12-16 May 1997.

C. Biino, M. Clément, N. Doble, K. Elsener, L. Gatignon, P. Grafström, U. Mikkelsen, A. Taratin, S. P. Møller, E. Uggerhøj, P. Keppler, and J. Major

First observation of the deflection of a 33 TeV Pb ion beam in a bent Silicon crystal
Proceedings from 1997 Particle Accelerator Conference, PAC'97, Vancouver, B.C., Canada, 12-16 May 1997.

C. Biino, M. Clément, N. Doble, K. Elsener, L. Gatignon, P. Grafström, U. Mikkelsen, K. Kirsebom, S.P. Møller, E. Uggerhøj, and T. Worm

The influence of radiation damage on the deflection of high energy beams in bent silicon crystals
Proceedings from 6th European Particle Accelerator Conference, EPAC-96, Sitges 10-14 th June 1996, Spain.

M.H. Holzscheiter, E. Uggerhøj... (54 authors):

Antihydrogen Production and Precision Experiments.
Int.Conf. on Low Energy Antiproton Physics LEAP 1996.

K. Paludan, G. Laricchia, P. Ashley, V. Kara, J. Moxom, H. Bluhme, H. Knudsen, U. Mikkelsen, S.P. Møller, E. Uggerhøj, E. Morenzoni:

Ionization of the rare gases by particle/antiparticle impact.
Journal of Phys. B. **30** (1997) 3951. **XX Int. Conf**. on the Physics of Electronic and Atomic Collisions, Vienna (1997) WE 159.

K. Paludan, H. Bluhme, H. Knudsen, U. Mikkelsen, S.P. Møller, E. Uggerhøj, E. Morenzoni:
Single,double and triple ionization of Ne, Ar, Kr, and Xe by 30-1000 keV p^- impact.
XX Int. Conf. on the Physics of Electronic and Atomic Collisions, Vienna (1997) WE 160. J.Phys.**B 30** 3951 1997.

Erik Uggerhøj:
Crystal Channeling of High Energy Beams.
Conference Proceeding. Submitted to QABP 98.

Thesis (EA)

Ulrik Mikkelsen
Experimental Investigations of the Interaction of Multi-GeV Particles with Strong Crystalline Fields.
Ph.D. Thesis 1998